



THE HONG KONG  
POLYTECHNIC UNIVERSITY

香港理工大學

Pao Yue-kong Library

包玉剛圖書館

---

## Copyright Undertaking

This thesis is protected by copyright, with all rights reserved.

**By reading and using the thesis, the reader understands and agrees to the following terms:**

1. The reader will abide by the rules and legal ordinances governing copyright regarding the use of the thesis.
2. The reader will use the thesis for the purpose of research or private study only and not for distribution or further reproduction or any other purpose.
3. The reader agrees to indemnify and hold the University harmless from and against any loss, damage, cost, liability or expenses arising from copyright infringement or unauthorized usage.

### IMPORTANT

If you have reasons to believe that any materials in this thesis are deemed not suitable to be distributed in this form, or a copyright owner having difficulty with the material being included in our database, please contact [lbsys@polyu.edu.hk](mailto:lbsys@polyu.edu.hk) providing details. The Library will look into your claim and consider taking remedial action upon receipt of the written requests.

Pao Yue-kong Library, The Hong Kong Polytechnic University, Hung Hom, Kowloon, Hong Kong

<http://www.lib.polyu.edu.hk>

**EXPLOITING THE POTENTIAL OF WIND TURBINES  
TO PROVIDE FREQUENCY SUPPORT**

**XIAOGE LIU**

**PhD**

**The Hong Kong Polytechnic University**

**2019**



**The Hong Kong Polytechnic University**

Department of Electrical Engineering

**Exploiting the Potential of Wind Turbines to  
Provide Frequency Support**

**Xiaoge LIU**

A thesis  
submitted in partial fulfillment of the requirements for  
the degree of Doctor of Philosophy

**August 2018**



## **CERTIFICATE OF ORIGINALITY**

I hereby declare that this thesis is my own work and that, to the best of my knowledge and belief, it reproduces no material previously published or written, nor material that has been accepted for the award of any other degree or diploma, except where due acknowledgement has been made in the text.

\_\_\_\_\_ (Signed)

\_\_\_\_\_ Xiaoge LIU \_\_\_\_\_ (Name of student)



*To my parents,*

*LIU Jiangbo and GAO Dongqin*



## **Abstract**

The wind energy technology emerges as one of promising techniques for satisfying growing power demand as well as reducing carbon dioxide emission. During recent years, the penetration level of wind energy has experienced continuous growth. However, compared with conventional power plants, the characteristics of wind power plants are different, and thus the wind power plants can impose significant challenges on the power system control and operation.

In order to maintain the stability of power system, some transmission system operators have stipulated that the wind power plants are required to regulate their performance. According to the technical rules specified by these system operators, the wind power plants ought to participate in voltage control and frequency regulation if necessary. To fulfill these requirements, various control schemes applied in wind turbines have been put forward.

The research in this thesis aims at developing new control schemes exploiting the potential of each variable speed wind turbine for frequency control. The research background and motivation are introduced in Chapter 1. Chapter 2 summarizes the technical requirements for wind power integration issued in recent years. The classical modelling of variable speed wind turbine and relevant control strategies are illustrated in Chapter 3. Based on a comprehensive review on the frequency control strategies designed for individual wind turbine, combined frequency control schemes enabling the variable speed wind turbine to provide frequency response are proposed in Chapter 4. Chapter 5

reveals that the control methodology presented in Chapter 4 can also be implemented in the offshore wind farm connected to VSC-HVDC system. The simulation results verify the effectiveness of the proposed frequency control schemes. Conclusions and future scope are provided in Chapter 6.

## **Publications Arising from The Thesis**

### **Technical Papers in Refereed Journals**

- [1] **Xiaoge LIU**, Zhao XU, and Kit Po Wong, “Recent Advancement on Technical Requirements for Grid Integration of Wind Power,” *Journal of Modern Power Systems and Clean Energy*, vol. 1, no. 3, pp. 216-222, 2013.
- [2] **Xiaoge LIU**, Zhao XU, ZHAO Jian, “Combined Primary Frequency Control Strategy of Permanent Magnet Synchronous Generator-Based Wind Turbine,” *Electric Power Components and Systems*, pp. 1-15, 2019.
- [3] **Xiaoge LIU**, Zhao XU, “Coordinated Frequency Control Scheme of Offshore Wind Farm Connected to VSC-HVDC,” *Electric Power Components and Systems* (Under second round review)

### **Conference Papers in Refereed Proceedings**

- [1] **Xiaoge LIU**, Zhao XU, Kit Po Wong, and Loi Lei Lai, “Power Smooth Control for DFIG under Extreme Operating Gust,” in *PES General Meeting/ Conference & Exposition, 2014 IEEE*, 2014, pp. 1-5: IEEE.



## **Acknowledgements**

I would be grateful to my chief supervisor, Prof. Zhao Xu, for his help and support provided when I studied in The Hong Kong Polytechnic University. Under his supervision, I have learnt critical thinking and research methodology. Besides, I have also acquired important skills on writing research articles and making academic presentations with his help.

I would like to express my gratitude to my parents for their unconditional support and endless love. During the past years, they are always on my side and give me valuable suggestions when necessary.

I would like to appreciate the financial support and research resources provided by The Hong Kong Polytechnic University. By using these resources, I can keep up with the development of relevant fields and conduct my research smoothly.

Moreover, I would like to thank Confucius for his excellent wisdom left in this world. From his experience, I have learnt how to live in this society and how to tackle the difficulties in my life.

The last but not the least, I would like to appreciate the care and support offered by my colleagues and friends in Hong Kong. When I need help, all of you will give me a hand in time and help me to deal with problems. Besides, I have learnt a lot by communicating with you. I will always cherish the memories of the time we spent together.



# Table of Contents

CERTIFICATE OF ORIGINALITY .....	5
Abstract .....	iii
Publications Arising from The Thesis.....	v
Acknowledgements .....	vii
Table of Contents .....	ix
List of Figures .....	xiii
List of Tables.....	xvi
Abbreviations .....	xvii
Chapter 1 Introduction .....	1
1.1 Research Background.....	1
1.2 Research Motivation .....	3
1.3 Thesis Layout .....	5
Chapter 2 Overview of Technical Requirements Specified for Wind Power Plants .....	9
2.1 Introduction.....	9
2.2 Technical Regulation for Wind Power Plant under Normal Condition .....	10
2.2.1 Technical Regulation of Active Power Control .....	11
2.2.2 Technical Regulation of Reactive Power Control.....	16
2.3 Technical Regulation of Wind Power Plant under Grid Fault .....	19
2.3.1 Technical Regulation of Low Voltage Ride Through.....	20
2.3.2 Technical Regulation of Reactive Current Support .....	23
2.4 Summary .....	26
Chapter 3 Overview of Construction and Conventional Operation of Variable Speed Wind Turbine .....	29
3.1 Construction of Variable Speed Wind Turbine.....	29
3.1.1 Aerodynamics of Wind Turbine .....	29
3.1.2 Shaft Train System .....	30
3.1.3 Pitch Angle Control .....	32

3.1.4	Configurations of Variable Speed Wind Turbine .....	33
3.2	Conventional Operation of Variable Speed Wind Turbine.....	35
3.2.1	Conventional Operation of VSWT under Normal Condition .....	35
3.2.2	Inner-loop Control Techniques Applied in Power Converters of VSWT..	40
3.2.3	Operation of VSWT under Grid Faults.....	41
3.2.4	Operation of VSWT Considering Material Fatigue.....	47
3.3	Power Smoothing Control of Variable Speed Wind Turbine .....	48
3.3.1	Introduction.....	49
3.3.2	Modelling of DFIG-WTs for Study .....	51
3.3.3	The Proposed Power Smoothing Control Scheme.....	53
3.3.4	Simulation Results .....	58
3.4	Summary .....	63
Chapter 4	Control Schemes Exploiting the Potential of Wind Turbines to Provide Frequency Support .....	65
4.1	Introduction.....	65
4.2	PMSG-WT Model for Study.....	69
4.2.1	Conventional Control Schemes Applied in Individual PMSG-WT.....	69
4.2.2	Modelling of Drive Train System.....	70
4.2.3	Modelling of Pitch Angle Controller .....	71
4.2.4	Conventional Control Schemes Applied in RSC and GSC .....	71
4.3	The Proposed Primary Frequency Control Scheme for PMSG-WT.....	72
4.3.1	Overview of The Proposed Control Scheme .....	72
4.3.2	Control Scheme to Realize the De-loading Operation of PMSG-WTs .....	75
4.3.3	Extended Rotor Speed Control Applied in RSC.....	78
4.3.4	Modified DC-Link Voltage Control Applied in GSC.....	79
4.4	Simulation Results .....	81
4.4.1	System Frequency Decline under Constant Wind Speed .....	84
4.4.2	System Frequency Rise under Constant Wind Speed.....	88
4.4.3	System Frequency Decline under Variable Wind Speed .....	92

4.5	Summary .....	98
Chapter 5 Coordinated Frequency Control Scheme for Offshore Wind Farm Integrated to VSC-HVDC System .....		
5.1	Introduction .....	101
5.2	System Model for Study .....	105
5.2.1	Overview of the Studied System.....	105
5.2.2	Model and Conventional Control of Individual Wind Turbine .....	105
5.3	The Proposed Coordinated Frequency Control Strategy for VSC-HVDC Connected Offshore Wind Farm .....	107
5.3.1	Overview of the Proposed Control Scheme .....	107
5.3.2	Extended Rotor Speed Control Applied in VSWTs.....	108
5.3.3	Modified DC-link Voltage Control Applied in VSC-HVDC .....	112
5.4	Simulation Results .....	113
5.4.1	System Frequency Decline under Constant Wind Speed.....	115
5.4.2	System Frequency Rise under Constant Wind Speed .....	118
5.4.3	System Frequency Decline under Variable Wind Speed .....	121
5.5	Summary .....	127
Chapter 6 Conclusions and Suggestions for Future Research .....		
6.1	Conclusions .....	129
6.2	Suggestions for Future Research.....	131
6.2.1	Improvement of Proposed Frequency Control Schemes.....	131
6.2.2	The Impacts of Proposed Frequency Control Schemes .....	132
6.2.3	Development of Multiple Wind Turbines Control Schemes.....	132
Appendices .....		B-1
References .....		B-3



## List of Figures

Figure 1.1 Trend of global wind power capacity [1] .....	1
Figure 2.1 Requirements of active power in Danish grid code [17] .....	12
Figure 2.2 Basic regulation of the active power generated by each WPP in Germany [18] .....	13
Figure 2.3 Requirements of frequency control for wind power plants of which the generated power is higher than 25MW in Denmark [17] .....	13
Figure 2.4 Operating range of each WPP in Germany [18] .....	18
Figure 2.5 Operating range of individual wind turbine in German grid code [18] .....	19
Figure 2.6 Operating range of Danish WPPs [17] .....	19
Figure 2.7 LVRT regulation specified in Danish grid code [17] .....	21
Figure 2.8 LVRT regulation specified in Germany [18] .....	21
Figure 2.9 LVRT regulation in Irish grid code [20] .....	22
Figure 2.10 LVRT regulation applied in Alberta, Canada [19] .....	22
Figure 2.11 LVRT regulation specified in Chinese grid code [21] .....	23
Figure 2.12 Regulation of reactive current support in Danish grid code [17] .....	25
Figure 2.13 Regulation of reactive current support in German grid code [18] .....	25
Figure 3.1 The relationship between power coefficient and tip speed ratio .....	30
Figure 3.2 Pitch angle control system .....	32
Figure 3.3 Conceptual sketch of individual DFIG-WT .....	33
Figure 3.4 Conceptual sketch of individual PMSG-WT .....	34
Figure 3.5 Schematic diagram of typical ORSC .....	36
Figure 3.6 Typical power characteristics of VSWT .....	38
Figure 3.7 Schematic diagram of OPC .....	38
Figure 3.8 DC-link voltage control in GSC .....	39
Figure 3.9 Control technique used in RSC .....	53
Figure 3.10 The flowchart of the proposed PSC scheme .....	56
Figure 3.11 The system model for simulation .....	58
Figure 3.12 The EOG profile used in case study .....	59
Figure 3.13 The variation of active power produced by the DFIG-WT under EOG .....	60
Figure 3.14 The rotor speed variation under EOG .....	60
Figure 3.15 The shaft torque variation under EOG .....	61
Figure 4.1 Configuration of a typical PMSG-WT .....	70
Figure 4.2 Model of pitch angle controller .....	70
Figure 4.3 Typical method to perform MPPT control .....	70
Figure 4.4 Overview of the proposed control scheme .....	73
Figure 4.5 Extended rotor speed control used in RSC .....	74
Figure 4.6 Modified DC-link voltage control used in GSC .....	75
Figure 4.7 $C_p - \lambda$ characteristic .....	76
Figure 4.8 Control technique to realize de-loading operation .....	77
Figure 4.9 Model of power system for case study .....	82

Figure 4.10 System frequency performance in Case. A .....	85
Figure 4.11 Performance of wind turbine rotor speed in Case. A .....	85
Figure 4.12 DC-link voltage performance in Case. A .....	86
Figure 4.13 Performance of active power produced by PMSG-WT in Case. A.....	86
Figure 4.14 Power coefficient performance in Case. A.....	87
Figure 4.15 System frequency performance in Case. B.....	89
Figure 4.16 Performance of wind turbine rotor speed in Case. B.....	89
Figure 4.17 DC-link voltage performance in Case. B .....	90
Figure 4.18 Performance of active power produced by PMSG-WT in Case. B.....	90
Figure 4.19 Power coefficient performance in Case. B .....	91
Figure 4.20 Variable wind speed profile used in Case. C.....	92
Figure 4.21 System frequency performance in Case. C (100~180s) .....	92
Figure 4.22 Performance of wind turbine rotor speed in Case. C (100~180s) .....	93
Figure 4.23 DC-link voltage performance in Case. C (100~180s).....	93
Figure 4.24 Performance of active power produced by PMSG-WT in Case. C (100~180s) .....	94
Figure 4.25 Power coefficient performance in Case. C (100~180s).....	94
Figure 4.26 System frequency performance in Case. C (170~220s) .....	95
Figure 4.27 Performance of wind turbine rotor speed in Case. C (170~220s) .....	96
Figure 4.28 DC-link voltage performance in Case. C (170~220s).....	96
Figure 4.29 Performance of active power produced by PMSG-WT in Case. C (170~220s) .....	97
Figure 4.30 Power coefficient performance in Case. C (170~220s).....	97
Figure 5.1 Typical layout of an offshore wind farm connected to a VSC-HVDC transmission system .....	105
Figure 5.2 A typical MPPT control method used in this research .....	106
Figure 5.3 Overview of the proposed frequency control scheme .....	108
Figure 5.4 Control scheme to achieve de-loading operation .....	109
Figure 5.5 Extended rotor speed control scheme used in each VSWT.....	110
Figure 5.6 Modified DC-link voltage control scheme applied in VSC-HVDC system	113
Figure 5.7 Configuration of the power system model for case study .....	114
Figure 5.8 Performance of system frequency in Case. A .....	116
Figure 5.9 Performance of wind turbine rotor speed in Case. A .....	116
Figure 5.10 Performance of DC-link voltage of the VSC-HVDC system in Case. A...117	117
Figure 5.11 Performance of active power injected into the main grid in Case. A.....117	117
Figure 5.12 Performance of system frequency in Case. B.....	119
Figure 5.13 Performance of wind turbine rotor speed in Case. B.....	119
Figure 5.14 Performance of DC-link voltage of the VSC-HVDC system in Case. B...120	120
Figure 5.15 Performance of active power injected into the main grid in Case. B .....	120
Figure 5.16 Variable wind speed profile used in Case. C.....	122
Figure 5.17 Performance of system frequency in Case. C (100~180s) .....	123
Figure 5.18 Performance of wind turbine rotor speed in Case. C (100~180s) .....	123

Figure 5.19 Performance of DC-link voltage of the VSC-HVDC system in Case. C (100~180s) ..... 124

Figure 5.20 Performance of active power injected into the main grid in Case. C (100~180s) ..... 124

Figure 5.21 Performance of system frequency in Case. C (170~220s) ..... 125

Figure 5.22 Performance of wind turbine rotor speed in Case. C (170~220s) ..... 126

Figure 5.23 Performance of DC-link voltage of the VSC-HVDC system in Case. C (170~220s) ..... 126

Figure 5.24 Performance of active power injected into the main grid in Case. C (170~220s) ..... 127

## List of Tables

Table 2.1 Grid codes selected for review.....	10
Table 2.2 The regulation of active power production for frequency control in Canada [19].....	14
Table 2.3 The regulation of active power generated by Chinese WPP [21].....	15
Table 2.4 The power factor ranges specified in Canada, Ireland and China [19-21] .....	18
Table 3.1 The value of b .....	54
Table 3.2 The switch conditions for EOG detection.....	57
Table 3.3 The setting of parameters.....	61
Table 4.1 Frequency performance of Case. A .....	87
Table 4.2 Wind turbine performance of Case. A .....	87
Table 4.3 Frequency performance of Case. B.....	91
Table 4.4 Wind turbine performance of Case. B .....	91
Table 4.5 Frequency performance of Case. C.....	98
Table 5.1 Frequency performance of Case. A .....	118
Table 5.2 Wind turbine performance of Case. A .....	118
Table 5.3 Frequency performance of Case. B.....	121
Table 5.4 Wind turbine performance of Case. B .....	121
Table 5.5 Frequency performance of Case. C.....	125

## **Abbreviations**

### *Acronyms*

FSWT	fixed speed wind turbine
VSWT	variable speed wind turbine
DFIG-WT	doubly fed induction generator based wind turbine
PMSG-WT	permanent magnet synchronous generator based wind turbine
TSO	transmission system operator
WPP	wind power plant
POC	power of connection
CSG	conventional synchronous generator
CPP	conventional power plant
MPPT	maximum power point tracking
LVRT	low voltage ride through
TSR	tip speed ratio
RSC	rotor-side converter
GSC	grid-side converter
LIDAR	light detecting and ranging
ORSC	optimal rotor speed control
OPC	optimal power control
PI controller	proportional-integral controller
HCS	hill climb search

RSRE	rotor speed reference estimating
IOPC	improved optimal power control
CVDP	combined vector and direct power control
IGBT	Insulated Gate Bipolar Transistor
EMF	electromotive force
SVC	static var compensator
STATCOM	static synchronous compensator
BPF	bandpass filter
EOG	extreme operating gust
IEC	International Electrotechnical Commission
PSC	power smoothing control
TGL	torque gradient limiter
PEC	power error control
EIC	emulated inertia control
DOPFC	de-loading operation based primary frequency control
ESS	energy storage system
P controller	proportional controller
D controller	derivative controller
ROCOF	rate of change of frequency
PV system	photovoltaic system
OWPP	offshore wind power plant
VSC-HVDC	voltage source converter based high voltage direct current

PD controller	proportional-derivative controller
WFS-VSC	wind farm side voltage source converter
GS-VSC	grid side voltage source converter

### *Symbols*

$f$	power system frequency
$n$	rotor speed in r/min
$p$	number of pole pairs
$P_m$	the mechanical power captured by individual wind turbine
$C_P$	power coefficient
$\lambda$	tip speed ratio (TSR)
$\beta$	pitch angle
$\rho$	air density
$R$	blade radius
$V_w$	wind speed
$\omega_r$	actual value of rotor speed
$C_P^{max}$	maximum value of power coefficient
$\lambda_{opt}$	optimal tip speed ratio
$T_m$	mechanical torque of each wind turbine
$T_e$	electrical torque of each wind turbine
$\omega_t$	turbine speed

$T_{sh}$	shaft torque
$H_t$	inertia constant of turbine
$D_t$	damping coefficient of turbine
$\theta_t$	shaft twist angle
$\omega_b$	the base value of rotating speed
$H_g$	inertia constant of generator
$D_g$	damping coefficient of generator
$K_{sh}$	stiffness constant
$D_{sh}$	mutual damping of shaft
$H_L$	inertia constant in one-mass model
$\beta_{opt}$	optimal value of pitch angle
$\beta_{max}$	upper bound of pitch angle
$\beta_{min}$	lower bound of pitch angle
$\omega_{r.max}$	upper bound of rotor speed
$P_{e.ref}$	reference of electrical power
$\omega_{r.ref}$	reference of rotor speed
$\omega_{r.min}$	lower limit of rotor speed
$P_{rate}$	rated power of individual wind turbine
$U_{DC.N}$	normal value of DC-link voltage
$U_{DC}$	actual value of DC-link voltage
$i_{qs}, i_{ds}$	d-q components of stator current

$i_{dr}, i_{qr}$	d-q components of rotor current
$DL_{del.N}$	the de-loading level of each wind turbine under normal condition
$P_m^{MPPT}$	the maximum power for a given wind speed
$P_m^{del.N}$	the captured power under de-loading level $DL_{del.N}$
$C_P^{del.N}$	sub-optimal power coefficient with de-loading level $DL_{del.N}$
$\lambda'_{del.N}$	lower-than-optimal TSR for de-loading operation
$\lambda_{del.N}$	higher-than-optimal TSR for de-loading operation
$f_N$	nominal value of frequency
$P_m^{del.f}$	desirable value of mechanical power for frequency control
$C_{DC}$	capacitance
$\Delta U_{DC}$	variation of DC-link voltage
$\Delta f$	variation of system frequency
$U_{DC.min}$	minimum value of DC-link voltage
$U_{DC.max}$	maximum value of DC-link voltage
$f_{min}^{WT}$	frequency value when the de-loading level becomes zero
$f_{nadir}$	frequency nadir
$f_{final}$	final value of frequency
$P_{e.hvdc}$	the active power provided by the DC capacitor in VSC-HVDC
$U_{DC.hvdc}$	voltage of DC capacitor in VSC-HVDC
$C_{DC.hvdc}$	capacitance of capacitor in VSC-HVDC
$U_{DC.hvdc.min}$	minimum voltage of DC capacitor in VSC-HVDC

$U_{DC.hvdc.max}$  maximum voltage of DC capacitor in VSC-HVDC

$f_{min}^{hvdc}$  frequency value when  $U_{DC.hvdc.min}$  is achieved

# Chapter 1 Introduction

## 1.1 Research Background

The public awareness on energy crisis and climate change inspire researchers and engineers to develop new techniques of renewable energy. It is expected that the integration of renewable energy can satisfy the increasing power demand and contribute to the reduction of carbon dioxide emission.

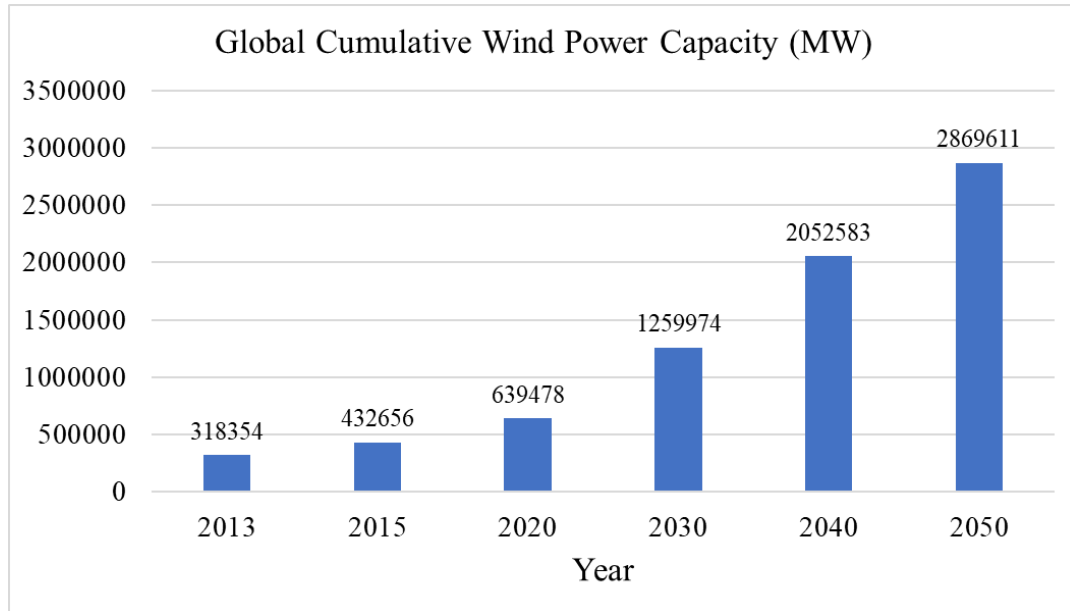


Figure 1.1 Trend of global wind power capacity [1]

So far, wind energy has been regarded as a mature technology and the integration level of wind power has increased continuously during recent years, especially in China, America and Europe [1]. The data presented in [1] show that the global capacity of wind power has increased to 433GW by the end of 2015. Based on historical data and current

policy on energy and climate, reference [1] also projects the future capacity of wind energy. The trend of wind power capacity installed globally is shown in Figure 1.1.

In the early 1970s, fixed speed wind turbines (FSWTs) were very popular in industry [2]. A number of FSWTs based wind farms were constructed in Europe and America [2]. Under normal condition, the operating range of each FSWT is quite narrow, and the reactive power in power system can be consumed by the induction generator installed in each FSWT [2]. For reactive power compensation, these wind power plants were usually equipped with capacitor banks [2].

In the 1990s, manufacturers began to produce variable speed wind turbines (VSWTs) [2]. Compared to FSWT, the operating range of VSWT is enlarged significantly. Therefore, each VSWT can extract more power from wind. In addition, due to the development of power electronic techniques, it is not required for each VSWT to absorb the reactive power from utility network. So far, the type of VSWT has become the mainstream in market.

Nowadays, two concepts of VSWT are widely used in industry: doubly fed induction generator based wind turbine (DFIG-WT) and permanent magnet synchronous generator based wind turbine (PMSG-WT). To realize variable speed operation, it is necessary to install AC/DC/AC converters in each DFIG-WT or PMSG-WT.

The characteristics of VSWTs are different from that of conventional power plants. In the past, the impact of low penetration of wind energy on power system could be neglected. Since the capacity of wind turbines incorporated into the power system experienced sustainable increase during recent years, transmission system operators

(TSOs) have stipulated that the wind power plants (WPPs) should be able to reinforce power system stability. According to the requirements specified in these grid codes, the WPPs should perform frequency control actions if power imbalance occurs. During a grid fault, the wind turbines should have the ability to survive and contribute to voltage stabilization.

Traditionally, the WPPs concentrate on energy harvesting, and thus maximum power point tracking (MPPT) control is applied in individual VSWT. Owing to the revision of the technical rules, various research endeavors have been devoted to the development of novel control schemes for VSWTs so that the requirements specified in grid codes can be fulfilled.

## 1.2 Research Motivation

To protect synchronous machines and other appliances, the system frequency should be kept constant. In the past, the power system consisted of conventional synchronous generators (CSGs). Because the CSGs are excited by DC exciters and the stator of each CSG is linked to the power system directly, the electricity produced by the CSG can be delivered to the power system without any conversion. Moreover, the relationship between rotor speed of the CSG and system frequency can be described as follows:

$$np = 60f \quad (1.1)$$

where  $n$  is generator speed in r/min,  $p$  is the number of pole pairs and  $f$  is system frequency.

This equation illustrates that system frequency is explicitly associated with the rotor speed of CSG. Therefore, the power imbalance can not only lead to rotor speed variation, but

result in frequency deviation as well. It is noteworthy that if frequency deviates, CSGs can offer inertia response naturally.

The system frequency control framework based on the characteristics of CSGs has been well-established. Under normal condition, each conventional power plant (CPP) equipped with CSGs should preserve primary reserve. If a frequency excursion occurs, the frequency proportional controller, which is installed in each CPP to perform primary frequency control, will be activated. Armed with such controller, the CPP can change the valve position if frequency deviates so that the mechanical power acquired by CSG can be adjusted. Consequently, the power system can regain a new equilibrium point. It is notable that due to the application of the frequency proportional controller, the frequency deviation caused by power imbalance can be arrested, but the system frequency cannot be restored. To eliminate the steady-state error of system frequency and recover the primary reserve, secondary frequency control should be implemented in practice.

System frequency stability can be influenced by the increasing penetration level of wind energy, especially for small scale isolated power grids [3], [4]. Different from CSGs, the rotor speed of each VSWT is no longer coupled with system frequency. Unlike the CSG excited by DC exciter, the generator in DFIG-WT is excited by AC current produced by rotor-side converter. For PMSG-WT, although the generator can be self-excited by permanent magnet, the stator is not linked to the power system directly. As a result, the relationship between system frequency and rotor speed of the VSWT cannot be described by (1.1), and therefore neither DFIG-WT nor PMSG-WT can provide inertia support automatically. If the CSGs are replaced by the VSWTs gradually, the system inertia

constant will reduce significantly. In that case, the power system can be more sensitive to disturbances. In addition to the decrease of system inertia constant, the variable wind speed can cause power imbalance unexpectedly, and thus the system frequency can fluctuate.

In order to mitigate the adverse impacts of VSWTs, the grid codes stipulated by some TSOs in Europe have required WPPs to provide frequency response, especially if power consumption is low [5]. Inspired by this, researchers have proposed various frequency control schemes enabling each VSWT to take part in frequency regulation.

In this thesis, a comprehensive review on these frequency control methods is provided. Furthermore, a combined frequency control scheme exploiting the potential of each PMSG-WT to provide frequency response is developed in this research. This scheme includes an extended rotor speed control and a modified DC-link voltage control. By using the extended rotor speed control, both the reserve acquired from de-loading operation and kinetic energy stored in rotor can be deployed together to perform frequency control. Besides, the modified DC-link voltage can utilize the electrical energy preserved in DC capacitor to enhance system inertia response. It is noteworthy that the extended rotor speed control can also enable the DFIG-WT to participate in frequency control. Moreover, in this thesis, the control methodology proposed for each PMSG-WT is also applied to the offshore wind farm which is connected to main power grid through VSC-HVDC system so that the performance of onshore system frequency can be improved.

### **1.3 Thesis Layout**

The contents of each chapter are summarized as follows:

**Chapter 2** reviews the grid codes issued in recent years. In this chapter, the technical regulations applied in different regions are compared and analyzed. The specifications on active power production and reactive power adjustment, which can particularly affect the performance of WPPs, are investigated. This chapter illustrates that as the penetration level of wind power rises, the TSOs in different countries demand that the wind power plants should make more contribution to the power system stability.

The construction and conventional operation of variable speed wind turbines are introduced in **Chapter 3**. This chapter presents the operation of wind turbines under normal condition and grid faults. The control schemes aiming at reducing the mechanical fatigue of each VSWT are also discussed. In addition, a power smoothing control (PSC) scheme enabling VSWT to alleviate the power fluctuation caused by the extreme operating gust is provided in this chapter. On detecting the extreme operating gust, the PSC can adjust the electromagnetic torque automatically, and thus the fluctuation of the active power can be effectively attenuated.

As described in Section 1.2, some TSOs have stipulated that WPPs are required to regulate power output for frequency control. **Chapter 4** presents a combined control scheme exploiting the potential of PMSG-WT to perform frequency control. By operating in de-loading mode, the wind turbine can keep the power reserve under normal condition. If frequency deviates, the extended rotor speed control in the proposed control strategy can adjust the rotor speed accordingly. As a result, not only the power reserve can be utilized to regulate system frequency, but the kinetic energy stored in rotor can be

extracted to provide frequency response as well. Besides, armed with the modified DC-link voltage control, the DC capacitor can exploit the energy to perform additional frequency control actions. The case study in this chapter proves that the frequency performance can be improved if the wind turbines are equipped with the proposed control scheme. As mentioned before, the extended rotor speed control discussed in this chapter can also be applied to each DFIG-WT for frequency control.

Inspired by the research presented in Chapter 4, a control scheme coordinating the VSC-HVDC system with offshore wind farm to provide frequency response is discussed in **Chapter 5**. Like the control scheme described in Chapter 4, the over-speeding based de-loading operation should be implemented by each wind turbine so that the power reserve can be acquired in advance. If the system frequency deviation occurs, the proposed control scheme will be triggered in order to enable the wind turbines and the VSC-HVDC system to participate in frequency regulation. Furthermore, the rotor speed of each wind turbine can be adjusted by applying the extended rotor speed control so that both power reserve and kinetic energy stored in rotor can be deployed to mitigate power imbalance. Meanwhile, the participation of the VSC-HVDC system in primary frequency control is realized by activating the modified DC-link voltage control. Apart from relevant theoretical analysis, the simulation results aiming at validating the effectiveness of the proposed coordinated frequency control scheme are also included in this chapter.

Finally, main conclusions and several interesting topics for future research are provided in **Chapter 6**.



# **Chapter 2 Overview of Technical Requirements Specified for Wind Power Plants**

## **2.1 Introduction**

As the integration level of wind energy increases rapidly during recent year, power system control and operation may be affected significantly [6], [7]. To mitigate the adverse effects of wind power, the WPPs should fulfill relevant technical requirements.

The operating rules designed for the CSGs based CPPs are mature enough. According to these rules, these CPPs are required to provide ancillary service to balance active power. In addition, if a grid fault occurs, the CPPs should be able to enhance system voltage stability [2].

Based on the existing operating principles of CPPs, TSOs in some countries such as UK, Denmark and China have issued relevant grid codes stipulating the technical regulations for WPPs. The performance of each WPP should satisfy the requirements described in these specifications [8].

Similar to the technical requirements of CPPs, the WPPs should contribute to power balancing under normal condition [8], [9]. Besides, the recent grid codes also demand that wind turbines should be able to conform to the specifications of low voltage ride through (LVRT) and inject reactive current to the power system if a grid fault occurs so that the system voltage stability can be reinforced [8], [9]. Considering the penetration level of

wind energy is increasing continuously, these technical regulation may be improved further in the future [8].

The technical requirements specified in these grid codes can drive the manufactures and researchers to develop new techniques for wind turbines [9]. To satisfy the requirements in the grid codes, various control schemes have been proposed during recent years. For instance, several frequency control methods applied in individual wind turbine have been provided in [3], [10], [11]. Besides, the control strategies to enhance the LVRT capability of each wind turbine have been designed in [12-14].

Relevant discussions on the grid codes for WPPs have been conducted in [7-9], [15], [16]. In this chapter, the technical regulations listed in Table 2.1 are reviewed. These technical guidelines are representative, for the development of wind power utilization in these countries is very rapid. The regulations on wind turbine operation under normal condition are discussed in Section 2.2, and the technical specifications under grid faults are investigated in Section 2.3.

Table 2.1 Grid codes selected for review

Country	TSO	Issue Year	Grid Codes
Denmark	Energinet.dk	2009	[17]
Germany	TenneT	2012	[18]
Canada	Aeso	2013	[19]
Ireland	EirGrid	2012	[20]
China	State Grid Corporation of China (SGCC)	2009	[21]

## **2.2 Technical Regulation for Wind Power Plant under Normal Condition**

### 2.2.1 Technical Regulation of Active Power Control

The requirements on active power control aim to regulate the active power production of each WPP. Conventionally, WPPs are required to capture maximum power from wind [22]. Since more and more wind turbines are integrated into the power grid, more control functions, which must be performed by each WPP if necessary, have been included into the grid codes issued recently [22].

According to recent technical regulations, each WPP should be able to participate in frequency regulation. The requirements of frequency control specified in Denmark and Germany have been presented in Figure 2.1-Figure 2.3. It is noteworthy that if the system frequency lies in the dead-band defined by the TSOs, the wind turbines installed in each WPP should operate continuously. As shown in these figures, the frequency dead-band is set as 49.5 Hz~50.2 Hz in Denmark [17]. In Germany, the frequency control of each WPP is not required to be triggered if the frequency varies from 49.00 Hz to 50.5 Hz [18].

However, if the frequency deviation exceeds the dead-band, it is necessary for the WPPs to adjust their active power output. Figure 2.2 shows that in Germany, less active power should be generated by the WPPs if the frequency is over 50.2 Hz [18]. In Denmark, the WPPs should behave according to the power-frequency curves depicted in Figure 2.3. Furthermore, if the frequency lies in the interval  $[f_1, f_2]$  or  $[f_3, f_4]$ , the droop requirements should be satisfied and frequency response should be provided by the WPPs [15], [17]. The Danish grid code also specifies the duration and accuracy of the frequency response. In addition, in Denmark, the voltage information acquired at the power of connection

(POC) point should be considered when the WPPs perform these active power control actions.

Similarly, the Chinese, Irish and Canadian system operators have also determined the frequency dead-bands used in practice [19-21]. The grid code issued in China requires the WPPs to operate normally if frequency varies between 49.5 Hz and 50.2Hz. The frequency dead-band in Ireland is set as 49.5 Hz-51.0 Hz. In Canada, the normal frequency is 60 Hz [19], [20]. The details of the technical regulation specified in Canadian grid code is provided in Table 2.2 [19].

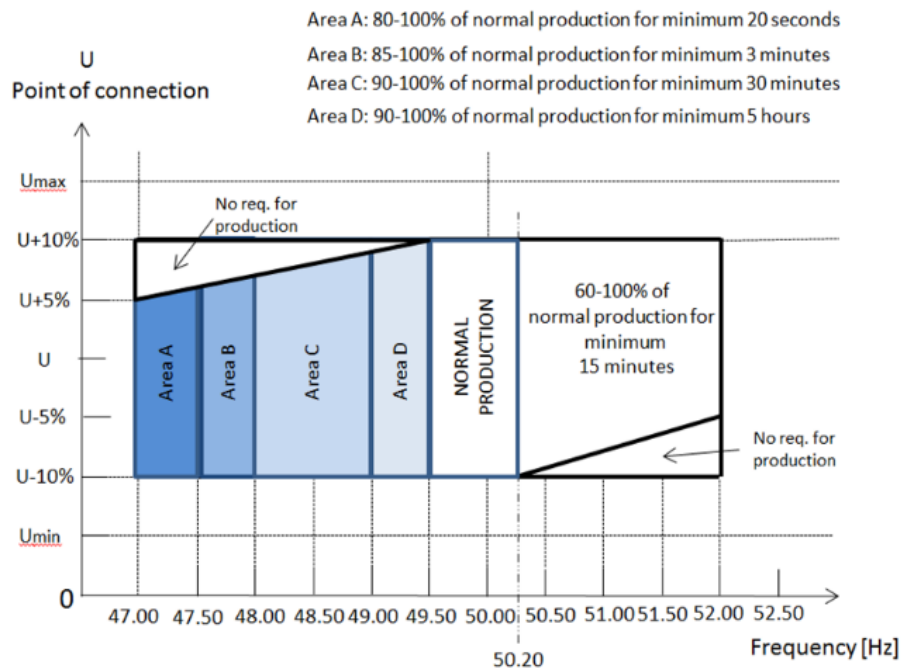


Figure 2.1 Requirements of active power in Danish grid code [17]

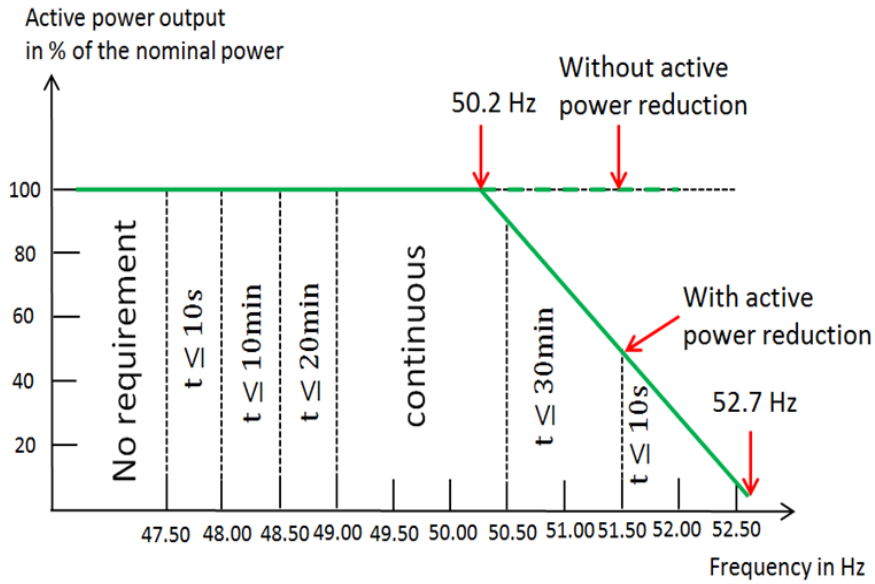


Figure 2.2 Basic regulation of the active power generated by each WPP in Germany [18]

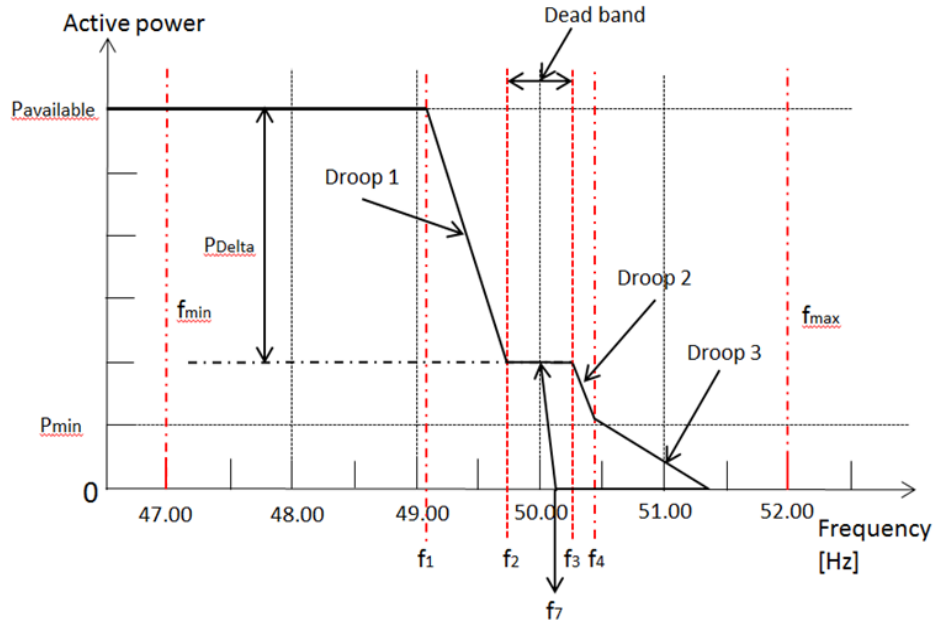


Figure 2.3 Requirements of frequency control for wind power plants of which the generated power is higher than 25MW in Denmark [17]

Table 2.2 The regulation of active power production for frequency control in Canada [19]

Frequency (Hz)	Minimum Time Delay
>61.7 Hz	0 seconds
61.6 Hz to 61.7 Hz	30 seconds
60.6 Hz to <61.6 Hz	3 minutes
>59.4 Hz to <60.6 Hz	Continuous Operation
>58.4 Hz to 59.4 Hz	3 minutes
>57.8 Hz to 58.4 Hz	30 seconds
>57.3 Hz to 57.8 Hz	7.5 seconds
>57.0 Hz to 57.3 Hz	40 cycles
$\leq 57.0$ Hz	0 seconds

The frequency deviation is caused by the imbalance between power generation and demand. To participate in frequency control, the WPPs should keep certain reserve capacity in advance [7], [22]. If frequency deviates, the reserve can be employed, and thus the WPPs can provide frequency response [7], [22]. Up to now, many papers have proposed various control schemes enabling wind turbines to provide frequency support [3], [10], [11].

The grid codes for WPPs also specify the constraints of power gradient so that the power ramp of each WPP can be limited if necessary [23]. These requirements may differ in different regions. The power gradient limits for the WPPs in China are provided in Table 2.3 [21]. In Ireland, the range of power ramp is from 1MW per minute to 30 MW per minute [20]. It is noteworthy that when the TSOs formulate the regulation of power ramp, the characteristics of conventional power plants should be considered [22].

Table 2.3 The regulation of active power generated by Chinese WPP [21]

The installed capacity of wind farm (MW)	10 min maximum ramp rate (MW)	1 min maximum ramp rate (MW)
<30	10	3
30-150	Installed capacity/3	Installed capacity /10
>150	50	15

Due to the variable wind speed, the active power produced by each WPP can fluctuate significantly. In order to smooth the power, some research articles suggest that energy storage systems (ESSs) such as flywheels, batteries and super-capacitors can be installed in wind farms [24]. However, the installation of the ESSs can lead to the dramatic increase of investment. In addition, some coordinated control methods, which aim to smooth the power generated by individual wind turbine by regulating pitch angle or changing the voltage of DC capacitor, have been designed [24], [25].

To fulfill the technical requirements on frequency control and power ramp, a centralized wind farm controller may be optional. Such controller should dispatch reference signals to individual wind turbine according to wind speed condition and the situation of each wind turbine [22]. More discussion on the control scheme for each WPP can be considered in the future.

Usually, the maximum power point tracking (MPPT) control is applied in each wind turbine in order to maximize the power captured from wind. If the frequency control is implemented to the WPPs in real-time, the MPPT control may be influenced in practice. The effect on MPPT control can also be investigated in the future.

### **2.2.2 Technical Regulation of Reactive Power Control**

The regulation of reactive power is associated with system voltage stability [26]. In the grid codes cited for this review, the specifications on reactive power adjustment under normal condition are commonly described by using power factor curves [26]. In Spain, not only the technical requirements on reactive power control are refined, but a commercial mechanism for power factor regulation is set up as well [27].

To develop the control schemes of reactive power regulation for each WPP, it is necessary to study the characteristics of the wind turbines. During the 1970s, fixed speed wind turbines (FSWTs) based on induction generator were widely erected in wind farms [2], [28]. However, owing to the application of induction generator, such wind turbines can only consume reactive power provided by power grid rather than inject reactive power to the power system [2]. Consequently, if a large number of FSWTs are connected to the power system, the power system stability can be affected greatly, especially if a grid fault occurs [2]. Besides, the reactive power output of each FSWT cannot be adjusted in practice [2]. As a result, these FSWTs cannot participate in voltage stabilization automatically. In the past, the requirements on power factor were quite general in relevant grid codes [26]. For instance, the Danish grid guidelines issued in 2000 allowed the WPPs to operate without injecting or absorbing reactive power, and the requirements on reactive power control were not very strict [26], [29]. Considering the FSWTs cannot generate reactive power, capacitor banks can be installed in the WPPs for reactive power compensation [28].

Since 2001, the variable speed wind turbines (VSWTs) such as doubly fed induction generator based wind turbines (DFIG-WTs) have become dominate in industry [2], [28], [30]. In each VSWT, a rotor-side converter and a grid-side converter are applied. Besides, DC capacitors are usually installed in each VSWT. By controlling the converters, such DC capacitors can release or absorb the reactive power according to the situation of power system [2]. Therefore, VSWTs can regulate the output of reactive power to enhance system voltage stability.

As the technique of wind turbine develops, more principles on reactive power control have been included in the grid codes issued in recent years. In Denmark and Germany, the power factor of each WPP should be adjusted as Figure 2.4-Figure 2.6 depict. As specified in German guideline, the power factor of the WPP should range from 0.95 underexcited to 0.925 overexcited if the system voltage falls from 170kV to 140kV [18], [31]. Moreover, the detailed requirements on reactive power control included in German grid code are shown in Figure 2.5. Table 2.4 presents the operating ranges of the power factor which are specified by the TSOs in Canada, Ireland and China.

As required by the TSOs in Canada, Ireland and China, the reactive power provided by each WPP should be varied with its active power output, while the German and Danish grid codes demand that the WPPs ought to adjust the reactive power according to the magnitude of system voltage [17], [18], [31]. These technical requirements are usually expressed by the curves describing the relationships between active power production and power factor or the mappings from system voltage to power factor.

Table 2.4 The power factor ranges specified in Canada, Ireland and China [19-21]

TSO	Country	Power Factor Range
aeso	Canada	-0.95 to 0.9 [19]
EirGrid	Ireland	0.85 lagging to 0.85 leading [20]
SGCC	China	0.95 lagging to 0.95 leading [21]

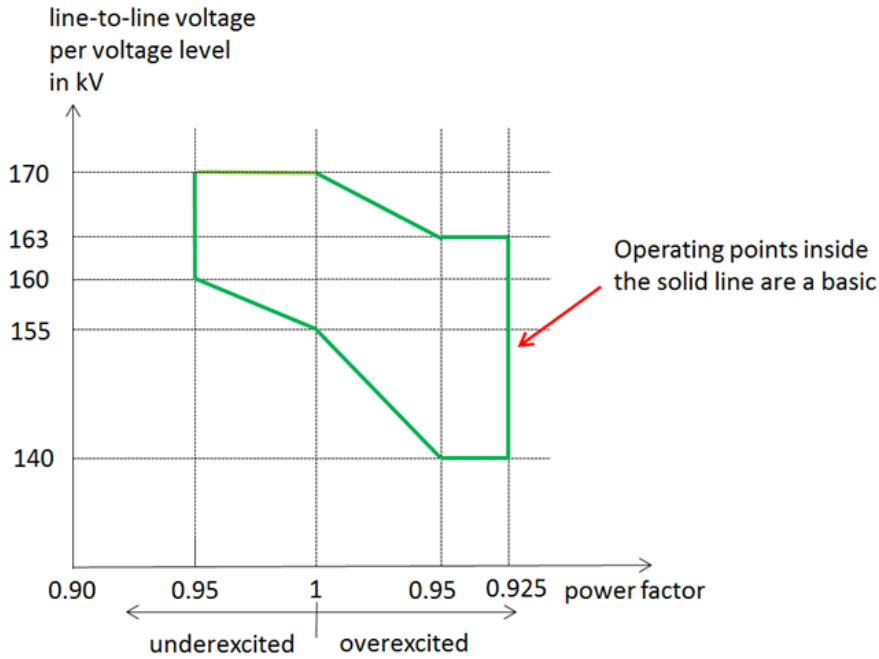


Figure 2.4 Operating range of each WPP in Germany [18]

In order to fulfill the technical requirements mentioned above, the potential of VSWTs can be exploited [31]. Additionally, the application of reactive power compensators such as static synchronous compensators (STATCOMs) or static var compensators (SVCs) can be considered [31]. Furthermore, considering the penetration level of wind energy is growing continuously, the control methods enabling the WPPs to provide voltage support can be discussed further in the future.

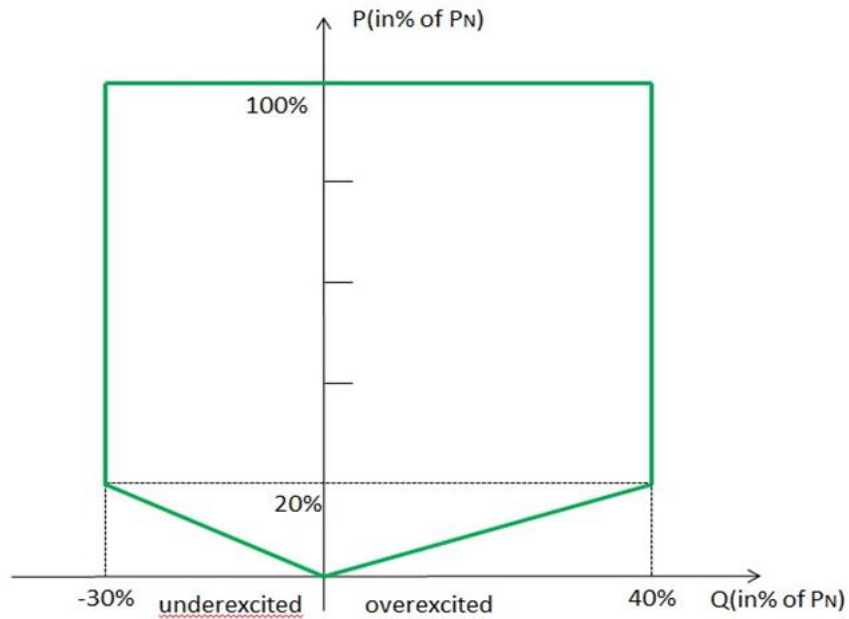


Figure 2.5 Operating range of individual wind turbine in German grid code [18]

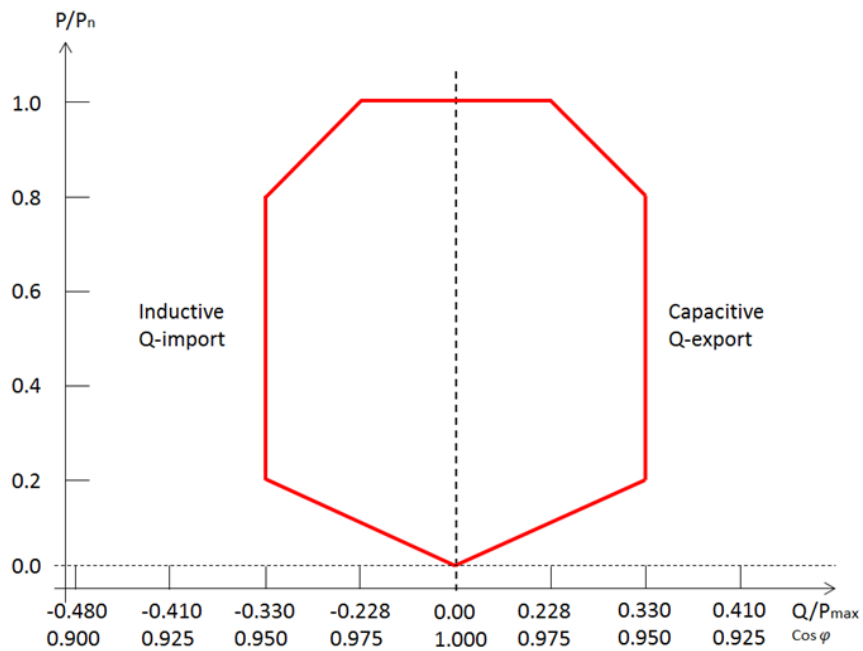


Figure 2.6 Operating range of Danish WPPs [17]

### 2.3 Technical Regulation of Wind Power Plant under Grid Fault

### **2.3.1 Technical Regulation of Low Voltage Ride Through**

During past years, the capacity of wind power was relatively small so that the effect on power system could be neglected [15], [32]. At that time, if a grid fault occurs, TSOs permitted the wind turbines to disconnect themselves from the transmission network [32]. Since more and more wind turbines are installed and participate in power supply during recent years, the instantaneous tripping of the wind turbines may lead to voltage collapse [33]. In order to enhance system voltage stability, the grid codes issued recently require the wind turbines to keep connecting to the power grid and provide reactive current during the fault. These requirements are termed as low voltage ride through (LVRT) [32]. The details of the LVRT regulation specified in different countries are presented in Figure 2.7- Figure 2.11.

In Denmark, the LVRT requirements must be fulfilled if a one, two or three phases fault occurs. According to Figure 2.7, the wind turbines in each WPP should not be tripped if a fault lies in Area A. In the event of a fault lying in Area B, the wind turbines should not only stay online, but inject reactive current as well. However, the wind turbines are allowed to be disconnected themselves if a fault is located within Area C [17]. The regulation of LVRT specified in China, Ireland and Canada are described in Figure 2.9- Figure 2.11 [17-21].

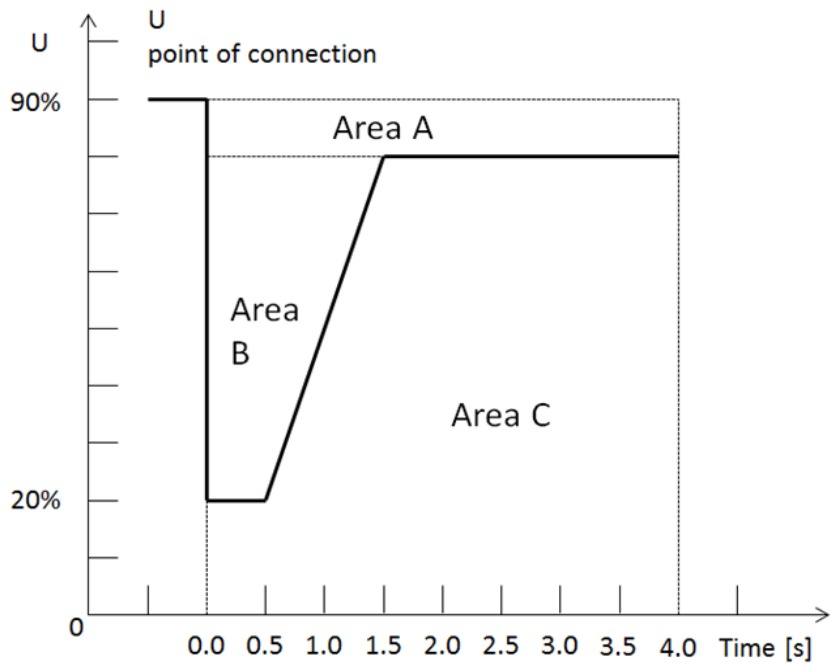


Figure 2.7 LVRT regulation specified in Danish grid code [17]

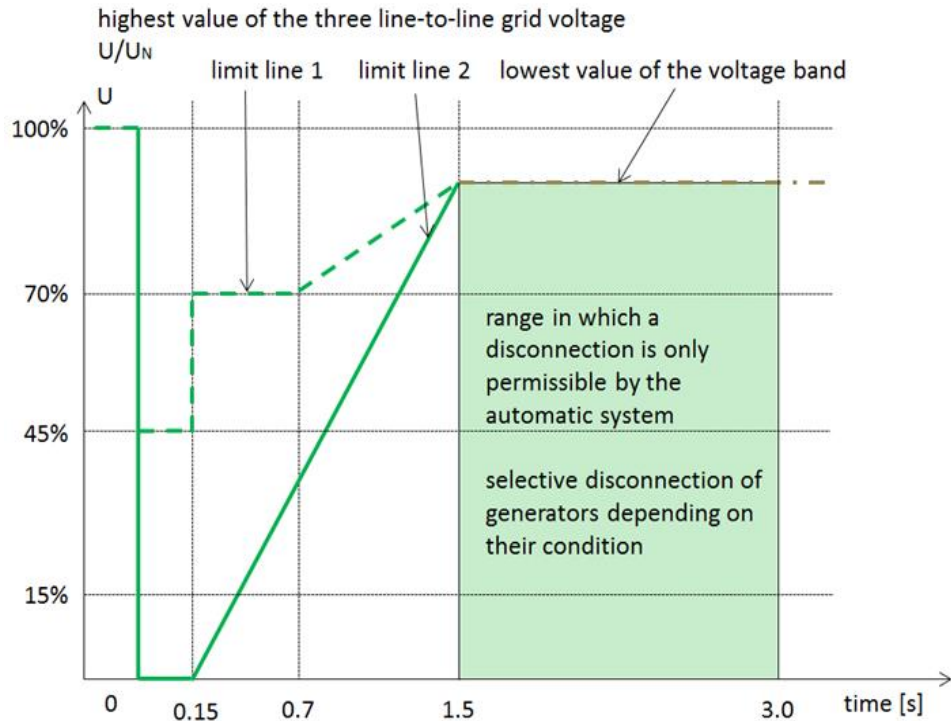


Figure 2.8 LVRT regulation specified in Germany [18]

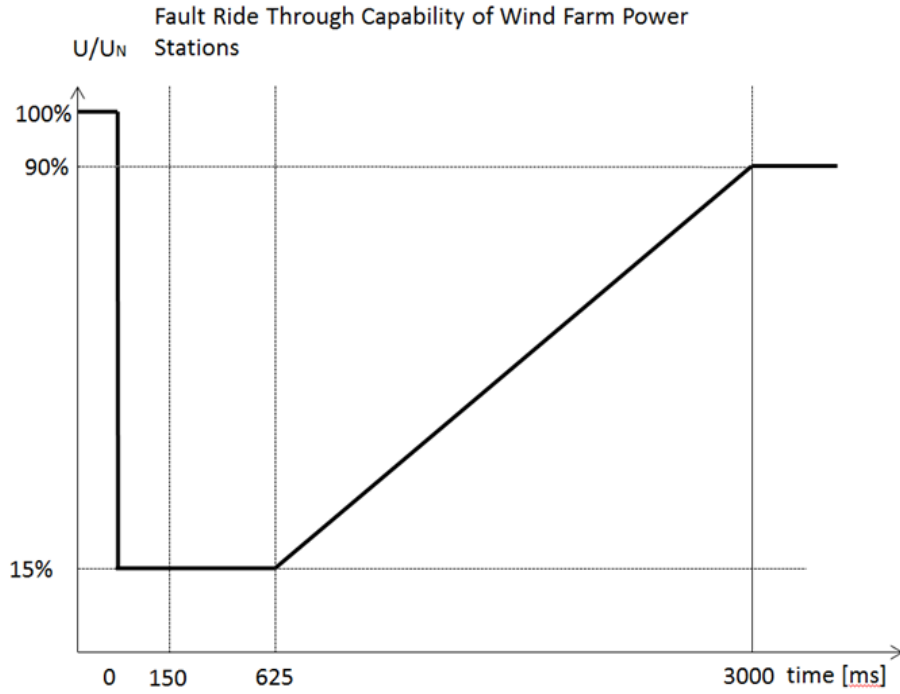


Figure 2.9 LVRT regulation in Irish grid code [20]

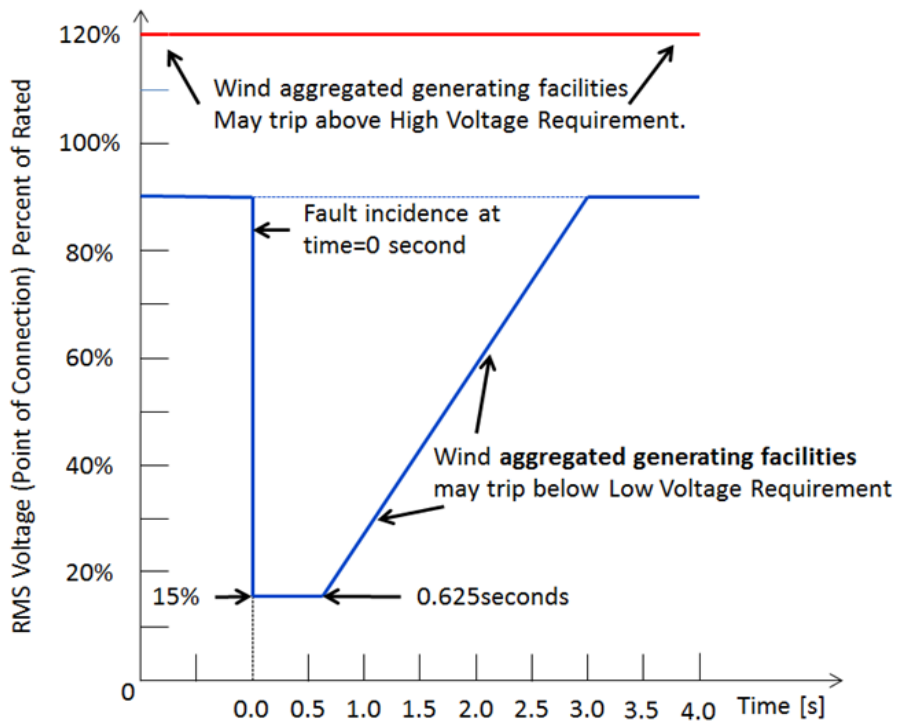


Figure 2.10 LVRT regulation applied in Alberta, Canada [19]

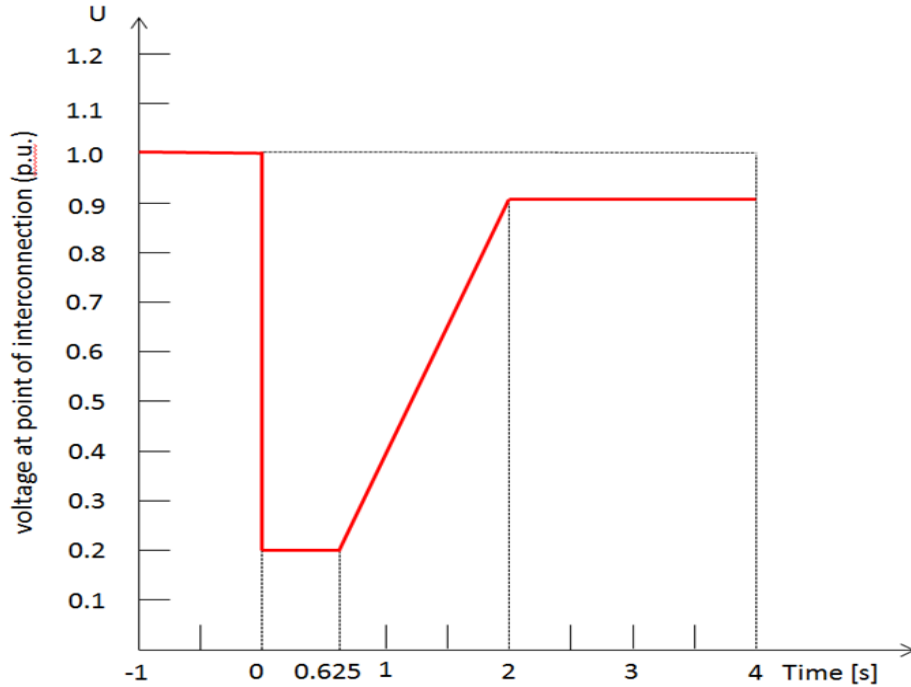


Figure 2.11 LVRT regulation specified in Chinese grid code [21]

The rule of LVRT defined in Germany is shown in Figure 2.8. It seems that such LVRT principle is the most complicated. If a grid fault lying in the area above Limit Line 1 occurs, the power system should remain stable. Besides, the wind turbines should keep connecting to the power system on condition that the system voltage lies in the area above the Limit Line 2. It is noteworthy that the grid fault may cause the current in each wind turbine to increase dramatically so that the converters are blocked. In that case, these wind turbines, which may become uncontrollable, can be tripped during the fault [18].

### 2.3.2 Technical Regulation of Reactive Current Support

According to the discussion in Section 2.2, due to the application of induction generator, it seems impossible to use the FSWTs for voltage stability enhancement. Considering that more and more VSWTs have been installed during recent years, these

wind turbines can provide additional reactive current to the power system by controlling the converters [12].

Figure 2.12-Figure 2.13 show the detailed regulations on reactive current injection which are applied in Denmark and Germany, respectively. According to the Danish grid code, the WPPs should make the reactive current supply a priority during the faults lying in Area B [17]. After having detected a voltage dip, the WPPs in Germany should be able to generate reactive current within 20ms [18].

Apart from the reactive power supply, the injection of active power during a voltage dip is also encouraged in some countries such as Ireland [14], [20]. It should be noted that due to the voltage sags, the overcurrent and overvoltage in VSWTs should be considered so that the power electronic devices installed inside can be protected from damaging [13], [14]. Furthermore, the Irish TSO specifies that the active power generated by WPPs ought to be proportional to the remaining voltage during a grid fault [20].

To avoid the power surge, some grid codes require that each WPP should limit the active power gradient after the system voltage recovers [26]. More specifically, the active power rate of individual WPP in Germany must be ranged from 10% to 20% of rated power per second [18].

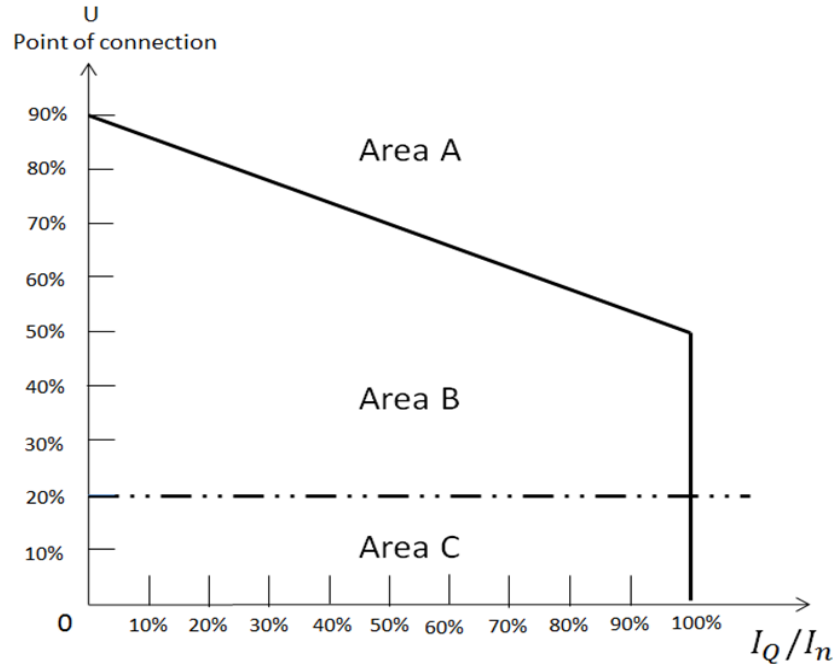


Figure 2.12 Regulation of reactive current support in Danish grid code [17]

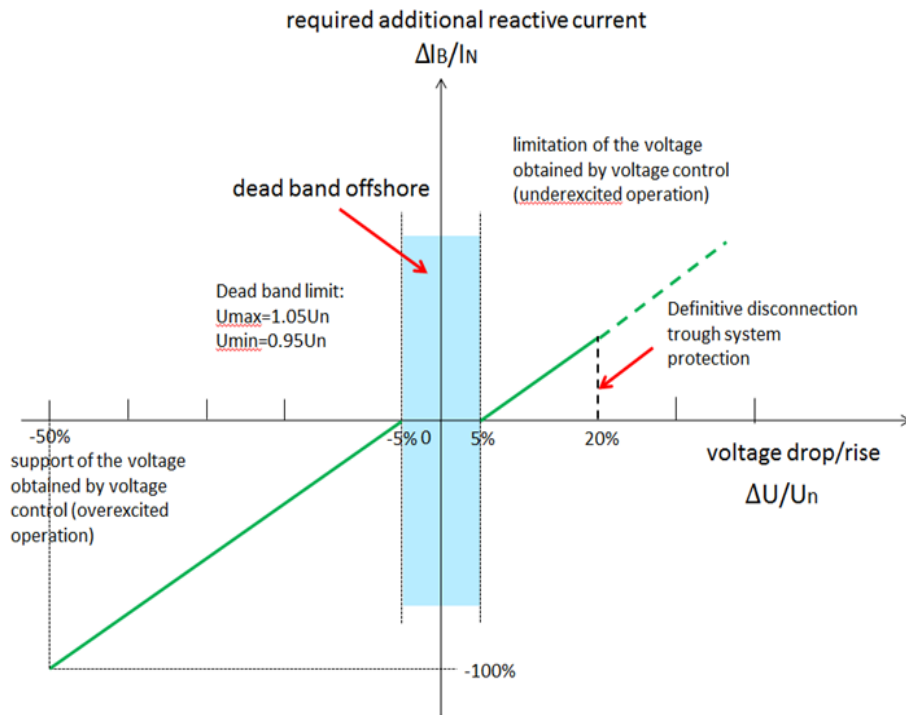


Figure 2.13 Regulation of reactive current support in German grid code [18]

As mentioned above, the potential of each VSWT can be exploited for reactive current supply [13], [14]. From a technical viewpoint, the DC capacitors installed in each DFIG-WT or PMSG-WT can be employed to provide reactive power by controlling the converters. Various control schemes enabling the VSWTs to generate the reactive power during a grid fault have been designed [14]. It is expected that some of these control strategies can be applied in the immediate future. If these control methods are implemented, the VSWTs can behave as STATCOMs after being subjected to a grid fault. It is noteworthy that the effects of wind turbine performance and wind speed condition on the implementation of these control strategies can be studied further.

## **2.4 Summary**

High penetration of wind energy can pose challenges to power system stability. As a result, it becomes necessary to evaluate and analyze the influence of wind power integration [32].

To tackle the challenges and avoid the instability of power system, TSOs in different countries have defined technical specifications so that the negative effects of WPPs can be mitigated. In this chapter, some grid codes stipulated in recent years are discussed.

Considering that the wind energy techniques are still evolving and penetration level of wind power is still growing, it can be expected that the grid codes may be refined further and more strengthened technical requirements may be included [32]. From this chapter, it can be learnt that the technical regulation has been reinforced in several aspects,

especially on reactive power supply and LVRT capability. These requirements aim to enhance the power system stability.

The innovation in wind power technology may be driven by the recent grid codes. Based on these regulations, the manufactures and researchers can contribute to the development of new devices or control techniques so that the requirements specified by the TSOs can be satisfied [9].



# Chapter 3 Overview of Construction and Conventional Operation of Variable Speed Wind Turbine

## 3.1 Construction of Variable Speed Wind Turbine

### 3.1.1 Aerodynamics of Wind Turbine

The basic aerodynamics of individual wind turbine can be regarded as fundamental knowledge of wind energy conversion. Such knowledge is investigated thoroughly in [2]. According to the wind turbine characteristics, the power extracted from wind  $P_m$  under a given wind speed can be expressed as follows [34]:

$$P_m = 0.5C_p(\lambda, \beta)\rho\pi R^2V_w^3 \quad (3.1)$$

$$C_p = 0.5176\left(\frac{116}{\gamma} - 0.4\beta - 5\right)e^{-\frac{21}{\gamma}} + 0.0068\lambda \quad (3.2)$$

$$\gamma = 1 / \left( \frac{1}{\lambda + 0.08\beta} - \frac{0.035}{\beta^3 + 1} \right) \quad (3.3)$$

In these equations,  $C_p$  is power coefficient, which is a function associated with the tip speed ratio (TSR)  $\lambda$  and pitch angle  $\beta$ ,  $\rho$  is air density,  $R$  is blade radius and  $V_w$  is wind speed. The TSR  $\lambda$  can be calculated as:

$$\lambda = \frac{\omega_r R}{V_w} \quad (3.4)$$

where  $\omega_r$  is rotor speed.

For a given wind speed, both the pitch angle and tip speed ratio can influence the value of power coefficient. As investigated in [2], in order to maximize the power

captured from wind, the pitch angle should be fixed at the optimal position, especially if the wind speed is below the rated value. The adjustment of pitch angle is discussed further in Section 3.1.3. Figure 3.1 describes the relationship between power coefficient and TSR on condition that the pitch angle is fixed.

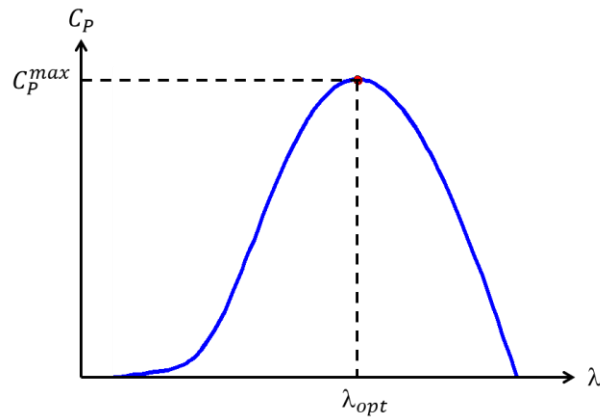


Figure 3.1 The relationship between power coefficient and tip speed ratio

In Figure 3.1,  $C_p^{max}$  represents the maximum value of power coefficient and the corresponding TSR is denoted by  $\lambda_{opt}$ . This figure shows that the extracted power can be maximized if and only if the wind turbine operates at the speed determined by  $\lambda_{opt}$ . Compared to the FSWTs, more power can be captured by VSWTs, because the rotor speed of each VSWT can be adjusted according to the power coefficient characteristics.

### 3.1.2 Shaft Train System

The shaft train system is the connection between wind turbine and generator [2]. In practice, both mechanical torque  $T_m$  and electrical torque  $T_e$  are applied on the shaft drive train system. As the connection is relatively soft in practice, the shaft drive train system may oscillate. Such oscillation may affect wind turbine operation and power system

stability [2]. Therefore, the representation of the shaft train system should be studied in detail [2].

So far, the shaft train system has been investigated in [2] and [35]. In [35], different types of the drive train model have been discussed and compared. The comparative study in [35] shows that the two-mass model is accurate enough to describe the performance of drive train and such model can be applied in the study of power system stability. A typical two-mass model can be described by following equations [2]:

$$T_m = \frac{0.5\rho\pi R^2 C_p(\lambda, \beta) V_w^3}{\omega_t} \quad (3.5)$$

$$\frac{d\omega_t}{dt} = \frac{1}{2H_t} (T_m - T_{sh} - D_t \omega_t) \quad (3.6)$$

$$\frac{d\theta_t}{dt} = \omega_b (\omega_t - \omega_r) \quad (3.7)$$

$$\frac{d\omega_r}{dt} = \frac{1}{2H_g} (T_{sh} - T_e - D_g \omega_r) \quad (3.8)$$

$$T_{sh} = K_{sh} \theta_t + D_{sh} \omega_b (\omega_t - \omega_r) \quad (3.9)$$

where  $T_m$  is mechanical torque,  $\omega_t$  is wind turbine speed;  $T_{sh}$  denotes shaft torque;  $H_t$  is inertia constant of wind turbine;  $D_t$  is damping coefficient of turbine;  $\theta_t$  is shaft twist angle,  $\omega_b$  is the base value of rotating speed;  $\omega_r$  is speed of rotor,  $H_g$  is inertia constant of generator,  $D_g$  is damping coefficient of generator,  $K_{sh}$  is the stiffness constant and  $D_{sh}$  is mutual damping of shaft.

Apart from the two-mass model, a lumped-mass model is also provided in [2]. Compared to the two-mass model, the lumped-mass model is simpler. Such model assumes that the shaft system is rigid enough [2]. In this model, the wind turbine inertia

and generator rotor inertia can be combined to acquire a single inertia constant  $H_L$ . The value of  $H_L$  can be computed by:

$$H_L = H_t + H_g \quad (3.10)$$

If the lumped-mass model is used, it is impossible to observe the torsion oscillation. In spite of this, the lumped-mass model can be used to establish a simplified wind turbine model, and thus some preliminary research results can be obtained.

### 3.1.3 Pitch Angle Control

As mentioned before, the power coefficient can be influenced by pitch angle and tip speed ratio. To maximize the power captured by blades, the pitch angle  $\beta$  is set to its optimal value  $\beta_{opt}$ . Usually, the optimal value of pitch angle is zero [2], [13].

If the wind speed becomes greater than rated value, the pitch angle will be varied to protect the wind turbine. Consequently, both the mechanical power and rotating speed can be limited. Although the extracted power is not optimized, the power output can be kept at the rated value [2].

To change the position of pitch angle, a pitch angle control system should be designed and implemented. A typical pitch angle controller described in [2] is presented as follows:

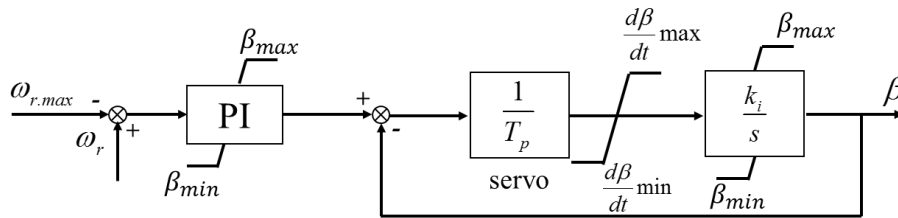


Figure 3.2 Pitch angle control system

In Figure 3.2,  $\omega_{r,max}$  is the upper limit of rotor speed.  $\beta_{max}$  is maximum value of pitch angle, while  $\beta_{min}$  denotes the lower bound of pitch angle.  $T_p$  and  $k_i$  represent the parameters used in the pitch angle control system.

### 3.1.4 Configurations of Variable Speed Wind Turbine

VSWTs can be divided into two categories: doubly fed induction generator based wind turbines (DFIG-WTs) and permanent magnet synchronous generator based wind turbines (PMSG-WTs). The configurations of individual DFIG-WT and PMSG-WT are different. The conceptual sketches of DFIG-WT and PMSG-WT are presented respectively:

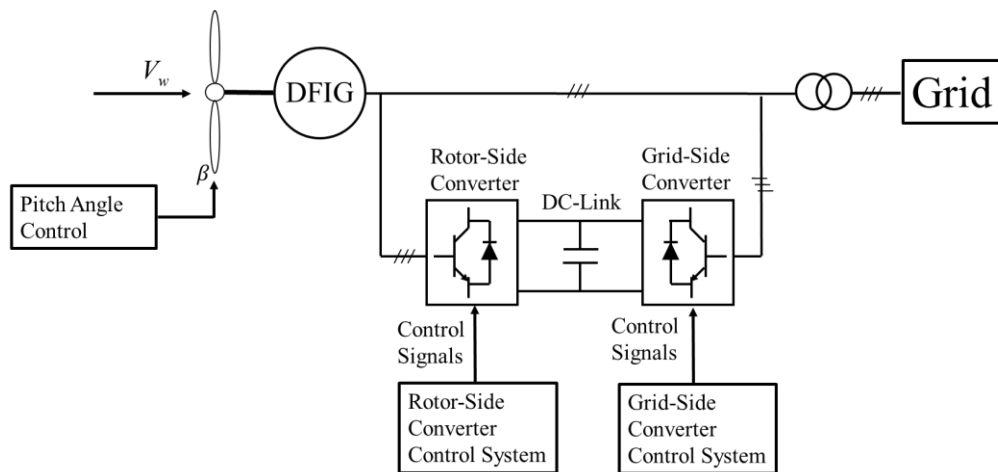


Figure 3.3 Conceptual sketch of individual DFIG-WT

Figure 3.3 shows the outline of individual DFIG-WT. As presented in this figure, the stator of DFIG-WT is connected to the power system directly. Besides, the connection between the rotor of induction generator and the power grid is achieved by using back-to-back converters [2]. Different from conventional synchronous generator, the rotor speed

of DFIG-WT is not required to be kept constant. To capture more power from wind, the rotor speed should be adjusted, and thus the rotor of the DFIG-WT may not operate at synchronous speed. It is important to note that the generator of the DFIG-WT should be excited by rotor-side converter (RSC) rather than DC source, for the frequency of the exciting current produced by the RSC can be variable. According to the information of rotor speed acquired in real-time, the RSC can adjust the frequency of the exciting current so that the electrical frequency produced by the DFIG-WT and the frequency of power grid can be the same value. Therefore, the DFIG-WT can realize sub-synchronous operation or super-synchronous operation. Considering that the slip of individual DFIG-WT is limited in practice, the rating power of each converter can be smaller than the rating power of the wind turbine.

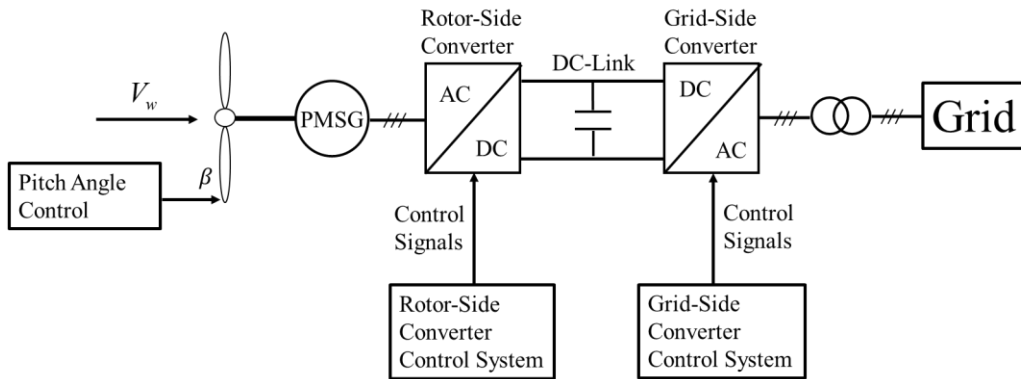


Figure 3.4 Conceptual sketch of individual PMSG-WT

Unlike the DFIG-WT, the stator of individual PMSG-WT is connected to the power system through back-to-back converters. Due to the application of permanent magnets, the rotor can be self-excited [36]. Therefore, the frequency of magnetic field is proportional to rotor speed [2]. It is noteworthy that each PMSG-WT should regulate rotor

speed in order to extract maximum power from wind. By using the RSC, the AC power produced by the generator in each PMSG-WT can be rectified to DC power. To deliver the power to the transmission network, it is necessary to install the grid-side converter (GSC) so that the DC power can be converted to AC power with rated frequency. Considering that all the power produced by the generator in the PMSG-WT can be injected to the converters, each converter and the PMSG-WT should have the same rated power. As a result, the cost of power electronic devices may increase.

## 3.2 Conventional Operation of Variable Speed Wind Turbine

### 3.2.1 Conventional Operation of VSWT under Normal Condition

Conventionally, MPPT control is performed by the RSC of each VSWT. The MPPT control is implemented when wind speed is lower than rated value and pitch angle is optimized [2]. If MPPT control is applied, the rotor speed can be adjusted so that the optimal TSR can be achieved, and the power maximization can be realized. To change the rotor speed for MPPT, the electrical torque or power should satisfy the following requirements where  $P_e$  represents the electrical power:

a) if  $\omega_r \leq \frac{\lambda_{opt} R}{V_w}$ , the wind turbine should accelerate and  $T_e \leq T_m$ ,  $P_e \leq P_m$

b) if  $\omega_r > \frac{\lambda_{opt} R}{V_w}$ , the wind turbine should decelerate and  $T_e > T_m$ ,  $P_e > P_m$

Based on Newton's laws of motion, the rotor speed can be varied by regulating the electrical torque or power properly. So far, optimal rotor speed control (ORSC) and optimal power control (OPC), both of which can be regarded as two typical MPPT

schemes, have been developed [37]. The two methods can provide setting principles of electrical power to realize MPPT control.

In ORSC, the reference of electrical power  $P_{e.ref}$  can be generated by rotor speed closed-loop controller [37]. Usually, a proportional-integral (PI) controller is applied in ORSC. The scheme of typical ORSC can be described as follows:

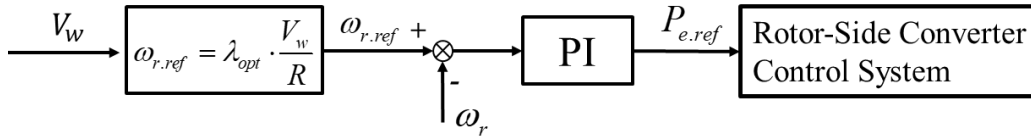


Figure 3.5 Schematic diagram of typical ORSC

In Figure 3.5,  $\omega_{r.ref}$  denotes the reference of rotor speed.  $\omega_r$  is the real value of the rotor speed. According to this figure, the  $\omega_{r.ref}$  is acquired by using  $V_w$  and  $\lambda_{opt}$ . Obviously, the information of wind speed may be required if the ORSC is implemented. Up to now, the light detecting and ranging (LIDAR) system has been designed in order to measure the wind speed accurately [38]. By using the LIDAR, the ORSC can be implemented in practice.

In addition, the  $\omega_{r.ref}$  can be produced by using other methods such as hill climb search (HCS) and rotor speed reference estimating (RSRE) [39], [40]. The HCS aims to track the optimal rotor speed by generating the  $\omega_{r.ref}$  step-by-step. If rotor speed is lower than its optimal value, the perturbation step should be set positive until the power captured by blades starts to reduce and vice versa [39]. The step size of the HCS should be set properly so that the wind turbine can reach the optimal operating point as soon as possible. If the step size is too large, even though the tracking speed of wind turbine can become

rapid, the oscillation of rotor speed may occur when the rotor speed is so closed to its optimal value [39], [41]. On the contrary, a smaller step size may lead to slower tracking speed [39], [41]. As a result, the wind turbine may spend too much time in tracking the optimal rotor speed, and thus less power may be extracted in practice. In order to track the optimal rotor speed efficiently without oscillating, a HCS algorithm with variable step size is designed in [41]. That paper suggests that a large step size can be used if the rotor speed is relatively far from its optimal value. As the wind turbine approaches to the optimal operating point, the step size should become smaller accordingly [41]. In this way, the efficiency of the HCS based ORSC can be ensured and the oscillation can be avoided.

The methodology of RSRE based ORSC is to estimate the reference of rotor speed by using the information of wind turbine operation such as mechanical torque [39], [40]. According to these information, the wind speed or the optimal rotor speed reference can be estimated by using artificial-intelligence techniques [39], [40]. However, the efficiency of RSRE based ORSC should be investigated further.

The control principle of OPC is based on the optimum power curve of VSWT. Figure 3.6 presents the typical power characteristics of the VSWT described in [34]. In this figure,  $\omega_{r.min}$  is the lower limit of rotor speed, while the maximum rotor speed is denoted by  $\omega_{r.max}$ .  $P_{rate}$  is the rated power of the wind turbine. The blue curves represent the extracted power under different wind speeds. The red curve, which is the optimum power curve, is formed from the operating points with maximum power under each wind speed. By analyzing the data, we can learn that the optimum power can be proportional to the cube of rotor speed.

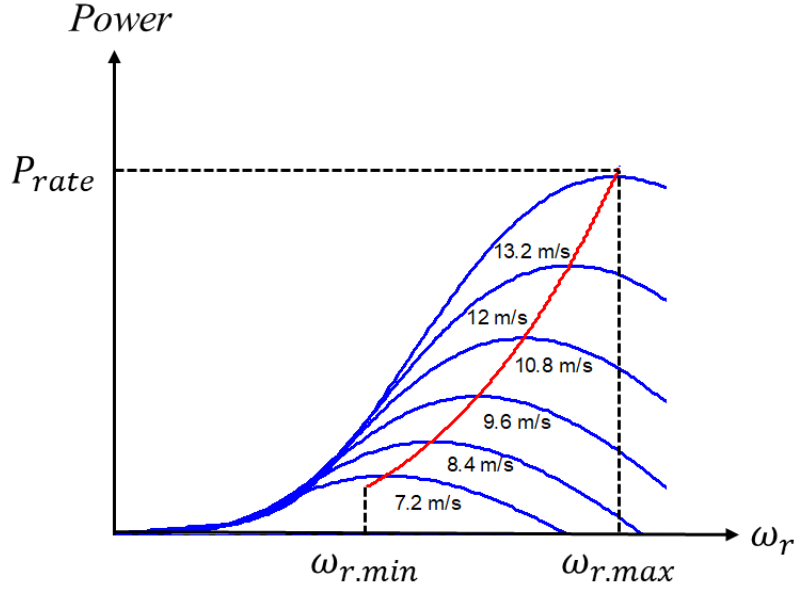


Figure 3.6 Typical power characteristics of VSWT

Based on the optimum power curve, the control law of OPC can be acquired. Such control law can be expressed by equation (3.11) or Figure 3.7. In this figure,  $K_{opt}$  is a constant which can be computed by (3.12).

$$P_{e.ref} = K_{opt} \cdot \omega_r^3 \quad (3.11)$$

$$K_{opt} = 0.5 \rho \pi R^5 \frac{C_p^{max}}{\lambda_{opt}^3} \quad (3.12)$$

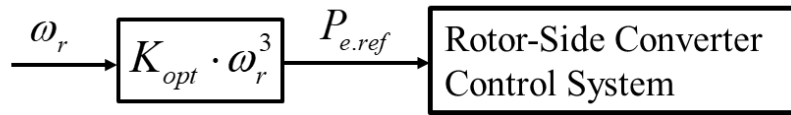


Figure 3.7 Schematic diagram of OPC

If the  $P_{e.ref}$  is generated by (3.11), the active power produced by the VSWT can automatically satisfy the MPPT control requirements mentioned above, and thus the MPPT control can be realized [37]. The OPC relies on the characteristics of each VSWT,

and no wind speed information is required. Compared to ORSC, no rotor speed closed-loop controller is included and the tracking speed of OPC is slower, but the active power produced by OPC can be smoother due to the existence of wind turbine inertia [42], [43].

The investigation of OPC performance has been provided in [42]. The analysis in that article reveals that the tracking speed of OPC can become smaller if the rotor speed is so close to its optimal value. To improve the efficiency of OPC, an improved OPC (IOPC) algorithm with constant bandwidth has been designed in [42]. The IOPC algorithm can be described as follows:

$$P_{e.ref}^{IOPC} = K_{opt} \cdot \omega_r^3 - k_f (P_m - k_{opt} \cdot \omega_r^3) \quad (3.13)$$

$P_{e.ref}^{IOPC}$  is the power signal generated by IOPC. Compared to conventional OPC, a feedforward item with a coefficient  $k_f$  is introduced. As a result, the tracking speed of IOPC can become higher and the extracted energy can increase. The method to determine the value of  $k_f$  is also provided in [42].

The GSC of each VSWT is used to stabilize the DC-link voltage [2]. By keeping the DC-link voltage stable, the active power generated by RSC can be sent to transmission network. The regulation of DC-link voltage can be attained by using the DC-link voltage controller, which is depicted as follows:

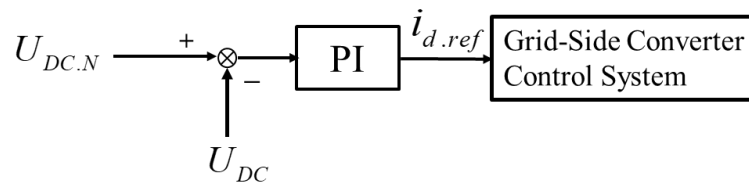


Figure 3.8 DC-link voltage control in GSC

In this figure,  $U_{DC.N}$  represents the normal value of DC-link voltage and  $U_{DC}$  is the DC-link voltage measured in real-time.  $i_{d.ref}$  denotes the reference of current component in d-axis. It is noteworthy that vector control technique is usually applied in GSC. The current component in d-axis  $i_d$  is commonly employed to adjust active power output, while the current component in q-axis is used to change reactive power. By controlling the value of  $i_{d.ref}$ , the active power passing through the GSC can be regulated, and thus the stabilization of DC-link voltage can be achieved.

### **3.2.2 Inner-loop Control Techniques Applied in Power Converters of VSWT**

The operation of the RSC and GSC in each VSWT can be realized by controlling Insulated Gate Bipolar Transistor (IGBT)-switches [2]. To regulate the active power and reactive power independently, direct control technique using switching tables or the vector control technique using PI controllers can be implemented in each power converter [36], [44]. Both of the two control techniques are developed from the control methods applied in induction motor [44]. The comparative analysis of the two control techniques has been provided in [45], [46]. According to the comparison presented in these articles, the dynamic response of direct control technique is faster. Moreover, the direct control technique is more robust than the vector control technique [45], [46]. In order to maintain the stability of the wind turbine control system, the parameters in vector control scheme should be tuned in practice. However, the hysteresis controllers involved in the direct control technique can cause significant power ripple, and thus the power quality may become worse [45], [46]. In [46], a control scheme combining the two techniques is

proposed. Such control scheme is named as combined vector and direct power control (CVDPC). The CVDPC has the advantages of the two control techniques. The simulation study proves that by using the CVDPC, the control performance can be improved and power ripple can become acceptable [46].

Apart from the specifications discussed in Chapter 2, TSOs also require that each WPP should fulfill the technical requirements on power quality. The studies in [47-49] provide different schemes to improve the power quality. Reference [47] proposes that the LCL filter can be used to mitigate the distortion caused by harmonics. A method to design the LCL filter is also discussed in that paper. Besides, a repetitive control technique is developed in [48]. The case study in [48] shows that the power quality can become better by using such control approach.

### **3.2.3 Operation of VSWT under Grid Faults**

As mentioned in Chapter 2, the penetration level of wind energy was relatively low in the past. At that time, the self-disconnection of wind turbines was allowed under a grid fault. Since the capacity of wind power experiences continuous increase during recent years, the grid codes specified by TSOs have demanded that the wind turbines should have the ability to keep connecting to the power system and inject reactive current if a grid fault occurs. Such requirements can be summarized by the term “low voltage ride through (LVRT)”. The regulations of LVRT in grid codes are presented in Chapter 2.

For the conventional synchronous generator, the voltage dip caused by short-circuit can lead to overcurrent in rotor and stator. For VSWTs, it is essential to investigate the

impacts of such grid faults on these wind turbines so that the control strategies of LVRT can be developed accordingly.

The influence of voltage sags on DFIG-WT has been studied in some papers [50-53]. These papers provide theoretical analysis of DFIG-WT performance under grid faults. According to these articles, the electromotive force (EMF) induced by stator flux linkage is proportional to the slip of each DFIG-WT [53]. Considering that the typical range of slip is from -0.3 to +0.3, the EMF is relatively small under normal condition [53]. If a grid fault arises, a DC current component will appear and a large EMF will occur [53]. The EMF with large magnitude can cause the overcurrent to act on the rotor circuit. Besides, the RSC can hardly provide an additional voltage component to attenuate the current magnitude, because the capability of RSC is limited [53]. As a result, the devices in RSC may be damaged by such overcurrent and thus the DFIG-WT may disconnect itself from the power grid to protect the devices [53]. Moreover, as the energy flows into the DC capacitor continuously, the DC-link voltage can become so high that the chopper protection will be activated [53].

The wind turbines could be self-disconnected in the past years, for the wind power capacity was relatively low and the impacts of wind turbines on power system could be neglected. However, the grid codes issued recently requires that the WPPs should act according to the LVRT regulation during a grid fault. More specifically, the WPPs should provide system support to avoid voltage collapse.

To satisfy the requirements specified by TSOs, some LVRT control methods should be designed and implemented. Considering that the grid faults may destroy the power

electronics devices installed in converters, the LVRT control strategies should protect the devices from damaging. Besides, the LVRT control schemes should enable wind turbines to provide reactive current in order to enhance system voltage stability.

So far, several LVRT control strategies have been proposed [13], [14], [53]. These control methods can be divided into four groups: crowbar protection, the demagnetizing method, limiting active power output and comprehensive LVRT control.

Conventionally, crowbar protection can be regarded as the most popular scheme to realize LVRT [53]. Considering that the rotor circuits will suffer overcurrent after a grid fault occurs, the crowbar circuits can be installed in each DFIG-WT. If the voltage of power grid dips, the crowbar protection will be activated, and the rotor can be short-circuited [2], [53]. In this way, the overcurrent will pass through the crowbar circuits rather than the RSC. It is noteworthy that the RSC can become uncontrollable if the crowbar protection is triggered and thus the wind turbine behaves as a conventional induction generator [53]. As a result, even though the damage to the devices in RSC can be avoided, the wind turbine can absorb reactive power from transmission network and the condition of power system may deteriorate. Besides, the cost of each wind turbine will increase, because additional hardware is necessary [53].

According to the studies in [52] and [53], the EMF which is caused by the negative sequence and DC components of stator flux linkage can lead to overcurrent. Based on this analysis, some demagnetizing methods are designed. The demagnetizing methods aim to alleviate the overcurrent as soon as possible by cancelling the transient components instead of short-circuiting the rotor [53-55]. In [54], a flux weakening control algorithm

is proposed. This control strategy can deal with the transient flux by controlling the rotor current, and thus the overcurrent caused by the fault can be mitigated [53]. However, the stator flux linkage estimation is of vital importance for the application of the flux weakening control [53]. Additionally, armed with such control strategy, the torque oscillation in each DFIG-WT can be very significant [53]. To overcome these drawbacks, a flux-linkage-tracking based LVRT method is put forward in [53]. By using this method, the rotor flux linkage should be adjusted according to the stator flux linkage during the grid fault. The case study shows that the overcurrent in rotor circuits can be alleviated and the torque oscillation can be relatively small [53].

Moreover, a simple LVRT control approach realized by changing the active power reference is discussed in [13]. According to the description in that article, the reference of active power or electrical torque can be set to zero if a grid fault is detected. Consequently, no active power is generated, and thus the magnitude of rotor current can become smaller.

The LVRT control schemes mentioned above aim at protecting the devices in individual DFIG-WT from destroying. However, the reactive current support which is required by modern grid codes is not considered. Recently, some comprehensive LVRT control strategies are developed [14], [55]. Reference [14] suggests that the active power output should be proportional to the magnitude of grid voltage. Consequently, if the grid voltage dips, the active power generated by the DFIG-WT can decrease accordingly and overcurrent in rotor can be avoided. In [55], a virtual damping flux-based control scheme is recommended. By using this method, the transient flux can decay rapidly, and thus the overcurrent in rotor can be alleviated. Besides, the electromagnetic torque can be

smoothed. Apart from the schemes aiming at protecting the devices in wind turbine, the strategies enabling the DFIG-WT to provide reactive power are also introduced in [14] and [55]. In each DFIG-WT, the RSC can generate reactive power by setting relevant control signals properly [55]. In addition, a cascading reactive power control scheme is presented in [2] and [14]. This control method coordinates the RSC and GSC installed in each DFIG-WT. Hence, the two converters can both contribute to reactive power support so that the voltage stability can be enhanced.

As mentioned before, the DC-link voltage in each DFIG-WT may rise dramatically if a grid fault occurs. The overvoltage of DC-link may damage the DC capacitors installed between the RSC and GSC. In order to protect the DC capacitors, a chopper protection method is usually applied. If the DC-link voltage is so high, the chopper protection will be activated. Hence, surplus active power can be consumed by the chopper circuits. Considering that power imbalance results in the rise of DC-link voltage, an improved DC-link voltage control method is discussed in [13] and [14]. In this method, a compensating item which reflects the variation of the power flowing into the DC capacitors is inserted into the GSC control system [13], [14], [56]. In this way, the power released by RSC can be injected into the power grid more quickly, and thus the DC-link voltage can be regulated [13], [14], [56].

Different from DFIG-WT, the generator of each PMSG-WT is not connected to the transmission network directly. As presented in Figure 3.4, the power produced by the PMSG-WT should flow into the RSC so that the AC power can be converted to DC power. By using GSC, the DC power can be transformed to AC power with rated frequency. Such

AC power can be delivered to the power system through the GSC. Consequently, even though a grid fault arises, the flux in generator side will not be influenced and the overcurrent will not be induced. However, due to the grid fault, less power can be absorbed by the power system. If the power generated by RSC is not limited, the surplus power will flow into the DC capacitor and charge it. Consequently, the DC-link voltage will increase rapidly. The overvoltage acting on the DC capacitor may interrupt the operation of the converters or even damage the devices [2]. In that case, the LVRT requirements cannot be satisfied.

To ensure the continuous operation of the two converters in the event of the grid fault, the installation of braking chopper is recommended in past years [2]. Like the chopper circuits applied in DFIG-WTs, the braking chopper in PMSG-WT will be activated on condition that the DC-link voltage exceeds the upper limit. In this way, the surplus active power can be dissipated by the chopper circuits [2].

References [57] and [58] propose that the power generated by RSC should be reduced if a voltage dip is detected. Based on this idea, some control schemes have been designed. Under normal condition, the MPPT control is implemented in RSC, whereas the active power reference in RSC should be constrained according to the magnitude of residual voltage when a grid fault occurs [57]. It should be noted that if the residual voltage is too low, little active power can be consumed by power system. In that case, even though the generated power is decreased, the excessive energy which has been stored in the DC capacitor cannot be consumed without chopper. To solve this problem, reference [58] introduces a control strategy arranging the RSC to participate in the DC-

link voltage stabilization during the grid fault. If this control method is implemented, the surplus active power can be stored as kinetic energy by adjusting rotor speed, and thus the power mismatch can be alleviated [58]. The case study in that article shows that by using this approach, the DC-link voltage can be maintained within normal range, and thus the activation of chopper may not be necessary [58].

In [58], not only a method to stabilize DC-link voltage is discussed, but a scheme for reactive power support is involved as well. In normal operation, the active power is controlled by the DC-link voltage controller. During a voltage sag, both the active power reference and reactive power reference in GSC should be given according to the technical requirements defined by TSOs [58]. In that case, the GSC can operate as a static synchronous compensator (STATCOM) and thus provide reactive power support for system voltage stability [58].

#### **3.2.4 Operation of VSWT Considering Material Fatigue**

Nowadays, it is necessary to install gearboxes in individual VSWT. Usually, it is expected that the gearboxes in each VSWT can be used for 20 years. However, the gearboxes should be replaced every 6-8 years in practice, for the torque vibration can act on gearbox-based drive train system [59]. Consequently, the cost for operation and maintenance can increase significantly [59].

In order to extend the lifetime of these gearboxes, various control methods aiming at damping the torsional vibration have been discussed [59]. In conventional electric drive system, the torsional oscillation is caused by the connection between the electric motor

and a mechanical load [59]. Such vibration can be damped by using motor torque control [59]. Inspired by this, the active vibration damping scheme can be included in the generator torque control algorithm of each VSWT [59]. The control strategy designed in [59] is based on a bandpass filter (BPF). Considering that the performance of BPF based control strategy can be affected by the uncertainty of parameters, a model based torsional damping controller is developed in [60]. Reference [61] put forward an indirect torque control method using STATCOM. In this method, the transient torque can be smoothed by regulating reactive current, and thus the torsional vibration can be alleviated [61]. Particularly, an active torsional vibration damping control method for PMSG-WTs is designed in [62]. This approach makes use of a speed feedback loop compensating the variation of rotor speed so that the torsional vibration damping action can be performed [62]. In addition, the impact of pitch angle on the dynamics of drive train is studied in [63]. That article also provides a control approach using the information of rotating speed for torsional vibration damping [63].

For individual VSWT, the active power control should not only enable each wind turbine to acquire maximum power from wind, but also reduce mechanical effort acting on the drive train system, especially in the event of gust wind. To satisfy the two control objectives, a power smoothing control algorithm for VSWTs is described in the following section.

### **3.3 Power Smoothing Control of Variable Speed Wind Turbine**

### 3.3.1 Introduction

In the last decade, the integration level of wind energy has increased continuously. It is expected that more power consumption can be satisfied by the wind power, and the carbon dioxide emission can be limited. However, the power system management can be affected by the wind energy [8], [31]. To deal with the technical challenges imposed by the wind power, WPPs should fulfill the technical requirements defined by TSOs [8].

Recently, VSWTs are commonly used in WPPs [44]. Different from the FSWT, each VSWT can adjust its turbine speed by applying maximum power point tracking (MPPT) control so that the power captured from wind can be maximized.

So far, the optimal rotor speed control (ORSC) strategy and the optimal power control (OPC) strategy have been proposed to realize MPPT control [37], [40], [44]. If the OPC is applied in the VSWT, the power provided by the wind turbine can be smooth, but the efficiency of power extraction is relatively low [42]. However, the ORSC based MPPT can track the optimal speed more quickly, and thus more power can be obtained by the wind turbine.

It is noteworthy that if the ORSC based MPPT is implemented in each VSWT, the fluctuation of the power generated by the wind turbine can be observed. Such power fluctuation may become significant on condition that wind speed changes rapidly [25]. Furthermore, the power fluctuation may deteriorate if the extreme operating gust (EOG), which has been specified by International Electrotechnical Commission (IEC), appears [64-66]. The fluctuation of the power produced by wind turbines may lead to the mismatch between power generation and demand. If the inertia constant of the isolated power

system is too small, the power imbalance may result in system frequency deviation [67]. Moreover, if the EOG occurs, the generator torque will change rapidly, and thus the shaft torque of the VSWT will oscillate. Consequently, the lifetime of gearbox can hardly be maintained [60]. In order to mitigate such negative impacts and limit maintenance cost, it is necessary to alleviate the power fluctuation caused by the EOG.

Up to now, various control schemes for power smoothing have been proposed [24]. The usage of the energy storage systems including flywheel, capacitor bank and battery has been discussed in [68-70]. However, if these devices are installed in WPPs, the investment can increase significantly [24]. The methods exploiting the potential capability of individual VSWT for power smoothing are developed in [25], [71], [72]. These articles suggest that the power smoothing control can be achieved by regulating rotor speed, DC-link voltage and pitch angle. In addition, reference [67] proposes an active power control scheme based on the risk evaluation of frequency excursion. According to the description in [67], the power generated by the wind turbine can be smoothed by setting the rotor speed reference properly. The strategies mentioned above are intended to attenuate the power fluctuation, but the typical condition of EOG is not taken into account [65], [66].

This section provides an active power control scheme aiming at alleviating the power fluctuation during the EOG. Furthermore, a power smoothing controller based on direct torque control is proposed. Moreover, a detection module is included so that the power smoothing control can be activated in time. The simulation study can demonstrate that the proposed control scheme is effective. In addition, the results show that the shaft torque in

drive train can become smoother by applying the proposed method, and thus the negative effects on the gearbox used in the VSWT could be mitigated to some extent [73].

### 3.3.2 Modelling of DFIG-WTs for Study

#### A. Model of Wind Turbine

In this research, a DFIG-WT model, which is based on the description in [13], is built up for study.

The wind turbine aerodynamics indicates that the mechanical power  $P_m$  and the mechanical torque  $T_m$  acting on the DFIG-WT can be expressed by (3.14) and (3.15):

$$P_m = 0.5C_p \rho \pi R^2 V_w^3 \quad (3.14)$$

$$T_m = \frac{0.5C_p \rho \pi R^3 V_w^2}{\lambda} \quad (3.15)$$

where  $C_p$  is power coefficient,  $\rho$  is the air density,  $R$  is the radius of the wind turbine,  $V_w$  is wind speed,  $\lambda$  is tip speed ratio,  $\beta$  is pitch angle [25]. The following equations show the calculation of  $C_p$  [13], [25]:

$$C_p = 0.22 \left( \frac{116}{\gamma} - 0.4\beta - 5 \right) e^{-\frac{12.5}{\gamma}} \quad (3.16)$$

$$\gamma = \frac{1}{\frac{1}{\lambda + 0.08\beta} - \frac{0.035}{\beta^3 + 1}} \quad (3.17)$$

The pitch angle can be fixed (usually  $\beta=0$ ) if wind speed is below the rated value, and thus MPPT control can be realized. The pitch angle will be adjusted on condition that the

wind speed is greater than the rated value so that the power output and turbine speed can be limited [2], [13].

As mentioned in 3.1.2, a two-mass model can be adopted to describe the performance of the drive train system [2], [35]. The study in [2] shows that the two-mass model can be described as below:

$$\frac{d\omega_t}{dt} = \frac{1}{2H_t} (T_m - T_{sh} - D_t \omega_t) \quad (3.18)$$

$$\frac{d\theta_t}{dt} = \omega_b (\omega_t - \omega_r) \quad (3.19)$$

$$\frac{d\omega_r}{dt} = \frac{1}{2H_g} (T_{sh} - T_e - D_g \omega_r) \quad (3.20)$$

$$T_{sh} = K_{sh} \theta_t + D_{sh} \omega_b (\omega_t - \omega_r) \quad (3.21)$$

$$T_e = L_m (i_{qs} i_{dr} - i_{ds} i_{qr}) \quad (3.22)$$

where  $\omega_t$  is turbine speed,  $H_t$  and  $H_g$  are the inertia constants of turbine and generator, respectively.  $T_{sh}$  is shaft torque,  $T_e$  is generator torque.  $D_t$ ,  $D_g$  and  $D_{sh}$  are the damping coefficients of the turbine, rotor and shaft, respectively.  $K_{sh}$  is stiffness of the shaft system.  $\theta_t$  is shaft twist angle.  $\omega_b$  is base speed,  $\omega_r$  is rotor speed [2].  $L_m$  is mutual inductance.  $i_{qs}$  and  $i_{ds}$  are the d-q components of stator current.  $i_{dr}$  and  $i_{qr}$  are the d-q components of rotor current [2], [13].

## B. Model of Converters

In each DFIG-WT, the MPPT control is usually realized by rotor-side converter (RSC), and the DC-link voltage regulation is commonly performed by grid-side converter (GSC) [2], [13].

The control scheme of RSC described in [13] and [14] is displayed in Figure 3.9, where  $\omega_{r.ref}$  is the rotor speed reference and  $\omega_r$  is the actual value measured in real-time.

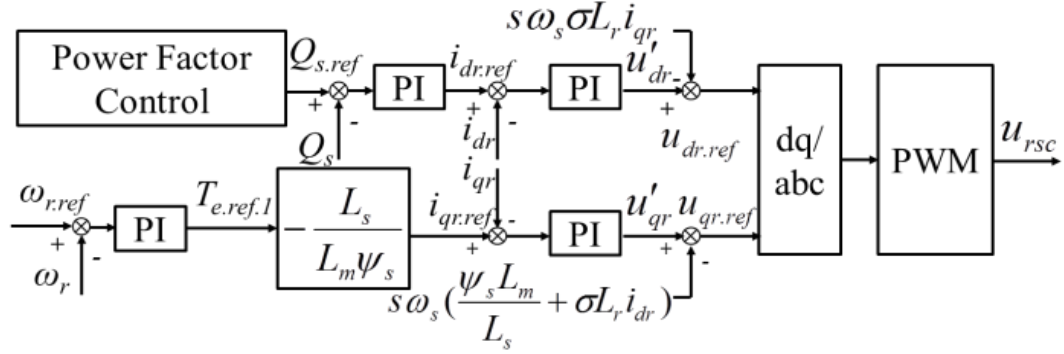


Figure 3.9 Control technique used in RSC

A typical ORSC based MPPT control method is applied herein. The rotor speed reference  $\omega_{r.ref}$  can be derived from the following equations [13], [37]:

$$\omega_{r.ref} = \sqrt{\frac{T_m}{K_{opt}}} \quad (3.23)$$

$$K_{opt} = \frac{\rho \pi R^5 C_p^{max}}{2 \cdot \lambda_{opt}^3} \quad (3.24)$$

where  $K_{opt}$  is the optimal constant,  $C_p^{max}$  is the maximum power coefficient and  $\lambda_{opt}$  is corresponding tip speed ratio. According to the error between  $\omega_{r.ref}$  and  $\omega_r$ , the electrical torque reference  $T_{e.ref.1}$  can be produced by the PI controller [13], [37].

### 3.3.3 The Proposed Power Smoothing Control Scheme

#### A. Power Smoothing Control Scheme

The power smoothing control (PSC) will be activated on detecting the EOG. In this study, three objectives should be attained by applying the PSC: 1) to attenuate the power

fluctuation, 2) to extract the power from wind as much as possible, 3) to switch back to MPPT control if the EOG terminates. Consequently, the electrical torque reference  $T_{e.ref.2}$  to realize PSC can be set as:

$$T_{e.ref.2} = \left( \frac{\omega_r}{\omega_{r.ref}} \right)^b \cdot T_m \quad (3.25)$$

which is similar to the OPC based MPPT proposed in [37]. In this equation,  $b$  is a parameter.

In this wind turbine model, the normal interval of rotor speed is between 0.7 p.u. and 1.1 p.u. Therefore, the value of  $b$  can be determined as Table 3.1 shows [13], [14]. As shown in this table, if wind speed is too high or too low, the  $\omega_{r.ref}$  may not lie in the normal range. In that case, the value of  $b$  should be set to zero, and thus the electrical torque will be equal to the mechanical torque. In this way, the rotor speed of the wind turbine can be kept constant so that the wind turbine can be protected to some extent.

Table 3.1 The value of  $b$

rotor speed condition	the value of $b$
$\omega_r = 0.7 \text{ p.u.} \&\& \omega_{r.ref} < 0.7 \text{ p.u.}$	0
Else	$> 0$
$\omega_r = 1.1 \text{ p.u.} \&\& \omega_{r.ref} > 1.1 \text{ p.u.}$	0

As EOG terminates, the difference between  $\omega_{r.ref}$  and  $\omega_r$  can be so small that  $T_{e.ref.2}$  approximates to  $T_m$ . However, the error between  $T_{e.ref.2}$  and  $T_{e.ref.1}$  can be significant. As a result, as the EOG disappears, power may change suddenly if electrical torque reference switches from  $T_{e.ref.2}$  to  $T_{e.ref.1}$  instantaneously. Such step change can

be avoided by applying a torque gradient limiter (TGL). The upper limit of TGL is set as 0.5 p.u./s in this research. Besides, because the acceleration of the DFIG-WT should be enlarged properly to eliminate the difference between  $\omega_{r.ref}$  and  $\omega_r$  more rapidly, a power error control (PEC) can be utilized when necessary. If  $|(T_{e.ref.1} - T_{e.ref.2}) \cdot \omega_r|$ , which is named as power error in this section, exceeds the bound  $\varepsilon_1$ , the PSC should be replaced by PEC. Moreover, the electrical torque reference to realize PEC  $T_{e.ref.3}$  and the switch conditions are listed as below:

if  $(T_{e.ref.1} - T_{e.ref.2}) \cdot \omega_r > \varepsilon_1$ ,

$$T_{e.ref.3} = k_1 \cdot T_m \quad (3.26)$$

if  $(T_{e.ref.1} - T_{e.ref.2}) \cdot \omega_r < -\varepsilon_1$ ,

$$T_{e.ref.3} = k_2 \cdot T_m \quad (3.27)$$

Assuming that the maximum active power of the DFIG-WT is denoted by  $P_{e.max}$ ,  $T_{e.ref.1}$ ,  $T_{e.ref.2}$  and  $T_{e.ref.3}$  cannot exceed  $P_{e.max}/\omega_r$  so that the devices installed in converters can be protected [74].

According to the description mentioned before, the proposed power smoothing control scheme under EOG is presented in Figure 3.10. The figure shows that the ORSC based MPPT technique is applied under normal condition. If the EOG appears, the MPPT control should be replaced by the power smoothing control.

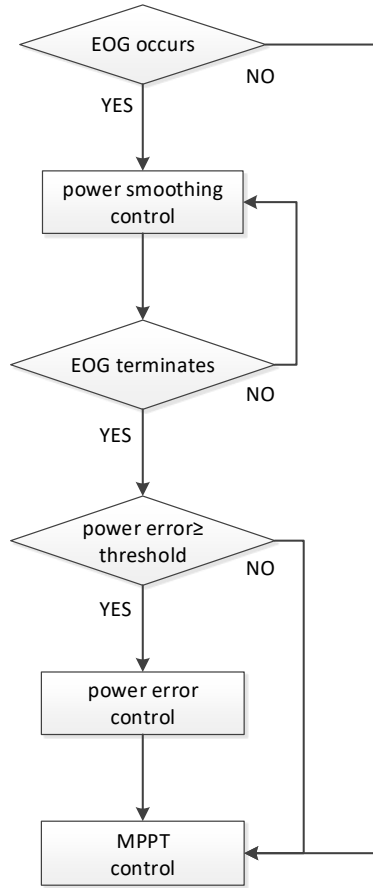


Figure 3.10 The flowchart of the proposed PSC scheme

### B. Module for EOG Detection

To detect the EOG accurately,  $\left| \frac{d\omega_{r.ref}}{dt} \right|$  and  $|\omega_{r.ref} - \omega_r|$  are employed to sense wind condition. In addition, the performance of power produced by wind turbine is evaluated by  $|\omega_{r.ref} - \omega_r|$ ,  $\left| \frac{d(\omega_r \cdot T_{e.ref.1})}{dt} \right|$  and the power error  $|(T_{e.ref.1} - T_{e.ref.2}) \cdot \omega_r|$  [41].

Table 3.2 The switch conditions for EOG detection

wind condition	power performance	events
$\left  \frac{d\omega_{r.ref}}{dt} \right  \leq \varepsilon_2$ && $ \omega_{r.ref} - \omega_r  \leq \varepsilon_3$	$\left  \frac{d(\omega_r \cdot T_{e.ref.1})}{dt} \right  \geq \varepsilon_4$    $ \omega_{ref} - \omega_r  \geq \varepsilon_5$    power error $\geq \varepsilon_1$	/
1	0	EOG does not occur; MPPT is applied all the time
0	1	EOG occurs; MPPT switches to PSC
1	1	EOG terminates; PSC switches to PEC
1	0	EOG terminates; PSC/PEC switches to MPPT

The switching conditions and the corresponding events recognized by the EOG detection module are listed in Table 3.2.  $\varepsilon_1$ - $\varepsilon_5$  denote the thresholds. In this study, the values of the thresholds can be obtained by using trial and error method.

The logic value of wind condition will be 1 if wind speed changes slowly. In that case, the power generated by the wind turbine will become smooth, and thus the logic value of power performance will be 0. When the EOG is detected, the logic value of wind condition will be 0 and the logic value of power performance will be 1 accordingly. As a result, the PSC should be activated.

As the EOG disappears, the logic value of wind condition will become 1. In spite of this, the power error may still be very large, and thus the logic value of power performance

is still 1. In that case, power error should be compared to  $\varepsilon_1$  to determine that whether PEC should be activated.

### 3.3.4 Simulation Results

The test system for simulation study is shown in Figure 3.11 [13], [14]. Such system is established under Matlab/Simulink environment [13], [14]. The parameters of the DFIG-WT used in this research have been provided in Appendix [13], [14]. Besides, according to IEC-61400, the typical EOG profile can be acquired [64-66].

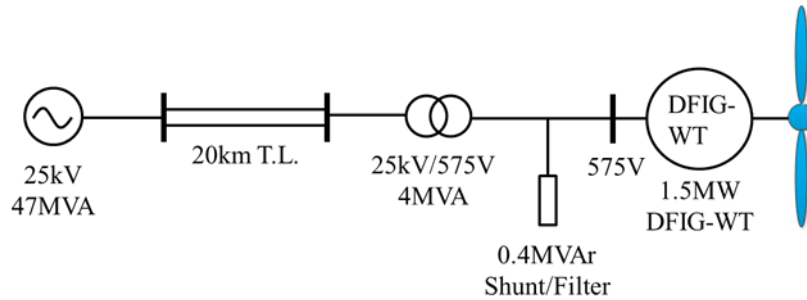


Figure 3.11 The system model for simulation

In this section, the performance of electrical torque and the behaviour of active power are emphasized. The effect of pitch angle is not considered. In addition, the DFIG-WT maintains unity power factor in this simulation [2], [13].

The thresholds  $\varepsilon_1$ - $\varepsilon_5$  in Table 3.3 and the value of TGL should be set properly so as to detect EOG successfully. Besides, the value of  $b$  in (3.25) should be selected appropriately so that an acceptable tradeoff between power smoothing and energy harvesting can be achieved. TGL can be set as  $\varepsilon_4$ . Besides, both the  $k_1$  in (3.26) and the  $k_2$  in (3.27) are necessary to be close to 1, and thus the error between  $\omega_{r.ref}$  and  $\omega_r$  can

be eliminated as soon as possible. In this section, all the parameters are determined by using trial and error approach. Table 3.3 provides the values of these parameters used in this simulation.

Figure 3.12 depicts the EOG profile in this study. This section considers the EOG with the recurrence period of one year [64-66]. As shown in Figure 3.12, the EOG in this simulation appears at 7 second and disappears at 17.5 second. Figure 3.13-Figure 3.15 provide the simulation results during the EOG.

As Figure 3.13 shows, by applying the detection module with the selected parameters, the PSC can be triggered within 2 seconds after the EOG occurs. Moreover, the PSC can be replaced by the PEC or MPPT after the EOG terminates.

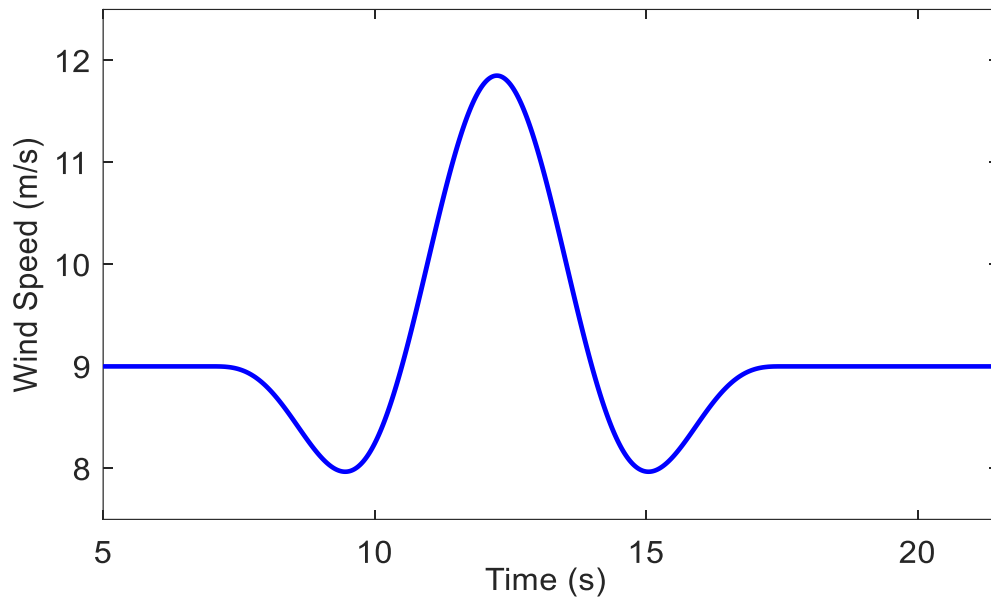


Figure 3.12 The EOG profile used in case study

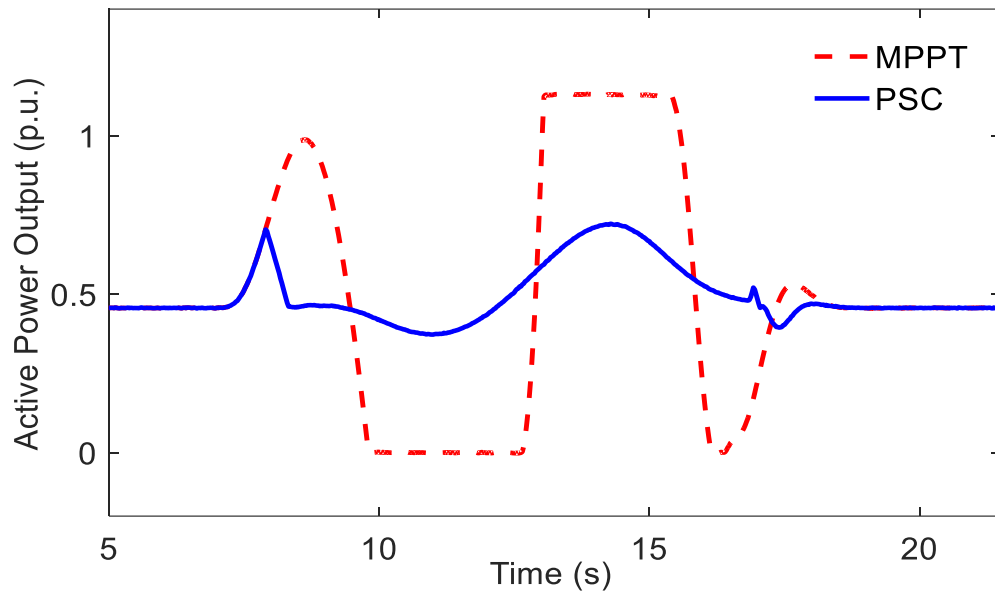


Figure 3.13 The variation of active power produced by the DFIG-WT under EOG

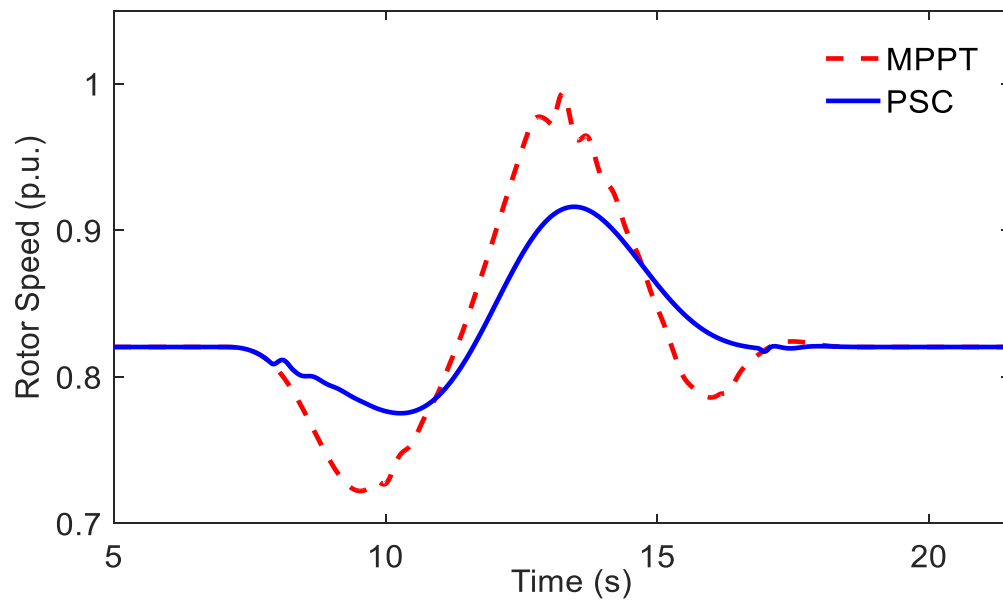


Figure 3.14 The rotor speed variation under EOG

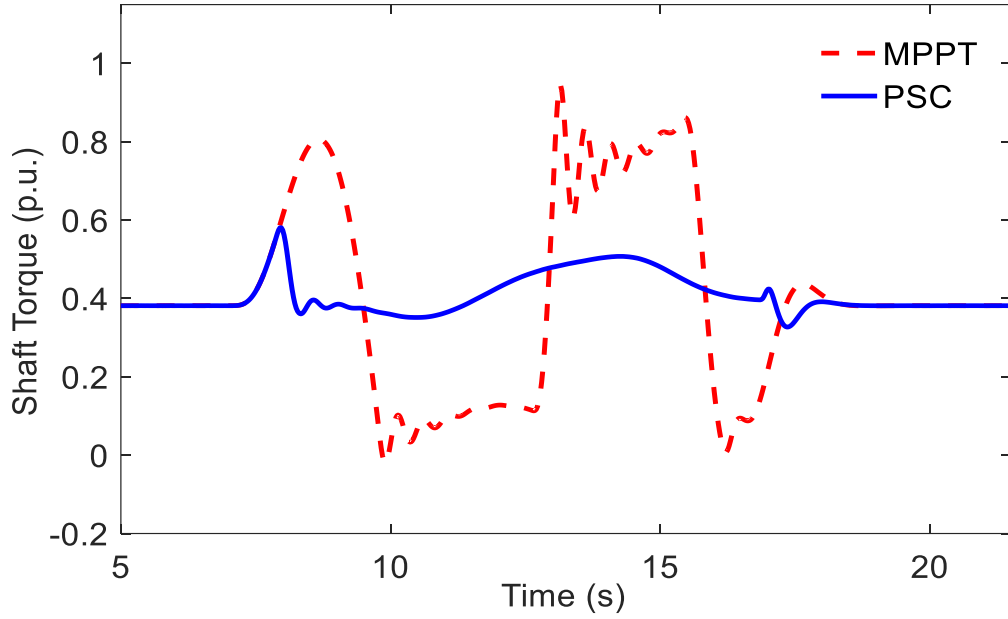


Figure 3.15 The shaft torque variation under EOG

Table 3.3 The setting of parameters

$\varepsilon_1$	$\varepsilon_2$	$\varepsilon_3$	$\varepsilon_4$	TGL	$\varepsilon_5$	b	$k_1$	$k_2$
0.25 p.u.	0.05 p.u./s	0.05 p.u.	0.5 p.u./s	0.5 p.u./s	0.1 p.u.	2.5	1.1	0.9

To assess the performance of the power produced by the DFIG-WT, the functions listed below can be considered [72]:

$$E_e = \int_{t_1}^{t_2} P_g(t) dt \quad (3.28)$$

$$P_{level} = \int_{t_1}^{t_2} \left| \frac{dP_g(t)}{dt} \right| dt \quad (3.29)$$

where  $E_e$  is the electrical energy produced by the DFIG-WT during the period  $[t_1, t_2]$ ,  $P_g(t)$  is the active power generated by the wind turbine.  $P_{level}$  is the function to evaluate

power fluctuation. The smaller  $P_{level}$  means that the power produced by the DFIG-WT is smoother [72].

As Figure 3.13 depicts, it can be learned that the fluctuation of power curve acquired from the MPPT based on ORSC is more significant, while the power curve acquired from the proposed PSC scheme is much smoother, for the variation of electrical torque is gradual. Furthermore, the  $P_{level}$  of proposed PSC scheme decreases to 34.58%.

Besides, the total energy extracted by the DFIG-WT  $E_w$  can be obtained by using (3.30):

$$E_w - E_e = \frac{1}{2} J_g [\omega_r(t_2)^2 - \omega_r(t_1)^2] \quad (3.30)$$

where  $E_w$  is the total energy captured from the wind,  $J_g$  is the total inertia of the wind turbine,  $\omega_r$  is the rotor speed [14]. It is noteworthy that the friction losses of the DFIG-WT are neglected in this study [14].

The  $E_e$  of MPPT based on ORSC and the  $E_e$  of PSC can be acquired from (3.28). In addition, the  $E_w$  of ORSC based MPPT and the  $E_w$  of PSC can be obtained by applying (3.30). Besides, the energy loss of PSC can be acquired if the  $E_w$  of ORSC based MPPT and the  $E_w$  of PSC are obtained [67].

In the event of EOG, according to Figure 3.14, if  $t_1 = 5s$  and  $t_2 = 21s$ , it can be obtained that  $\omega_r(t_2) = \omega_r(t_1)$  no matter which control scheme is applied. Therefore,  $E_w = E_e$ . Such equation indicates that the electrical energy produced by the wind turbine is equal to the wind energy captured by the wind turbine under EOG. As a result, the

energy loss can be computed by using the  $E_e$  of the MPPT based on ORSC and the  $E_e$  of PSC.

From (3.28) and (3.30), the energy loss of PSC under the EOG can be obtained. In this study, the energy loss caused by the application of PSC is 0.08%, which can be acceptable in practice [67]. Besides, as Figure 3.15 shows, the shaft torque obtained from PSC can be smoother. This result reveals that the proposed PSC scheme can alleviate the fluctuation of shaft torque under the EOG, and thus the negative effects on gearbox could be mitigated [60], [73].

### **3.4 Summary**

The control schemes of wind turbines under normal condition and grid faults are discussed in this chapter. Besides, the control strategies aiming to reduce the mechanical fatigue of each VSWT are also involved.

In addition, a power smoothing control method, which is intended to alleviate the power fluctuation caused by the EOG, is described in this chapter. Such control method adjusts the electrical torque directly, and therefore the power produced by each VSWT can be smoothed. The simulation study proves that the proposed PSC scheme is effective. Compared to the ORSC based MPPT control, the active power fluctuation can be attenuated by implementing the proposed power smoothing control. In addition, the proposed power smoothing control can also smooth the shaft torque during the EOG in order to maintain the lifetime of gearbox.



# **Chapter 4 Control Schemes Exploiting the Potential of Wind Turbines to Provide Frequency Support**

## **4.1 Introduction**

Driven by the public expectations for the sustainable development of society, the integration of wind energy has been promoted continuously during recent years [75]. As projected in the latest report published by the Global Wind Energy Council, more wind power plants (WPPs) will be installed in the foreseeable future [1].

In the past, the variable speed wind turbines (VSWTs) are arranged to extract the maximum power from the wind. Therefore, the maximum power point tracking (MPPT) control is applied in each VSWT [37]. However, as the penetration level of the wind energy increases rapidly, the impact of the VSWTs on power system frequency performance should be assessed thoroughly [3], [4]. Different from the conventional synchronous generators, some power electronic devices are applied in each VSWT so that the rotor speed of the VSWT is no longer strictly proportional to the system frequency [4]. As a result, if more and more VSWTs are installed to take the place of conventional power plants (CPPs) gradually, the inertia constant of such power system will decrease significantly [3]. In addition, owing to the variability of wind speed, the corresponding wind power can result in frequency fluctuation [76].

In order to maintain the power system stability, some TSOs in Europe have updated technical regulations for WPPs. According to the recent grid codes stipulated by British system operator, the WPPs should be able to provide frequency response, especially when power consumption is low [5].

Up to now, various control schemes enabling individual wind turbine to provide frequency support have been designed. According to the discussion in [3] and [75], these control methods can be generally put into two groups. One group can be named as the emulated inertia control (EIC), and the other group can be summarized as de-loading operation based primary frequency control (DOPFC). These control actions can be performed by either DFIG-WT or PMSG-WT.

By applying the EIC, the wind turbine can provide virtual inertia support so that the rate of change of system frequency can be attenuated [75]. To perform such control action, a frequency derivative controller can be inserted in each wind turbine, and thus the kinetic energy provided by rotor can be employed [77-79]. Besides, energy storage systems (ESSs) can also be utilized to perform EIC [77]. However, if the ESSs are installed, additional investment will be required [75].

The DOPFC can be performed on condition that the power reserve has been obtained by the wind turbine operating in de-loading mode under normal condition [3], [76], [80]. Since the de-loaded wind turbines cannot capture maximum power from wind, the electricity market mechanism should be modified in order to compensate the revenue loss of WPPs' operators [75], [81].

The DOPFC aims at employing the power reserve, which is acquired by each de-loaded wind turbine, to contribute to system frequency control. As described in [80-82], the DOPFC can be performed through pitch angle adjustment. If such method is applied, the power captured by the wind turbine can be regulated. However, mechanical fatigues may be caused by the variation of pitch angle [80]. In addition to the pitch angle regulation, some papers propose that the DOPFC can also be achieved if a frequency proportional controller, which can produce an active power compensation item, is applied into the RSC control system of each wind turbine [3], [76], [80], [83], [84]. It is noteworthy that in these control schemes, mechanical power variation is not explicitly involved. As a result, the wind turbine with these control strategies may not be able to adjust the mechanical power captured from wind in the event of frequency deviation [78], [82], [85].

Recently, PMSG-WTs have been widely used, especially in large wind farms [86]. Conventionally, the RSC is assigned to realize MPPT control, and the DC-link voltage stabilization is performed by the GSC [36]. As mentioned in Chapter 3, either direct control technique or vector control technique can be adopted as the inner-loop control scheme of the two converters [36], [44], [45]. In [87] and [88], a new control approach, which is based on a fractional-order controller, is put forward. According to the two articles, if such control strategy is implemented, the power quality of the converters can become better.

If the PMSG-WT is arranged to realize de-loading operation, both the kinetic energy stored in rotor and the power reserve can be used to provide frequency response. In addition, the DC capacitors can also perform frequency control if electrical energy is

deployed. The frequency control strategies employing the kinetic energy provided by rotor and the power reserve are proposed in [3], [5], [75], [76], [78-84], [89] and [90]. However, the participation of DC capacitors in frequency support provision can be discussed. The control schemes described in [4], [77], [85], [86], [91] and [92] focus on the emulated inertia control performed by each PMSG-WT, but the usage of power reserve for DOPFC realization can be investigated further.

To exploit the available resource provided by each PMSG-WT for frequency support provision as much as possible, this chapter describes a combined primary frequency control strategy. In this control scheme, an extended rotor speed control and a modified DC-link voltage control are included. The extended rotor speed control can adjust the power captured from wind by changing the turbine speed so that the power reserve can be utilized to regulate system frequency. In the meantime, the rotor speed variation indicates that the kinetic energy stored in the rotor can be utilized, and thus the EIC can be performed. Besides, the modified DC-link voltage control can change the DC-link voltage according to frequency deviation. In this way, the energy preserved in the DC capacitors can be deployed and additional emulated inertia support can be offered. Consequently, the transient performance of system frequency can be improved further.

Although the research presented in this chapter emphasizes the frequency control methods used in individual PMSG-WT, the extended rotor speed control scheme described here can also be applied in each DFIG-WT so that the potential of the DFIG-WT can be exploited for frequency regulation. Besides, it is noteworthy that the recent works on frequency control strategies applied in photovoltaic (PV) systems have also been

reviewed for this research. From these papers, it can be learnt that similar to the VSWTs, the PV systems can also acquire power reserve through de-loading operation, and such reserve can be deployed for frequency control as well [93-99]. Furthermore, a control scheme employing the power reserve and the DC capacitors together to provide frequency response is discussed in [98].

The rest of this chapter consists of four sections. Section 4.2 introduces the model of the PMSG-WT used in this research. The proposed control scheme is illustrated in Section 4.3. Simulation results are provided in Section 4.4 and the summary of this research is presented in Section 4.5.

## 4.2 PMSG-WT Model for Study

### 4.2.1 Conventional Control Schemes Applied in Individual PMSG-WT

Based on the description in [34], a model of a typical 2MW PMSG-WT is adopted for this study. Figure 4.1 shows the configuration of this model and the conventional control scheme applied in this wind turbine. In this figure,  $P_{e.ref}$  represents the active power command generated by MPPT control algorithm, and  $U_{DC.ref}$  denotes the reference of DC-link voltage.

According to the analysis on aerodynamics of this wind turbine, the mechanical power  $P_m$  can be calculated as follows [34]:

$$P_m = 0.5C_p(\lambda, \beta)\rho\pi R^2V_w^3 \quad (4.1)$$

$$C_p = 0.5176\left(\frac{116}{\gamma} - 0.4\beta - 5\right)e^{-\frac{21}{\gamma}} + 0.0068\lambda \quad (4.2)$$

$$\gamma = 1 / \left( \frac{1}{\lambda + 0.08\beta} - \frac{0.035}{\beta^3 + 1} \right) \quad (4.3)$$

In these equations,  $C_p$  is power coefficient;  $V_w$  is wind speed;  $\lambda$  is tip speed ratio (TSR);

$\beta$  is pitch angle;  $R$  is the radius of the blade;  $\rho$  is air density.

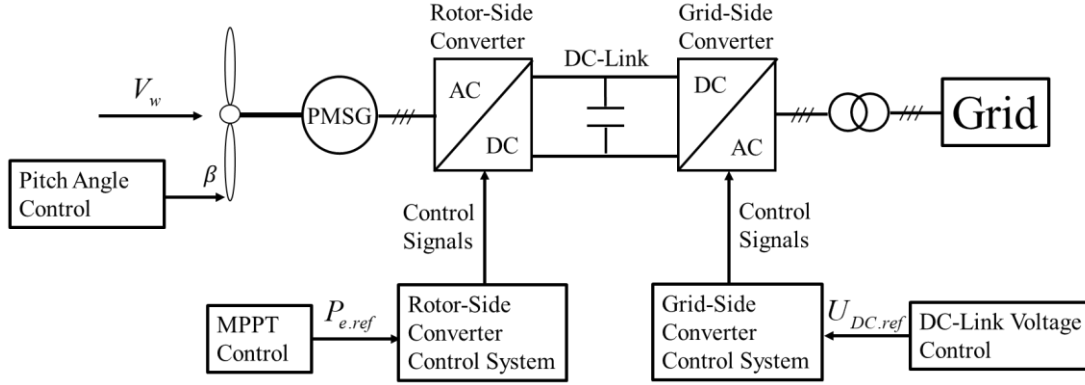


Figure 4.1 Configuration of a typical PMSG-WT

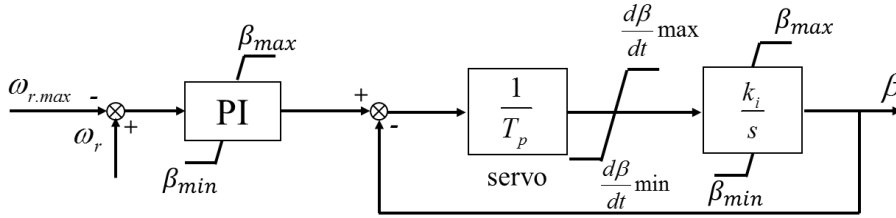


Figure 4.2 Model of pitch angle controller

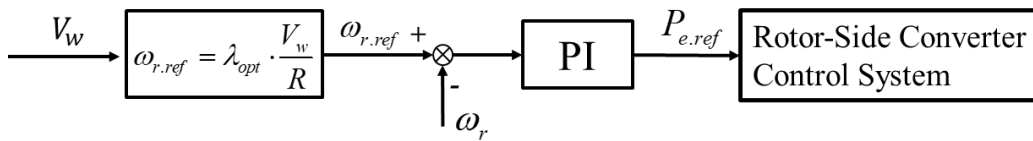


Figure 4.3 Typical method to perform MPPT control

#### 4.2.2 Modelling of Drive Train System

In this study, a two-mass model, which is accurate enough to describe the behavior of the drive train system, is established [2]. Such model is introduced in Chapter 3 and relevant details are provided in [2].

### 4.2.3 Modelling of Pitch Angle Controller

In order to realize MPPT control, the pitch angle  $\beta$  should be set as its optimal value  $\beta_{opt}$  if the wind speed is lower than the rated value [13]. However, as wind speed increases, the pitch angle control may be performed to limit the rotor speed and the power output of each wind turbine [2]. In this chapter, the pitch angle actuator described in [2] is applied. Such control system is sketched in Figure 4.2. As shown in this figure,  $T_p$  and  $k_i$  represent the parameters.

### 4.2.4 Conventional Control Schemes Applied in RSC and GSC

Conventionally, the MPPT control is implemented in the RSC of each PMSG-WT. The MPPT control can drive the wind turbine to operate at the optimal speed where the power captured by blades can be maximized. In [37], a typical rotor speed control loop based MPPT scheme is designed. Such MPPT control method is presented in Figure 4.3. In this figure, the rotor speed reference is denoted by  $\omega_{r.ref}$ , and the active power command generated by PI controller is represented by  $P_{e.ref}$ . In addition,  $\lambda_{opt}$  is the TSR where the extracted power is maximized.

As shown in Figure 4.1, GSC is used to keep the voltage of the DC capacitor stable by using the DC-link voltage control. Under normal condition, the DC-link voltage should remain constant so that the wind turbine can deliver the active power produced by RSC to the power grid [2]. Therefore, the  $U_{DC.ref}$  in the GSC control system should be fixed. In this research, the two converters are modelled according to the description in [36].

In practice, the WPPs should fulfill the requirements on power quality, which are specified in the grid codes. The power quality issues relate to the converter topology and the control techniques applied in the converters. Considering that the impact of the control scheme on frequency performance is emphasized in this chapter, further discussion on power quality issues can be carried out in the future.

## **4.3 The Proposed Primary Frequency Control Scheme for PMSG-WT**

### **4.3.1 Overview of The Proposed Control Scheme**

According to the discussion in Section 4.1, the power reserve can be obtained on condition that the wind turbine operates in de-loading mode. Such operation mode can be achieved if the wind turbine operates at a certain speed where the power coefficient is not optimal [3]. In this chapter, the over-speeding technique is applied to implement the de-loading operation, for additional kinetic energy can be acquired. In Section 4.3.2, the theoretical analysis and implementation of the de-loading operation are provided.

To deploy the power reserve acquired from de-loading operation to perform frequency control, an extended rotor speed control is applied. By using such control method, the rotor speed reference will reduce if the fall of system frequency is detected. As a result, the wind turbine will slow down and move towards the optimal operating point where more power can be extracted. In this way, both the power reserve and the kinetic energy preserved by rotor can be employed for frequency response provision. Different from the under-frequency event, if the system frequency rises, the setting point of the rotor speed will increase to make the wind turbine accelerate. Consequently, the power captured by the wind turbine will reduce, but more kinetic energy will be acquired.

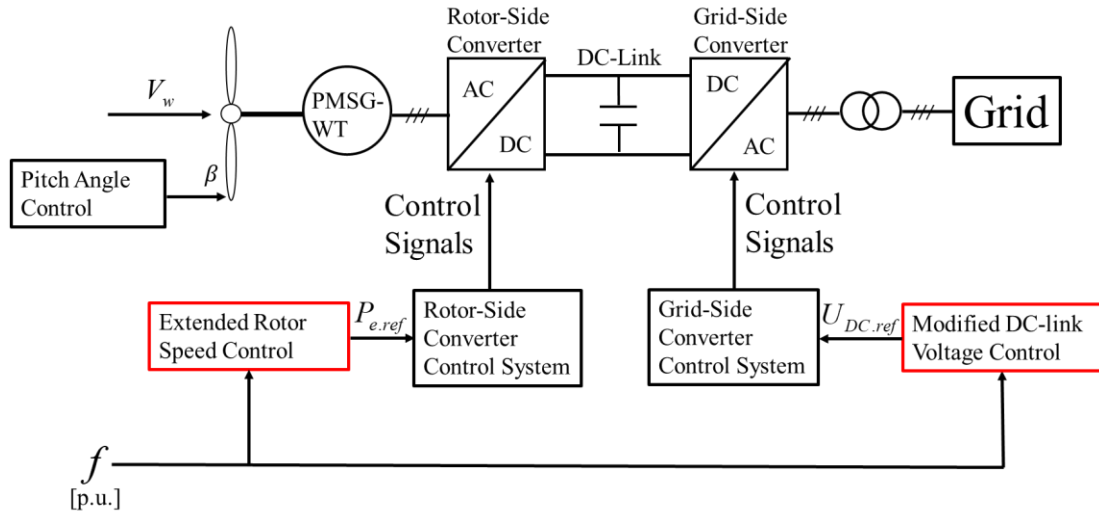


Figure 4.4 Overview of the proposed control scheme

In addition, the DC capacitor can contribute to improving frequency performance if a modified DC-link voltage control is applied. The modified DC-link voltage controller has been introduced in [91] and [92]. Such controller can adjust the value of DC-link voltage according to the frequency deviation, and thus the DC capacitor can provide frequency support by releasing or absorbing energy.

Figure 4.4 summarizes the combined control scheme enabling each PMSG-WT to provide frequency support. In Figure 4.5, the extended rotor speed control scheme, which is implemented by RSC, is depicted. The modified DC-link voltage control is sketched in Figure 4.6. The two control schemes are analyzed in Section 4.3.3 and 4.3.4, respectively.



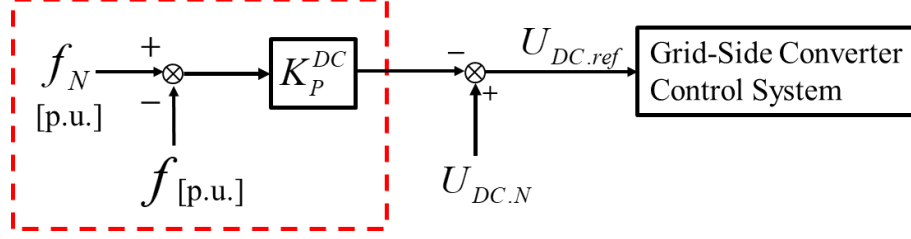


Figure 4.6 Modified DC-link voltage control used in GSC

### 4.3.2 Control Scheme to Realize the De-loading Operation of PMSG-WTs

As mentioned before, the wind turbine should be de-loaded to acquire power reserve if the system frequency varies within normal range. To describe the amount of power reserve, the de-loading level  $DL_{del.N}$  is defined according to the discussion in [100]. Such definition can be expressed by (4.4):

$$\begin{aligned}
 DL_{del.N} &= \frac{P_m^{MPPT} - P_m^{del.N}}{P_m^{MPPT}} \times 100\% \\
 &= \frac{0.5C_p^{\max} \rho \pi R^2 V_W^3 - 0.5C_p^{del.N} \rho \pi R^2 V_W^3}{0.5C_p^{\max} \rho \pi R^2 V_W^3} \times 100\% \\
 &= \frac{C_p^{\max} - C_p^{del.N}}{C_p^{\max}} \times 100\%
 \end{aligned} \tag{4.4}$$

in which  $P_m^{MPPT}$  is the maximum power that can be captured by the wind turbine and  $P_m^{del.N}$  is the power extracted by the wind turbine operating in de-loading mode.  $C_p^{\max}$  is the maximum value of power coefficient. The sub-optimal power coefficient is denoted by  $C_p^{del.N}$ . If a certain  $DL_{del.N}$  is given, the corresponding power  $P_m^{del.N}$  can be derived from (4.5):

$$P_m^{del.N} = P_m^{MPPT} (1 - DL_{del.N}) \tag{4.5}$$

To realize de-loading operation, the wind turbine should move away from the optimal operating point where the extracted power is maximized [76]. Assuming that the pitch

angle is fixed, the mapping from TSR  $\lambda$  to power coefficient  $C_p$  can be described by the curve shown in Figure 4.7.

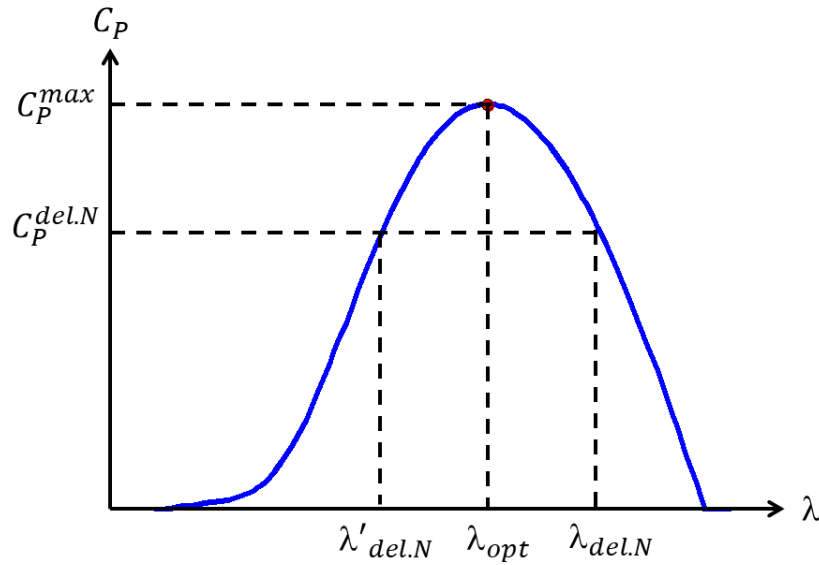


Figure 4.7  $C_p - \lambda$  characteristic

According to Figure 4.7, a certain  $DL_{del.N}$  can be acquired by using a lower-than-optimal TSR  $\lambda'_{del.N}$  or a higher-than-optimal TSR  $\lambda_{del.N}$  [101].  $\lambda_{del.N}$  indicates that  $C_p^{del.N}$  can be achieved by over-speeding, while  $\lambda'_{del.N}$  reveals that the wind turbine can operate in de-loading mode if an under-speeding technique is applied [76], [101]. As mentioned before, since more kinetic energy can be preserved by using the over-speeding technique,  $\lambda_{del.N}$  is selected to implement the de-loading operation [90].

The over-speeding technique to perform de-loading operation is shown in Figure 4.8, where  $\omega_{r.min}$  represents the minimum value of rotor speed. According to this figure, it can be observed that if the  $DL_{del.N}$  is given, the value of  $C_p^{del.N}$  can be acquired from (4.1).

By using the  $C_p^{del.N}$  and the  $C_p - \lambda$  characteristics, the TSR  $\lambda_{del.N}$ , which is greater than  $\lambda_{opt}$ , can be obtained accordingly.

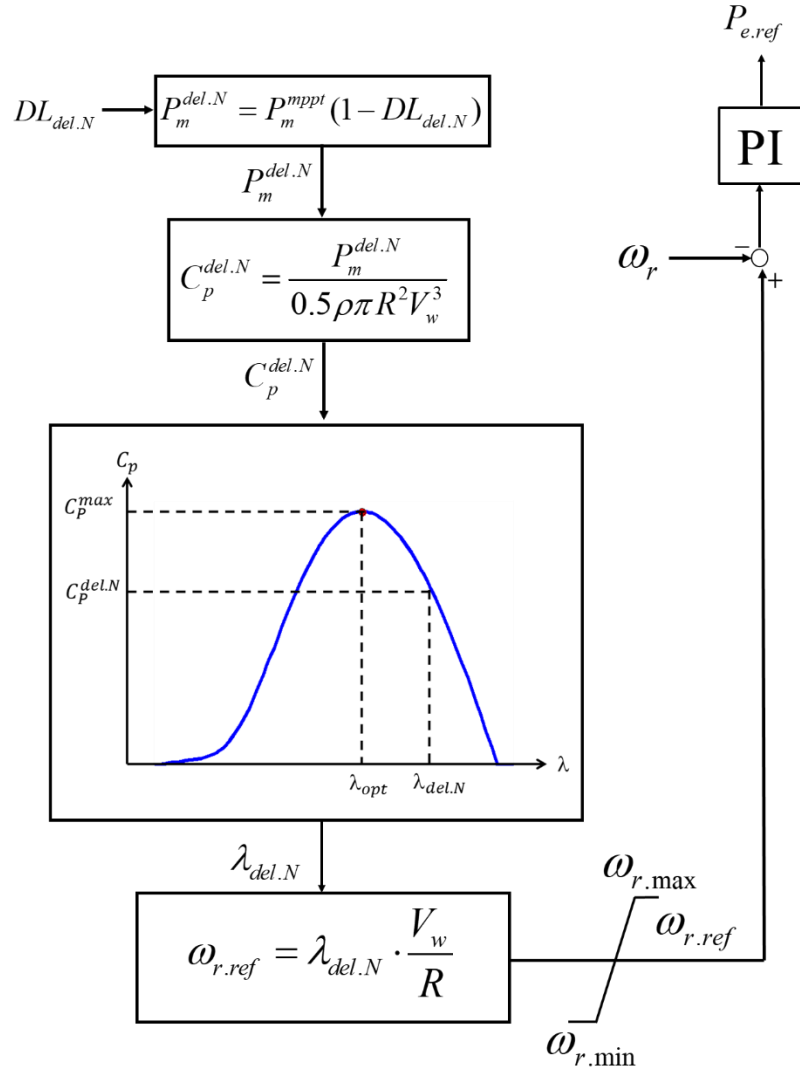


Figure 4.8 Control technique to realize de-loading operation

It is noteworthy that in this research, the pitch angle is assumed to be fixed. However, as mentioned in Section 4.2.3, the pitch angle will be varied to avoid overloading, on condition that the wind speed is higher than the rated value. Therefore, both rotor speed

adjustment and pitch angle control should be considered for the implementation of de-loading operation [80], [89], [90]. Further investigation on this topic can be conducted in the future. Besides, the wind speed information should be obtained in real-time if such control method is applied. According to the study in [38], the wind speed can be measured by using the light detection and ranging (LIDAR) system. It is expected that such technique can be more mature and cost-effective.

### 4.3.3 Extended Rotor Speed Control Applied in RSC

As discussed in Section 4.3.1, the decline of system frequency requires that each wind turbine should extract more power from wind, while less power should be captured if frequency rises. In order to satisfy such requirements, the rotor speed reference should be generated according to Figure 4.5.

In Figure 4.5,  $f$  denotes the actual frequency of power system, while  $f_N$  is the normal value of system frequency. If frequency deviates, the frequency proportional (P) controller with a parameter  $K_P$  can produce a compensating item, and thus the desirable value of mechanical power  $P_m^{del.f}$  can be obtained. The selection of  $K_P$  is discussed in Section 4.4. Once the  $P_m^{del.f}$  is determined, the corresponding power coefficient  $C_p^{del.f}$  and TSR  $\lambda_{del.f}$  can be acquired according to (4.1) and the  $C_p - \lambda$  characteristics. By using the value of  $\lambda_{del.f}$ , the reference of rotor speed  $\omega_{r.ref}$  can be updated automatically. From Figure 4.5, it can be observed that the  $\omega_{r.ref}$  should be sent to the PI controller so that the operating point of the wind turbine can be adjusted for frequency control.

By applying the control strategy shown in Figure 4.5, the decrease of system frequency can drive the wind turbine to move from de-loading operating point to optimal operating point. Consequently, each wind turbine can extract more power from wind, and thus additional active power can be injected into transmission network for frequency regulation. On detecting an over-frequency event, the wind turbine will accelerate to regain a new speed with a lower power coefficient so that less power will be captured.

Compared to the rotor speed control strategy discussed in [89], a frequency derivative (D) controller is inserted into the proposed control scheme shown in Figure 4.5. The parameter of the D controller is denoted by  $K_D$ . Since the rotor speed can be adjusted during the frequency excursion, the frequency D controller can employ the kinetic energy stored in rotor to realize EIC.

In addition, it is important to note that the soft connection between the turbine and generator may lead to torsion oscillation, and such oscillation can cause the system frequency to fluctuate [2]. If the frequency D controller is applied, the frequency fluctuation induced by the torsion oscillation can be attenuated to some extent.

#### **4.3.4 Modified DC-Link Voltage Control Applied in GSC**

Traditionally, the DC-link voltage in the PMSG-WT should remain stable in order to deliver the active power produced by RSC into transmission network. According to the investigation in [92] and [102], additional virtual inertia support can be acquired if the energy preserved by DC capacitor is exploited. Such idea can be realized by changing the DC-link voltage. As discussed in these papers, the DC capacitor can realize EIC if the

capacitor exploits the preserved energy to perform a power command generated by a frequency derivative controller [91], [102]. Such power command is denoted by  $P_e^{DC}$ , and the  $P_e^{DC}$  can be expressed by the following equation [91], [102]:

$$P_e^{DC} = U_{DC} \cdot C_{DC} \frac{dU_{DC}}{dt} = K_D^{DC} \cdot \frac{df}{dt} \quad (4.6)$$

where  $K_D^{DC}$  represents the parameter of the frequency derivative controller.

By using the integration principles, the expression of the energy extracted from the DC capacitor can be acquired as follows [91], [102]:

$$\int_{t_0}^t P_e^{DC} \cdot dt = \int_{U_{DC.N}}^{U_{DC}} U_{DC} \cdot C_{DC} \cdot dU_{DC} = \int_{f_N}^f K_D^{DC} \cdot f \cdot df \quad (4.7)$$

where  $t_0$  denotes the instant when frequency excursion is detected,  $U_{DC}$  is the actual value of the DC-link voltage, while  $U_{DC.N}$  is the normal voltage of DC capacitor.  $C_{DC}$  is the capacitance. Based on (4.7), the following equations can be acquired:

$$\frac{1}{2} C_{DC} (U_{DC}^2 - U_{DC.N}^2) = \frac{1}{2} K_D^{DC} (f^2 - f_N^2) \quad (4.8)$$

$$\frac{1}{2} C_{DC} [(U_{DC.N} + \Delta U_{DC})^2 - U_{DC.N}^2] = \frac{1}{2} K_D^{DC} [(f_N + \Delta f)^2 - f_N^2] \quad (4.9)$$

In (4.8) and (4.9), the deviation of DC-link voltage is denoted by  $\Delta U_{DC}$ , and variation of system frequency is represented by  $\Delta f$ . As discussed in [91], compared to  $U_{DC.N}$  and  $f$ , both  $\Delta U_{DC}$  and  $\Delta f$  are relatively small. Therefore,  $\Delta U_{DC}^2$  and  $\Delta f^2$ , which are the higher order terms in (4.9), can be neglected so that the simplified equations (4.10) and (4.11) can be obtained [91]:

$$C_{DC} \cdot U_{DC.N} \cdot \Delta U_{DC} = K_D^{DC} \cdot f_N \cdot \Delta f \quad (4.10)$$

$$C_{DC} \cdot U_{DC.N} \cdot (U_{DC} - U_{DC.N}) = K_D^{DC} \cdot f_N \cdot (f - f_N) \quad (4.11)$$

From (4.11), the desirable value of DC-link voltage can be described as follows:

$$U_{DC} = -K_P^{DC} \cdot (f_N - f) + U_{DC.N} \quad (4.12)$$

It is noteworthy that  $K_P^{DC}$  is also a parameter which can be derived from the following equation:

$$K_P^{DC} = \frac{K_D^{DC} \cdot f_N}{C_{DC} \cdot U_{DC.N}} \quad (4.13)$$

Figure 4.6 shows the modified DC-link voltage controller based on the equations (4.6)~(4.12). As mentioned in Section 4.3.1, such controller has been discussed in [91] and [92]. Furthermore, if the  $U_{DC.ref}$  is updated according to Figure 4.6, the DC capacitor can utilize the energy to enhance emulated inertia support.

If the controller depicted in Figure 4.6 is implemented, the reduction of system frequency can cause the voltage of DC capacitor to decrease so that the DC capacitor can release the electrical energy to provide frequency response. On detecting an over-frequency event, the DC-link voltage will be boosted so that the surplus power can be stored into the DC capacitor. It is obvious that the value of  $K_P^{DC}$  can influence the range of DC-link voltage variation. The setting of  $K_P^{DC}$  is briefly investigated in Section 4.4.

As mentioned in Section 4.2, each wind power plant should fulfill the requirements on power quality in practice. Several methods aiming at improving the power quality are introduced in [47-49]. In these works, the application of LCL filter and the implementation of repetitive control techniques are analyzed. The study on power quality issues can be conducted in the future.

## 4.4 Simulation Results

Figure 4.9 presents a small power system model established for simulation. In this system, 2 thermal power plants and 5 wind turbines are included. If power is balanced, the system frequency should be maintained at 50Hz. Based on [103], the parameters of the governors used in the thermal power plants can be obtained. The load damping coefficient is set as 1.5, which is a typical value provided in [104]. All the parameters used in the system are listed in Appendix. The initial power demand is set as  $(39.567+j2.7067)$  MVA.

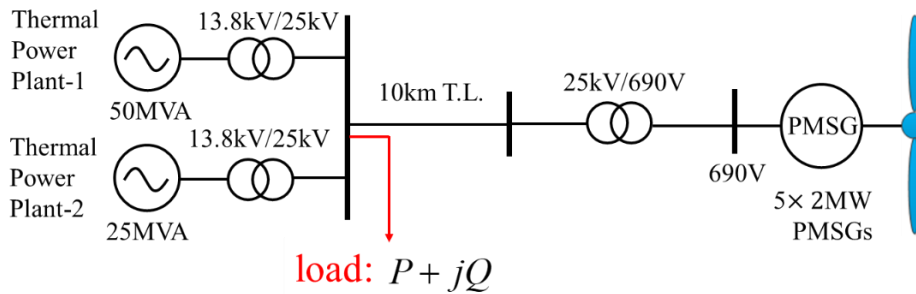


Figure 4.9 Model of power system for case study

In order to show the advantage of the proposed control scheme, three control strategies are applied in this research. These control strategies are illustrated as below:

**Strategy A:** The MPPT control is applied in each PMSG-WT, and thus the wind turbine cannot provide frequency response.

**Strategy B:** The extended rotor speed control is implemented in each PMSG-WT, but the modified DC-link voltage control is disabled.

**Strategy C:** Both the extended rotor speed control and the modified DC-link voltage control are applied in each PMSG-WT.

In this simulation, the value of  $K_p$  in Figure 4.5 is calculated according to (4.14):

$$K_p = \frac{P_m^{MPPT} - P_m^{del.N}}{f_N - f_{min}^{WT}} \times f_N \quad (4.14)$$

In (4.14),  $f_{min}^{WT}$  denotes the lower bound of control range, i.e. if the system frequency decreases to  $f_{min}^{WT}$ , the optimal rotor speed with maximum power coefficient should be achieved so that the wind turbine can release all the power reserve kept in advance. It is noteworthy that once an over-frequency event occurs, the  $K_p$  acquired from (4.14) is also used in the frequency control scheme proposed in Section 4.3. From (4.14), it can be learnt that if  $f_{min}^{WT}$  is greater, the wind turbine will be more sensitive to frequency excursion.

For simulation study, the  $DL_{del.N}$  of each PMSG-WT armed with Strategy B or C is set as 10%. In addition,  $f_{min}^{WT}$  is set as 49.8 Hz. Considering that this research emphasizes the utilization of power reserve acquired from de-loading operation, the value of  $DL_{del.N}$  is fixed in this section. Further discussion on the setting of  $DL_{del.N}$  will be conducted in the future.

Besides, the parameter  $K_p^{DC}$ , which is involved in the modified DC-link voltage control, can be derived from (4.15). In (4.15), the minimum voltage of DC capacitor is denoted by  $U_{DC.min}$ , and the maximum DC-link voltage is represented by  $U_{DC.max}$ . In this simulation,  $U_{DC.max}$  is set as 1.15 p.u. and  $U_{DC.min}$  is set as 0.85 p.u.. Consequently, the  $U_{DC.max}$  can be achieved if the system frequency increases to 50.2 Hz.

$$K_p^{DC} = \frac{U_{DC.N} - U_{DC.min}}{f_N - f_{min}^{WT}} \times f_N \quad (4.15)$$

To improve the performance of the proposed control scheme, it is necessary to set these control parameters properly. The selection of these parameters will be included in the future work.

If wind speed is constant, three indexes can be adopted to evaluate the frequency performance: the maximum absolute value of the rate of change of frequency, which is represented by maximum  $|ROCOF|$ , frequency nadir  $f_{nadir}$  and the final value of system frequency  $f_{final}$ . It is important to note that in this research, the  $f_{nadir}$  is defined as the frequency value measured when the maximum dynamic frequency deviation is achieved. Furthermore, for an under-frequency event, the  $f_{nadir}$  is the lowest value of frequency, while when frequency rises, the  $f_{nadir}$  is the peak value of frequency.

The transient behavior of system frequency can be assessed by using maximum  $|ROCOF|$  and  $f_{nadir}$ , and the steady-state performance of system frequency can be represented by  $f_{final}$ . Moreover, under variable wind speed, the mean value of  $|\Delta f|$ , which is acquired by averaging the absolute value of system frequency error, and  $f_{nadir}$  are applied to describe the frequency performance.

#### **4.4.1 System Frequency Decline under Constant Wind Speed**

*Case. A:* Wind speed is set as 8m/s and the load increases by (7.5+j0.75) MVA at 40s.

The simulation results of Case. A are shown in Figure 4.10-Figure 4.14. The data provided in Table 4.1 describe the behavior of system frequency, while the data listed in Table 4.2 represent the performance of each PMSG-WT. It is necessary to note that in

Case. A, the optimal rotor speed is 0.8 p.u., while the rotor speed of the wind turbine with 10% de-loading level is 0.9473 p.u..

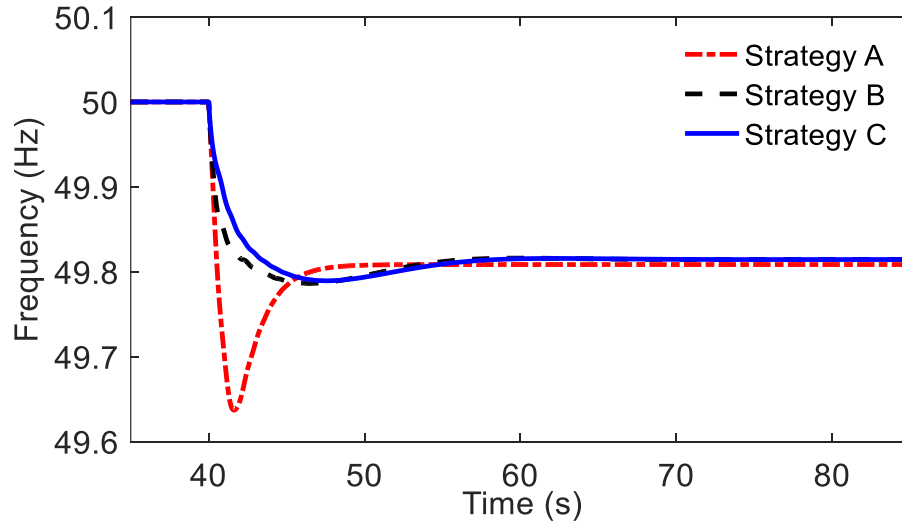


Figure 4.10 System frequency performance in Case. A

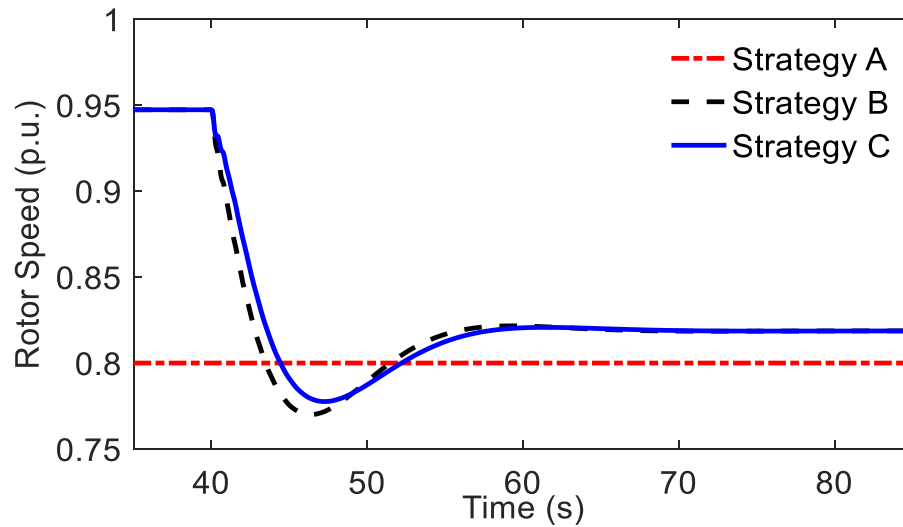


Figure 4.11 Performance of wind turbine rotor speed in Case. A

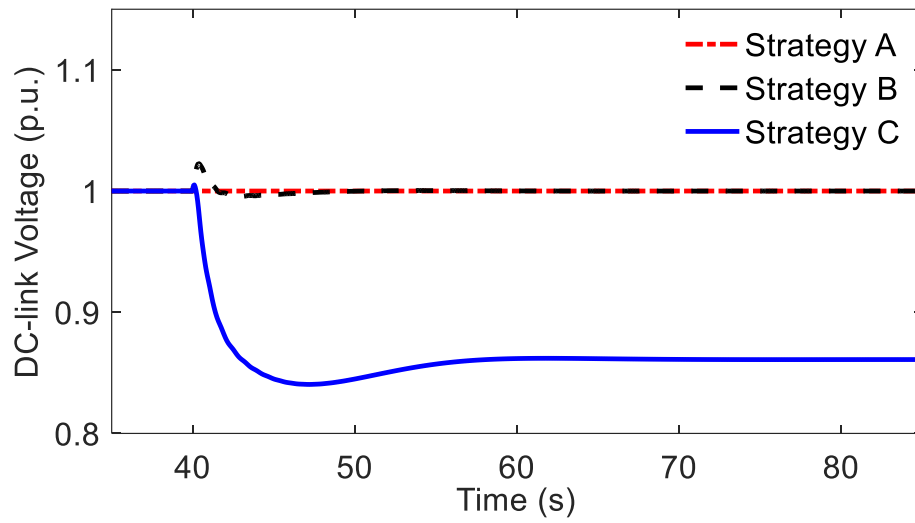


Figure 4.12 DC-link voltage performance in Case. A

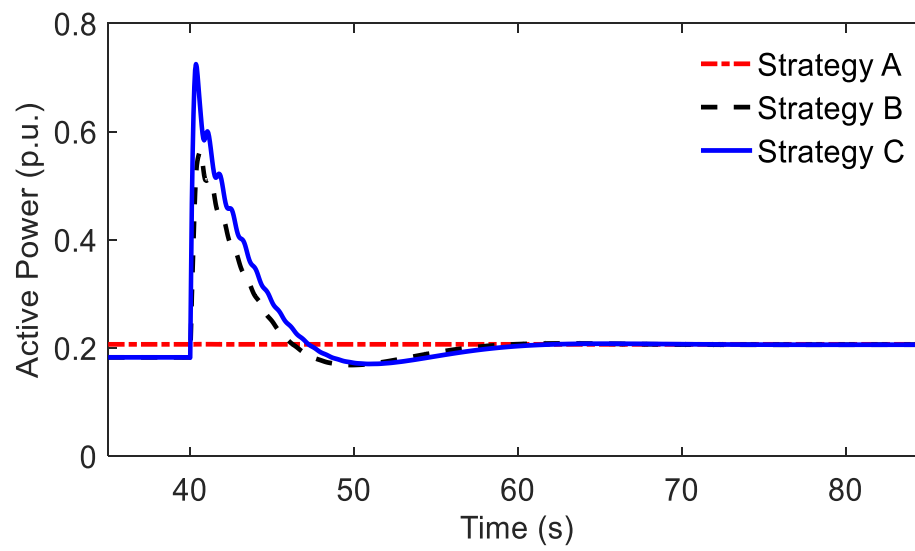


Figure 4.13 Performance of active power produced by PMSG-WT in Case. A

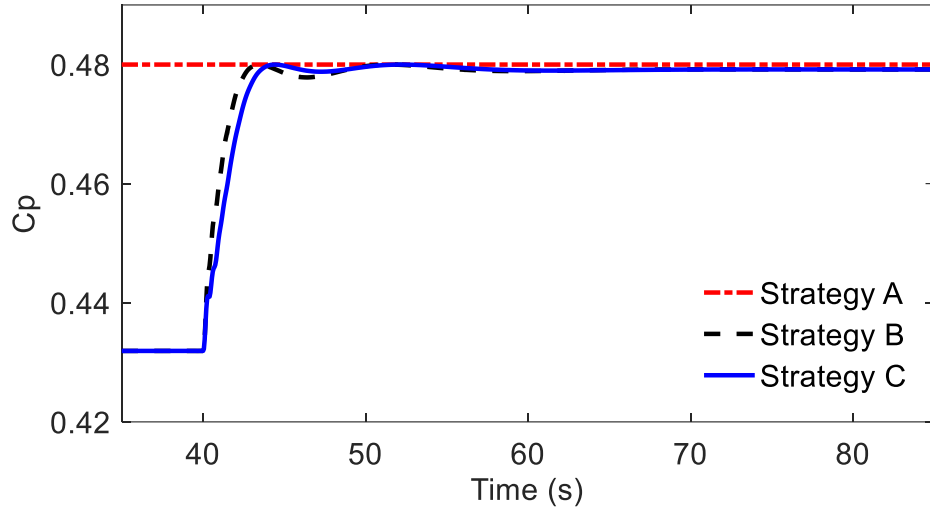


Figure 4.14 Power coefficient performance in Case. A

Table 4.1 Frequency performance of Case. A

Schemes	Maximum  ROCOF (Hz/s)	$f_{nadir}$ (Hz)	$f_{final}$ (Hz)
Strategy A	0.3884	49.6372	49.8087
Strategy B	0.3268	49.7864	49.8146
Strategy C	0.2988	49.7895	49.8146

Table 4.2 Wind turbine performance of Case. A

Schemes	Initial Value of $\omega_r$ (p.u.)	Final Value of $\omega_r$ (p.u.)	Initial Value of $P_m$ (p.u.)	Final Value of $P_m$ (p.u.)
Strategy A	0.8	0.8	0.2163	0.2163
Strategy B	0.9473	0.8187	0.1946	0.2159
Strategy C	0.9473	0.8187	0.1946	0.2159

From the data in Table 4.2, it can be learnt that by applying Strategy A, the rotor speed of each PMSG-WT remains at 0.8 p.u., and thus no frequency support is offered. Nevertheless, the wind turbine with Strategy B or C can decelerate from 0.9473 p.u. to

0.8187 p.u.. Therefore, the power captured from wind increases from 0.1946 p.u. to 0.2159 p.u.. Besides, the reduction of rotor speed implies that the wind turbine can release the kinetic energy preserved in rotor to the power system. As a result, the  $f_{nadir}$  is improved significantly, while the maximum  $|ROCOF|$  is attenuated. In addition,  $f_{final}$  can rise from 49.8087 Hz to 49.8146 Hz.

According to Figure 4.12, the DC-link voltage will decline by using Strategy C. Hence, the DC capacitor can extract electrical energy to provide additional frequency support. Furthermore, the  $f_{nadir}$  increases from 49.7864 Hz to 49.7895 Hz and the maximum  $|ROCOF|$  decreases from 0.3268 Hz/s to 0.2988 Hz/s. As the DC capacitor can only perform emulated inertia control, the index  $f_{final}$  will not be affected.

#### **4.4.2 System Frequency Rise under Constant Wind Speed**

*Case. B:* Wind speed is set as 8m/s and the load decreases by (7.5+j0.75) MVA at 40s

According to Figure 4.15 and Table 4.3, both the fastest frequency change rate and the greatest frequency overshoot can be observed if the Strategy A is implemented in each wind turbine. On the contrary, the wind turbine with Strategy B or Strategy C can accelerate when frequency rises. Therefore, the surplus power can be stored into the rotor and the power extracted from wind can be decreased. As a result, not only the maximum  $|ROCOF|$  and the peak value of system frequency can be alleviated, but the value of  $f_{final}$  reduces from 50.1901 Hz to 50.1849 Hz as well.

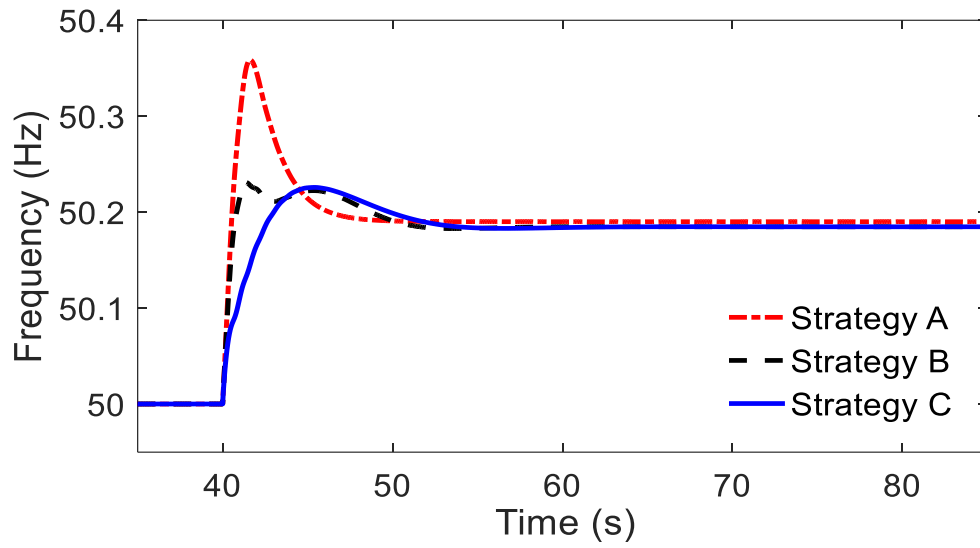


Figure 4.15 System frequency performance in Case. B

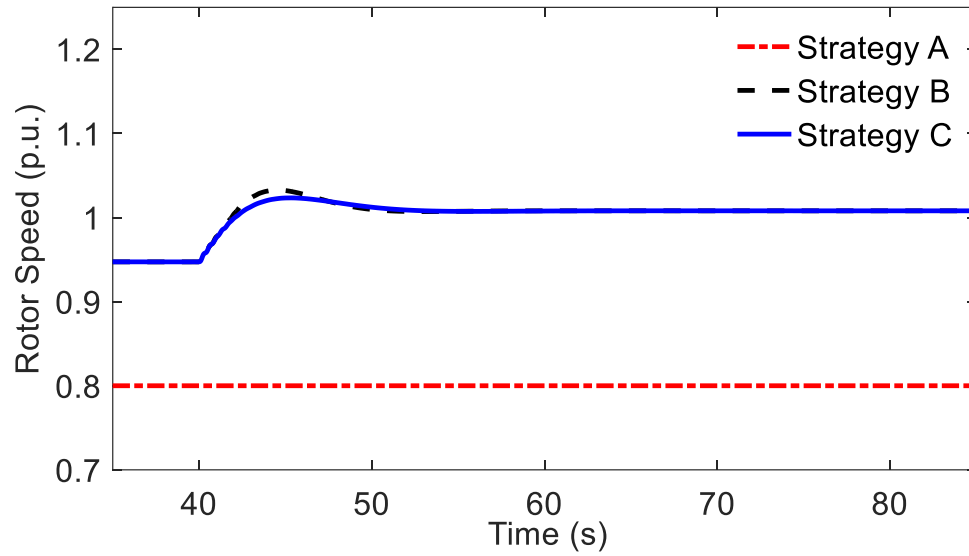


Figure 4.16 Performance of wind turbine rotor speed in Case. B

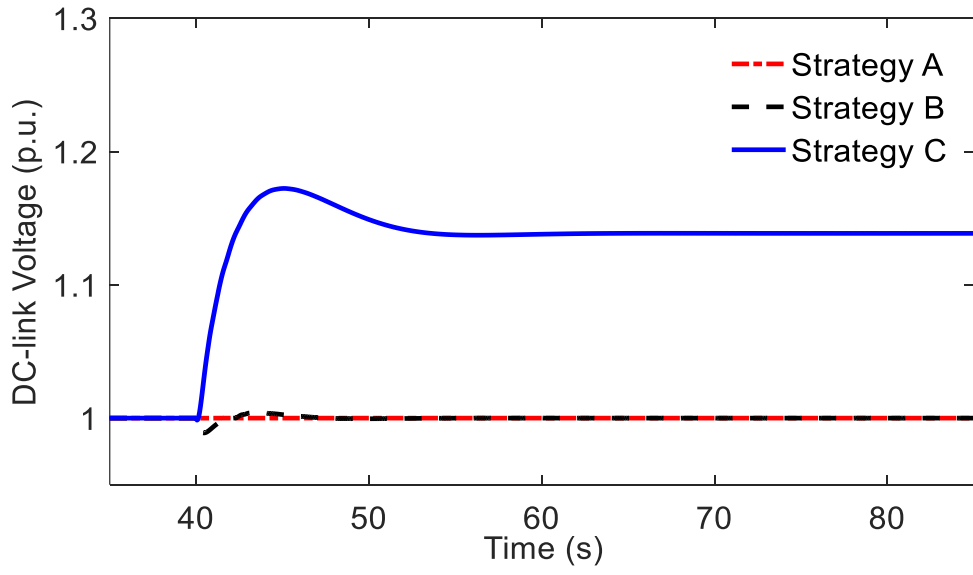


Figure 4.17 DC-link voltage performance in Case. B

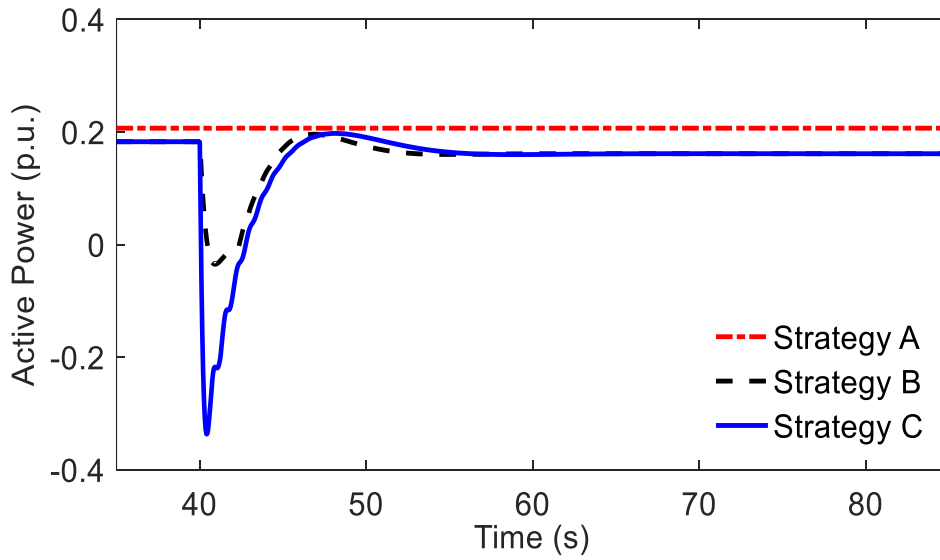


Figure 4.18 Performance of active power produced by PMSG-WT in Case. B

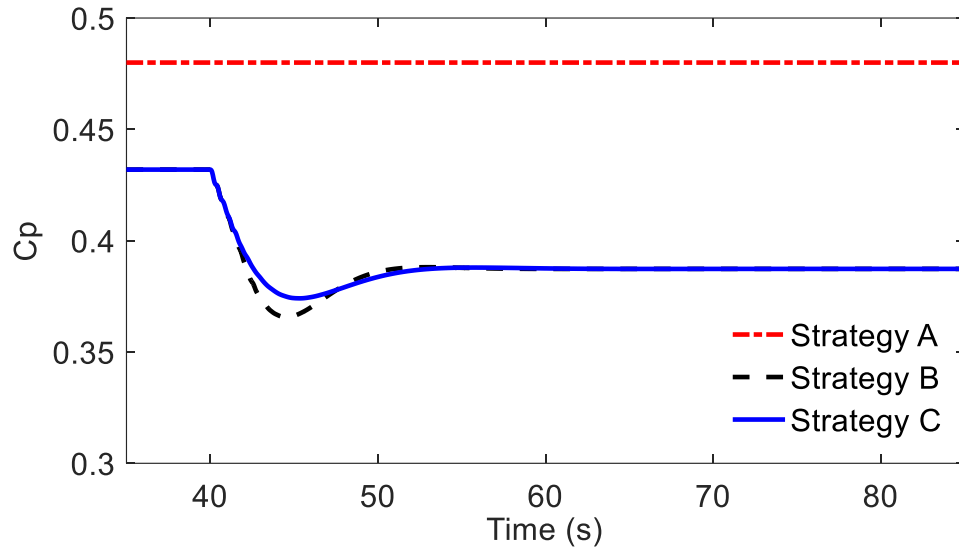


Figure 4.19 Power coefficient performance in Case. B

Table 4.3 Frequency performance of Case. B

Schemes	Maximum  ROCOF (Hz/s)	$f_{nadir}$ (Hz)	$f_{final}$ (Hz)
Strategy A	0.3822	50.3587	50.1901
Strategy B	0.3397	50.2310	50.1849
Strategy C	0.3087	50.2259	50.1849

Table 4.4 Wind turbine performance of Case. B

Schemes	Initial Value of $\omega_r$ (p.u.)	Final Value of $\omega_r$ (p.u.)	Initial Value of $P_m$ (p.u.)	Final Value of $P_m$ (p.u.)
Strategy A	0.8	0.8	0.2163	0.2163
Strategy B	0.9473	1.0080	0.1946	0.1745
Strategy C	0.9473	1.0080	0.1946	0.1745

Figure 4.17 shows that on detecting the over-frequency event, the Strategy C can cause the DC-link voltage to increase, and thus the surplus power can be absorbed by the DC capacitor. Consequently, the rate of change of frequency can become slower, and the

maximum dynamic deviation of system frequency can become smaller.

#### 4.4.3 System Frequency Decline under Variable Wind Speed

*Case. C* Wind speed is variable and the load increases by  $(7.5+j0.75)$  MVA at 180s

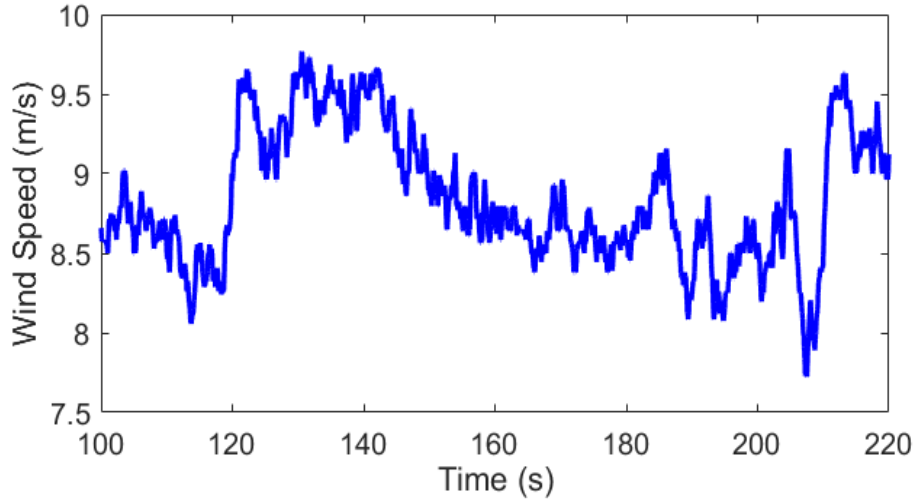


Figure 4.20 Variable wind speed profile used in Case. C

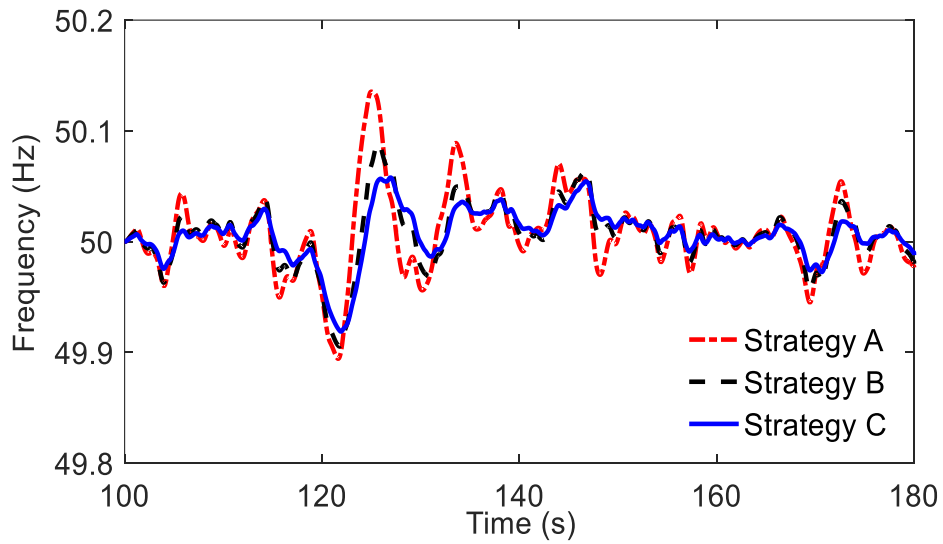


Figure 4.21 System frequency performance in Case. C (100~180s)

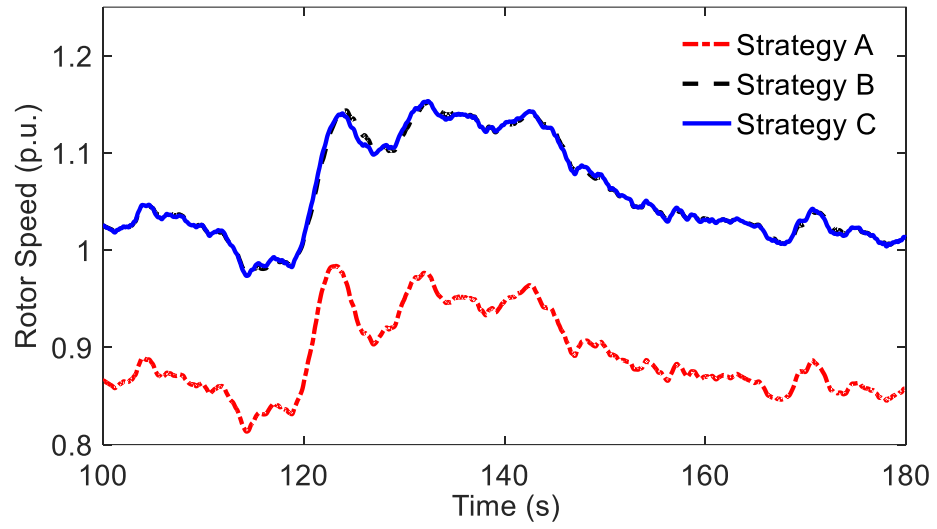


Figure 4.22 Performance of wind turbine rotor speed in Case. C (100~180s)

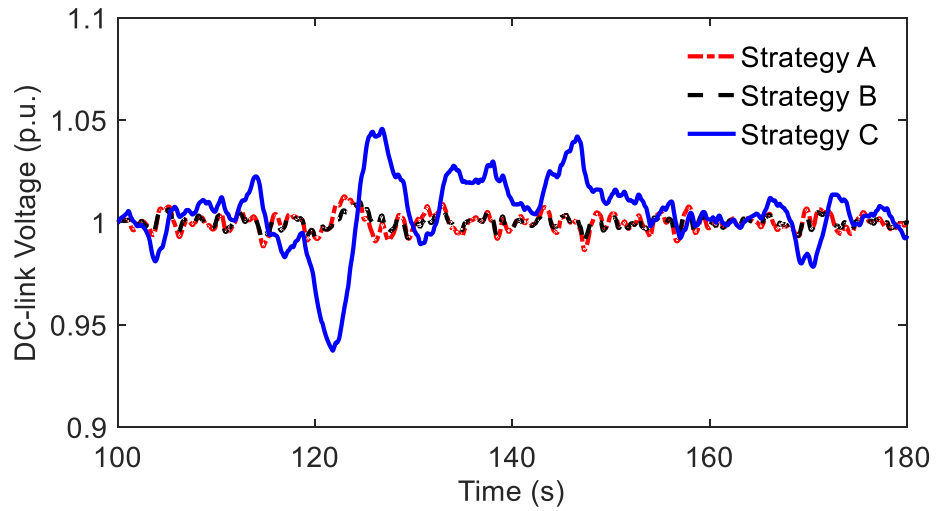


Figure 4.23 DC-link voltage performance in Case. C (100~180s)

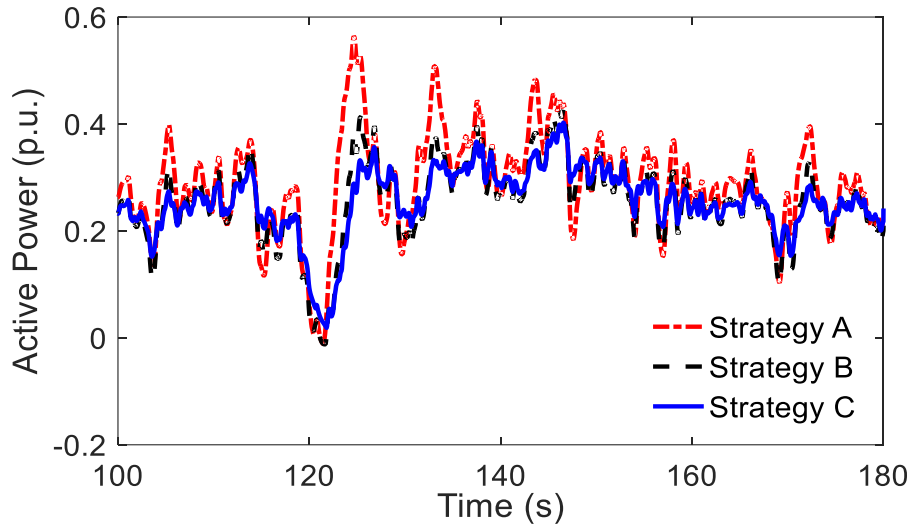


Figure 4.24 Performance of active power produced by PMSG-WT in Case. C (100~180s)

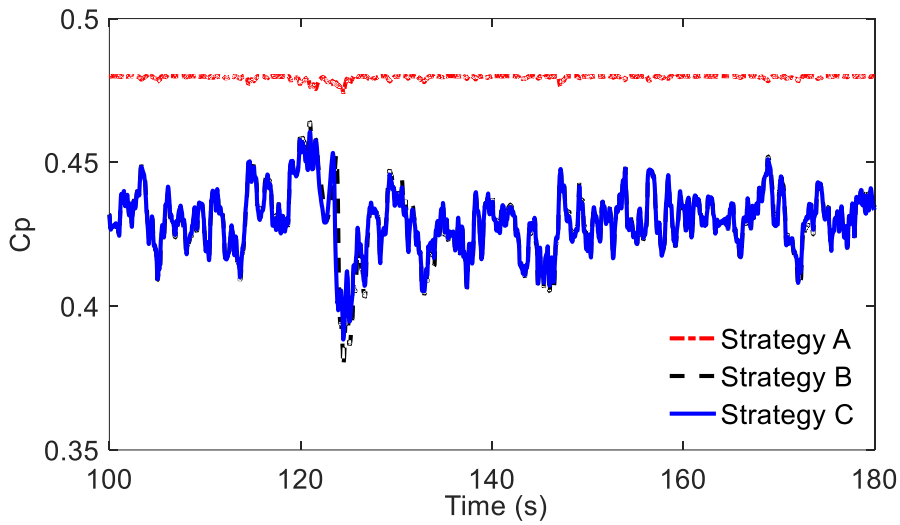


Figure 4.25 Power coefficient performance in Case. C (100~180s)

Figure 4.20 shows the profile of variable wind speed, which is applied in Case. C. The data of such wind speed profile can be acquired from [105]. It is noteworthy that the power consumption is constant during 100s~180s.

The simulation results during 100s~180s are provided in Figure 4.21-Figure 4.25. Moreover, the data describing the frequency performance can be found in Table 4.5. As shown in Figure 4.21, the fluctuation of system frequency can be caused by the variable wind speed. This figure also reveals that if Strategy B or C is applied, the frequency fluctuation can be mitigated effectively, for the two control strategies can both adjust the rotor speed of each wind turbine accordingly. In addition, due to the activation of modified DC-link voltage control, the electrical energy preserved in DC capacitor can be exploited to alleviate the frequency fluctuation further.

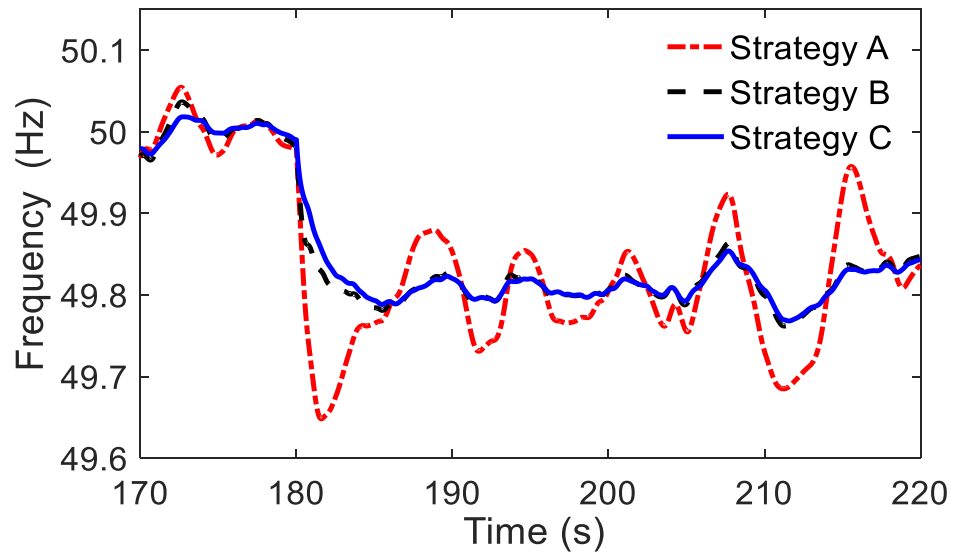


Figure 4.26 System frequency performance in Case. C (170~220s)

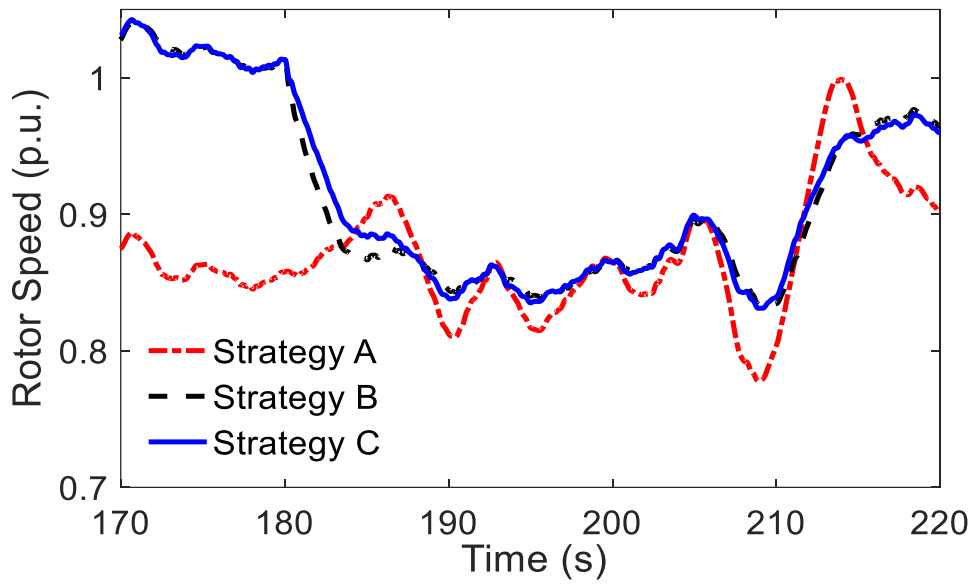


Figure 4.27 Performance of wind turbine rotor speed in Case. C (170~220s)

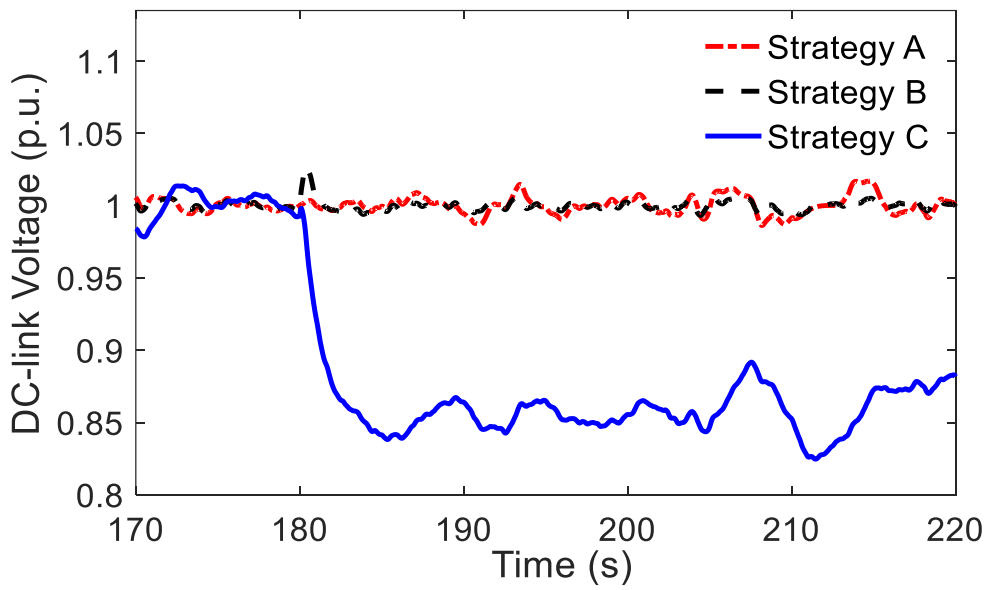


Figure 4.28 DC-link voltage performance in Case. C (170~220s)

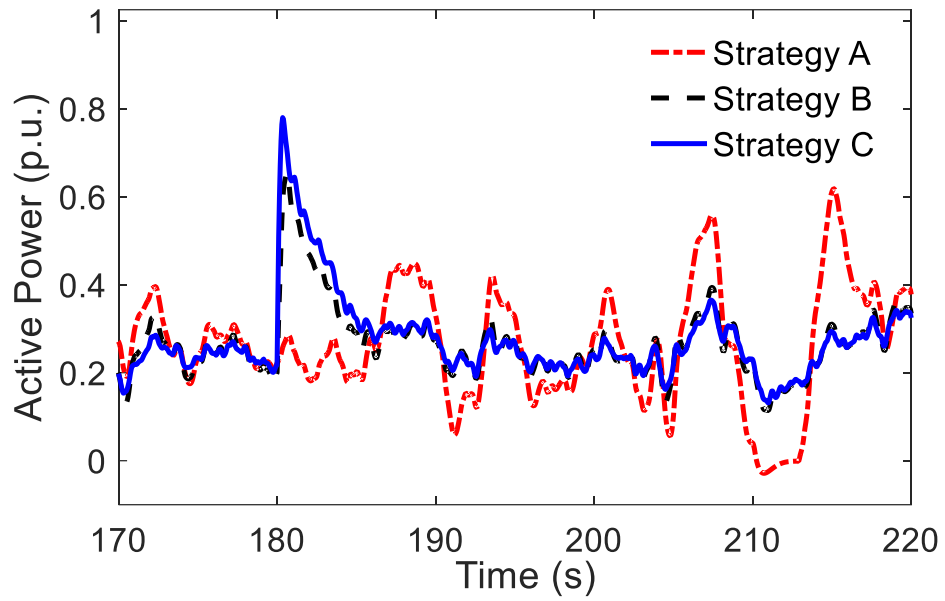


Figure 4.29 Performance of active power produced by PMSG-WT in Case. C (170~220s)

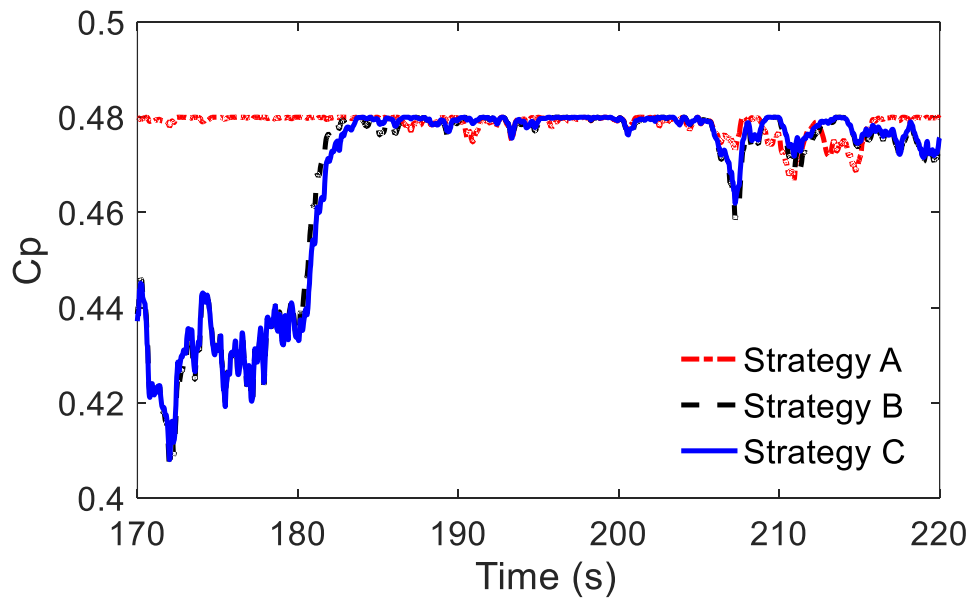


Figure 4.30 Power coefficient performance in Case. C (170~220s)

Table 4.5 Frequency performance of Case. C

Schemes	mean value of $ \Delta f $ (Hz) during 100s~180s	$f_{nadir}$ (Hz) during 170s~220s
Strategy A	0.0258	49.6480
Strategy B	0.0214	49.7619
Strategy C	0.0175	49.7681

Figure 4.26-Figure 4.30 presents the simulation results during 170s~220s. Relevant data are provided in Table 4.5. The figures and data prove that armed with Strategy B or C, the frequency decline leads to the deceleration of each PMSG-WT. As the rotor speed reduces, the kinetic energy stored in rotor can be extracted and the power captured by the wind turbine can increase. Consequently, the frequency nadir can become higher. Besides, if Strategy C is applied, the DC capacitor can participate in frequency control so that the performance of system frequency can be improved further.

## 4.5 Summary

This chapter describes a combined control strategy aiming at maximizing the frequency support provided by each PMSG-WT. In such control strategy, an extended rotor speed control and a modified DC-link voltage control are included.

In order to acquire the power reserve for ancillary service, the wind turbine should be de-loaded in advance. As soon as the frequency deviation occurs, the extended rotor speed control will be triggered, and thus the wind turbine can adjust the rotor speed accordingly. In this way, both the kinetic energy preserved in rotor and the power reserve obtained in advance can be employed to provide frequency response. In addition, the application of modified DC-link voltage control can result in the change of DC-link

voltage, and thus the energy kept in DC capacitors can be exploited to make the transient performance of system frequency become better. The simulation results prove that although no additional equipment is involved, the frequency stability can still be enhanced if the proposed control scheme is applied in each wind turbine.

For future work, several technical issues can be investigated further. Firstly, considering that the pitch angle can be activated if the wind is too strong, the participation of the pitch angle controller in frequency regulation can be discussed. Secondly, to optimize the performance of the proposed control strategy, the analysis on parameter selection can be carried out. Besides, since the amount of power reserve should be determined properly in practice, it is necessary to examine the setting of  $DL_{del.N}$ . Additionally, the methods to improve the power quality can also be explored.



# **Chapter 5 Coordinated Frequency Control Scheme for Offshore Wind Farm Integrated to VSC-HVDC System**

## **5.1 Introduction**

The global capacity of wind energy is growing continuously during recent years [1], [106]. In order to harvest offshore wind energy, some European countries promote the integration of offshore wind farms [107], [108]. Owing to the long distance between the onshore power system and the offshore wind farms, the voltage source converter based high voltage direct current (VSC-HVDC) transmission system can be applied so that the power produced by each offshore wind power plant (OWPP) can be delivered to the main grid economically [106], [109].

The effects of wind power on system frequency are briefly analyzed in Chapter 1 and Chapter 4. Since the wind speed is variable, the frequency of onshore power system may fluctuate [76]. In addition, the wind turbines cannot provide natural inertia support to the main grid, because the power electronic devices are involved in the VSC-HVDC system [106]. As more and more OWPPs are connected to the onshore power grid, the stability of system frequency may deteriorate [5].

To minimize these negative effects, the potential of the wind turbines and the VSC-HVDC system to provide frequency response can be investigated [110]. The studies in [102] and [111] recommend that the DC capacitors installed in the VSC-HVDC system

can be deployed to improve dynamic performance of system frequency. According to these papers, a frequency derivative controller can be inserted into the VSC-HVDC control system so that the energy preserved in the DC capacitors can be exploited to provide virtual inertia support.

Not only the DC capacitors in the VSC-HVDC system can be employed for frequency response provision, but the wind turbines in OWPPs can contribute to frequency control as well. According to Chapter 4, the control strategies enabling the wind turbines to participate in frequency regulation can be divided into two groups: EIC and DOPFC [3], [75]. The EIC aims to improve transient performance of system frequency by providing short-term active power support, while the objective of DOPFC is to perform primary frequency control by utilizing the power reserve kept by each wind turbine.

Similar to the control schemes described in [102] and [111], the frequency derivative controller can also be installed into the wind turbine control system so that the EIC can be realized by extracting the kinetic energy preserved in rotor [77-79].

In order to perform DOPFC, each wind turbine should operate in de-loading mode under normal condition to acquire the power reserve. It is noteworthy that the power reserve kept by the wind turbines may be necessary in practice, since the primary reserve provided by CPPs may not be enough to maintain the power system stability, especially if the integration level of wind power is very high. However, the de-loading operation indicates that the wind turbine cannot extract the maximum power from wind [3], [76], [80], [82], [83]. To encourage the OWPPs to keep the power reserve for frequency regulation, the modification of electricity market mechanism may be required [75], [81].

To achieve the objective of DOPFC, the power reserve obtained by each wind turbine should be deployed when frequency deviates. As studied in [3], [76], [80], [83], [84], DOPFC may be realized if a frequency proportional controller, which generates an active power item, is applied into the wind turbine control system. Nevertheless, it seems that these control schemes do not explicitly involve the adjustment of the mechanical power [82]. Hence, the wind turbine may not be able to employ the power reserve for frequency control [78], [82], [85]. According to the research in [82], each wind turbine can also perform DOPFC by regulating the pitch angle. However, it is important to note that the pitch angle variation can result in mechanical fatigue [80]. In [89], a frequency control method including a rotor speed control loop is put forward. As described in that paper, the mechanical power variation is considered, whereas the deployment of the kinetic energy preserved in rotor can be investigated further.

As investigated in Chapter 4, the wind turbine can provide frequency support by utilizing the kinetic energy stored in rotor and the power reserve derived from de-loading operation [89], [90]. In addition, the VSC-HVDC system can also contribute to frequency regulation if the energy preserved in the DC capacitors is deployed [102], [111]. Inspired by the research mentioned above, some coordinated control schemes enabling the VSC-HVDC connected OWPP to provide frequency response are designed in [106], [108], [110], [112-122]. According to the description in [106], [114], [116-118], both the wind turbines and the VSC-HVDC system can be assigned to provide emulated inertia response. In these papers, the realization of EIC is emphasized, while the implementation of DOPFC is not considered. In [108], [110], [112], [113], [115], [119-122], the wind turbines are

arranged to perform DOPFC, but the variation of mechanical power is not discussed thoroughly so that the power reserve may not be employed successfully [78], [82], [85]. It should be pointed out that the wind turbines can react to frequency excursions on condition that the frequency of onshore power system can be sensed by the OWPP [117]. Therefore, a communication system between the main power grid and the offshore wind farm may be necessary [111], [117].

In this chapter, a coordinated frequency control scheme exploiting the available resources provided by the VSC-HVDC system and the wind turbines is presented. In this control scheme, a modified DC-link voltage control is implemented in the VSC-HVDC system to regulate the DC-link voltage. In this way, the DC capacitors can utilize electrical energy to provide frequency response. In addition, an extended rotor speed control is applied in each wind turbine. Such control approach can employ the kinetic energy preserved in rotor and the power reserve obtained from de-loading operation to perform frequency control by adjusting the rotor speed. On detecting the frequency deviation, both the modified DC-link voltage control and the extended rotor speed control will be activated simultaneously to maximize the frequency support provided by the VSC-HVDC system and the OWPP. The simulation study proves that the proposed frequency control strategy is effective.

The rest of this chapter is summarized as follows: the system model used in this study is introduced in Section 5.2. Section 5.3 illustrates the proposed frequency control scheme. Section 5.4 presents the simulation results, and Section 5.5 provides the summary of this research.

## 5.2 System Model for Study

### 5.2.1 Overview of the Studied System

A typical configuration of an OWPP connected to a VSC-HVDC system is shown in Figure 5.1. In this research, 50 PMSG-WTs are installed in the offshore wind farm. According to Figure 5.1, the active power generated by the wind turbines can be collected by the wind farm side voltage source converter (WFS-VSC) in the VSC-HVDC system. The grid side voltage source converter (GS-VSC) can regulate the DC-link voltage, and thus the active power can be transmitted to the onshore power system.

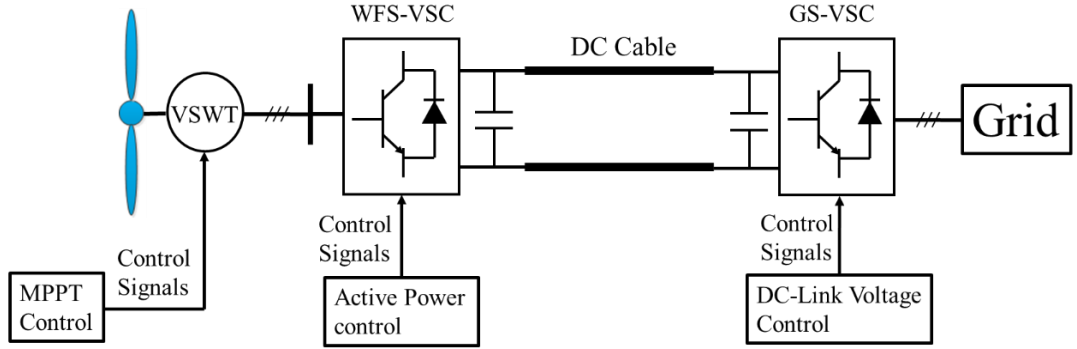


Figure 5.1 Typical layout of an offshore wind farm connected to a VSC-HVDC transmission system

### 5.2.2 Model and Conventional Control of Individual Wind Turbine

According to the characteristics of each wind turbine, the mechanical power  $P_m$  of the PMSG-WT can be calculated as follows [34]:

$$P_m = 0.5C_p(\lambda, \beta)\rho\pi R^2V_w^3 \quad (5.1)$$

$$C_p = 0.5176\left(\frac{116}{\gamma} - 0.4\beta - 5\right)e^{-\frac{21}{\gamma}} + 0.0068\lambda \quad (5.2)$$

$$\gamma = 1 / \left( \frac{1}{\lambda + 0.08\beta} - \frac{0.035}{\beta^3 + 1} \right) \quad (5.3)$$

where  $V_w$  is wind speed;  $R$  is the radius of the blade;  $\rho$  is air density;  $\beta$  is pitch angle;  $\lambda$  is tip speed ratio (TSR);  $C_p$  is power coefficient.

Conventionally, the MPPT control is applied in individual wind turbine to maximize the power captured from wind. As summarized in Chapter 3, reference [37] provides two methods for MPPT realization. Figure 5.2 shows a typical MPPT control strategy, which is applied in this study. In Figure 5.2, the command of rotor speed is represented by  $\omega_{r.ref}$ , while  $\omega_r$  is the real value.  $P_{e.ref}$  denotes the active power reference, and  $\lambda_{opt}$  represents the optimal TSR where the maximum power can be captured from wind.

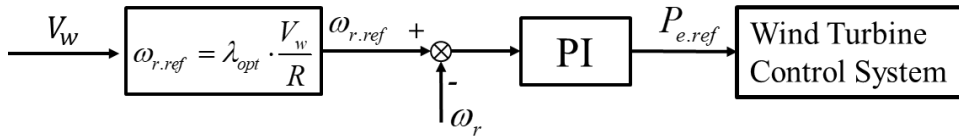


Figure 5.2 A typical MPPT control method used in this research

As discussed in [2], it is essential to establish a two-mass model so that the performance of the drive train system can be described accurately. The details of the two-mass model are provided in Chapter 3.

Moreover, the pitch angle controller is also included into the wind turbine model. If the wind speed is too strong, such controller will be activated in order to prevent the rotor speed from exceeding the upper limit. In this research, the pitch angle controller which is sketched in Figure 4.2 is adopted.

## **5.3 The Proposed Coordinated Frequency Control Strategy for VSC-HVDC Connected Offshore Wind Farm**

### **5.3.1 Overview of the Proposed Control Scheme**

Like the CPPs, the wind turbines should realize de-loading operation rather than MPPT operation in order to acquire the power reserve. Up to now, various methods to achieve de-loading operation are proposed [80]. According to the discussion in Section 4.3.2, the wind turbine can operate in de-loading mode by applying the over-speeding technique. The advantage of the over-speeding technique is that more kinetic energy can be obtained, and such energy can be utilized if necessary. The implementation of over-speeding technique based de-loading operation is also provided in Chapter 4.

The proposed coordinated frequency control approach is sketched in Figure 5.3. The extended rotor speed control, which is implemented in the wind turbine control system, aims at utilizing the kinetic energy preserved in rotor and the power reserve obtained from the de-loading operating mode to perform frequency control. In addition, the modified DC-link voltage control is applied in VSC-HVDC system in order to deploy the electrical energy preserved in DC capacitors to enhance frequency support. After being subjected to disturbance, both the extended rotor speed control and the modified DC-link voltage control will be activated so that all the available resources can be exploited for frequency regulation.

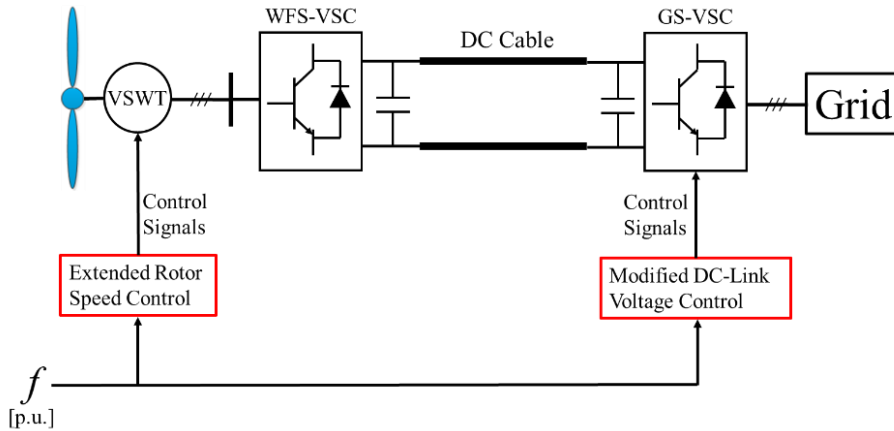


Figure 5.3 Overview of the proposed frequency control scheme

### 5.3.2 Extended Rotor Speed Control Applied in VSWTs

According to the discussion in Chapter 4, each wind turbine can achieve over-speeding technique based de-loading operation by applying the control method depicted in Figure 4.8. Such control scheme is also shown in Figure 5.4. Armed with the control method described in Figure 4.8, the wind turbine can operate at a rotating speed which is higher than the one determined by optimal TSR under normal condition. As a result, not only the power reserve can be acquired, but more kinetic energy can be obtained as well.

In order to employ the kinetic energy and power reserve provided by each wind turbine for frequency regulation, the extended rotor speed control, which is illustrated in Section 4.3.3, can be implemented into the wind turbine control system. The extended rotor speed control designed in Chapter 4 is also presented in Figure 5.5. Such control method can cause the rotor speed to change, and thus the mechanical power can be adjusted. In this way, the usage of power reserve can be realized. In addition, different from the control method discussed in [89], a frequency derivative (D) controller is applied.

Such controller can exploit the kinetic energy preserved in rotor so that the emulated inertia response can be enhanced further.

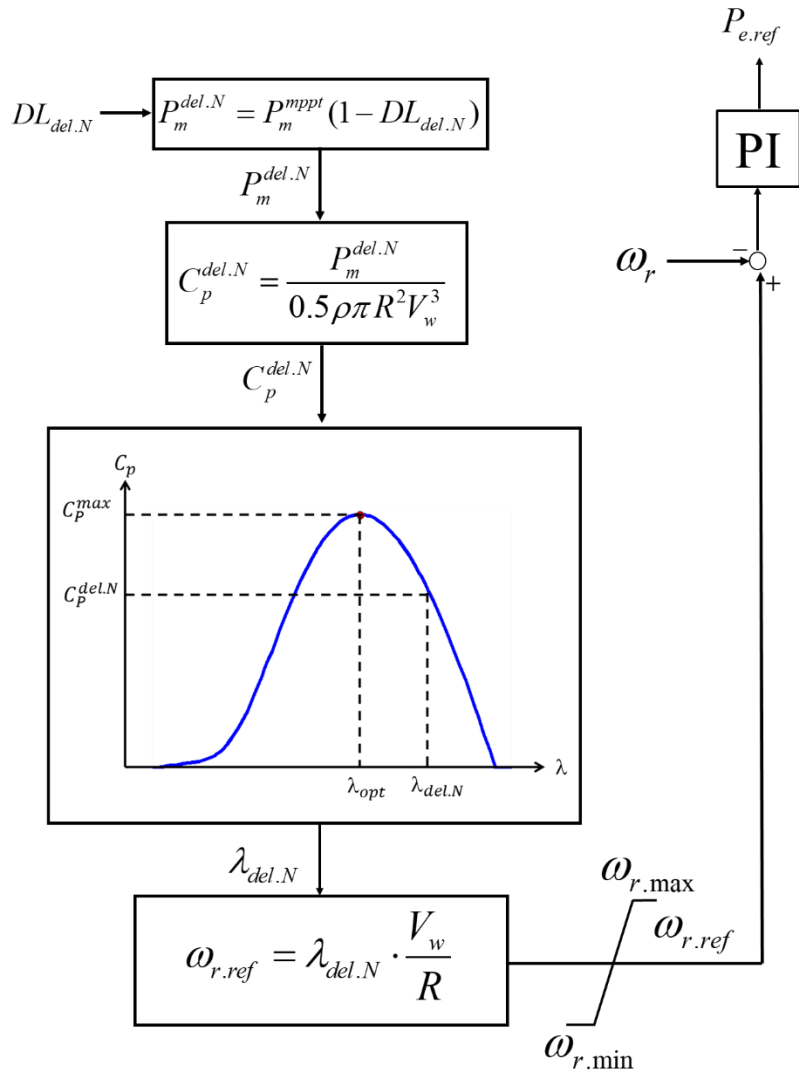


Figure 5.4 Control scheme to achieve de-loading operation

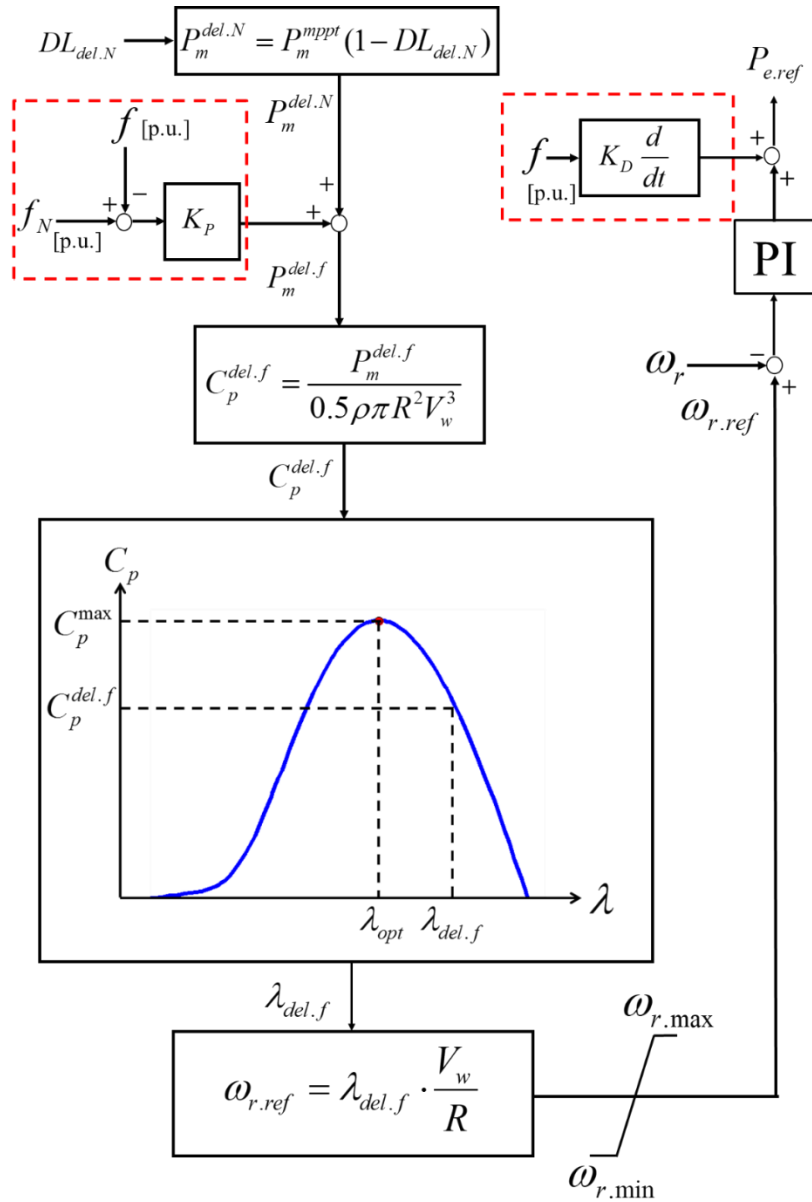


Figure 5.5 Extended rotor speed control scheme used in each VSWT

In Figure 5.5, the real-time system frequency is represented by  $f$ , and the normal system frequency is denoted by  $f_N$ .  $P_m^{del.f}$  is the desired mechanical power which should be captured from wind. To obtain the value of  $P_m^{del.f}$ , the  $P_m^{del.N}$  should be added to the item given by the frequency proportional (P) controller with the parameter  $K_P$ . One

method to determine the value of  $K_p$  is discussed in Section 5.4. If system frequency deviates, the value of  $P_m^{del.f}$  can be generated accordingly, then both the corresponding  $C_p^{del.f}$  and  $\lambda_{del.f}$  can be derived by using (5.1) and the  $C_p - \lambda$  characteristics described in Figure 4.7. By using the value of  $\lambda_{del.f}$ , the reference of rotor speed  $\omega_{r.ref}$  can be acquired and sent to the rotor speed controller. Hence, the wind turbine can be brought to a new operating point.

If the extended rotor speed control depicted in Figure 5.5 is applied, the wind turbine can operate at the sub-optimal point with a certain  $DL_{del.N}$  under normal condition. Once frequency falls, the wind turbine can move towards the optimal operating point by decelerating so that the power coefficient can become higher and more power can be captured by blades. In this way, both the kinetic energy provided by rotor and the power reserve kept in advance can be released and delivered to the power grid for frequency control. On the contrary, the wind turbine will speed up if frequency rises. As a result, the additional active power can be preserved by accelerating and less power can be extracted from wind so that the system power imbalance can be alleviated.

As mentioned in Chapter 4, the wind speed information should be available if the extended rotor speed control is utilized. To acquire the information of wind speed, reference [38] provides a light detection and ranging (LIDAR) system. Such technology is expected to be more mature and cost-effective. In addition, considering that the high wind speed can lead to the activation of the pitch angle control, the effect of pitch angle variation on frequency regulation can be investigated in the future.

### 5.3.3 Modified DC-link Voltage Control Applied in VSC-HVDC

As mentioned in Section 5.2.1, the VSC-HVDC system should regulate the DC-link voltage so that the active power produced by the OWPP can be transmitted to the onshore transmission network. According to the study in [102] and [111], the VSC-HVDC system can offer virtual inertia response by extracting the energy preserved in the DC capacitors. Such idea can be realized by using the modified DC-link voltage control, which can be derived from the frequency D controller [102]:

$$P_{e.hvdc} = U_{DC.hvdc} \cdot C_{DC.hvdc} \frac{dU_{DC.hvdc}}{dt} = K_{D.hvdc} \cdot \frac{df}{dt} \quad (5.4)$$

where the active power released by the DC capacitor is represented by  $P_{e.hvdc}$ , the value of DC-link voltage is denoted by  $U_{DC.hvdc}$ .  $C_{DC.hvdc}$  is the capacitance, and  $K_{D.hvdc}$  is the parameter of the D controller.  $f$  is the real frequency of the main grid.

According to the discussion in Chapter 4, a modified DC-link voltage control for frequency response provision can be obtained from (5.4). Such modified DC-link voltage controller, which is shown in Figure 5.6, can also be applied in VSC-HVDC system. By using this control approach, the DC-link voltage will decrease to release the energy if frequency drops. In addition, the voltage of the DC capacitor can be boosted on condition that the rise of system frequency is detected, and therefore the surplus active power can be stored by the capacitor.

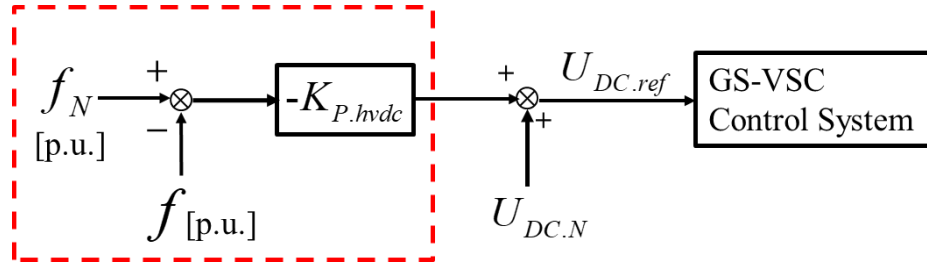


Figure 5.6 Modified DC-link voltage control scheme applied in VSC-HVDC system

## 5.4 Simulation Results

For simulation study, a power system including an offshore wind farm and a VSC-HVDC system is modelled. As shown in Figure 5.7, 50 PMSG-WTs are installed in the offshore wind farm. The OWPP connects to the onshore power system through the VSC-HVDC transmission system. The main power grid consists of two thermal power plants. The rated frequency of the main grid is set as 50 Hz. According to the data listed in [104], the load damping coefficient is set as 1.5. Reference [103] provides the parameters of the two conventional power plants. The parameters of other components can be found in the Appendix.

For comparison, the following control schemes are applied in this study:

**Scheme A:** The MPPT control is used in each wind turbine. Neither the OWPP nor the VSC-HVDC system participates in frequency control.

**Scheme B:** Only the wind turbines installed in the OWPP provide frequency support.

**Scheme C:** Both the VSC-HVDC system and the wind turbines contribute to frequency regulation.

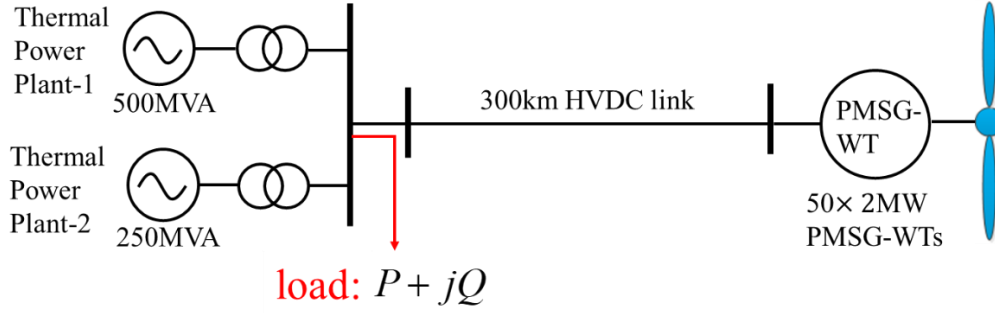


Figure 5.7 Configuration of the power system model for case study

Similar to Section 4.4, the  $DL_{del.N}$  of each wind turbine is fixed as 10%, for this study emphasizes the utilization of the power reserve. Furthermore, the parameter  $K_P$  can be obtained by:

$$K_P = \frac{P_m^{MPPT} - P_m^{del.N}}{f_N - f_{min}^{WT}} \times f_N \quad (5.5)$$

In (5.5),  $f_{min}^{WT}$  denotes the frequency value that requires the wind turbine to attain the optimal power coefficient. If frequency rises, the  $K_P$  obtained from (5.5) can also be applied in the extended rotor speed control. In this research,  $f_{min}^{WT}$  is set as 49.8Hz.

From Figure 5.6, it can be learnt that the setting of  $K_{P,hvdc}$  relates to the variation of DC-link voltage. In this research, the value of  $K_{P,hvdc}$  can be calculated as follows:

$$K_{P,hvdc} = \frac{U_{DC,hvdc.N} - U_{DC,hvdc.min}}{f_N - f_{min}^{hvdc}} \times f_N \quad (5.6)$$

If frequency decreases to  $f_{min}^{hvdc}$ , the minimum DC-link voltage  $U_{DC,hvdc.min}$  can be achieved. Besides, the  $K_{P,hvdc}$  derived from (5.6) is also used in the modified DC-link voltage on detecting an over-frequency event. In this section,  $U_{DC,hvdc.min}$  is set as 0.85

p.u. and the  $f_{min}^{hvd}$  is set as 49.8 Hz. The optimization of these control parameters will be discussed further in the future.

The simulation results under constant wind speed are presented in Section 5.4.1 and 5.4.2. Like the case study in Chapter 4, the final value of system frequency  $f_{final}$ , the frequency nadir  $f_{nadir}$  and the rate of change of frequency (ROCOF) are used to evaluate the frequency performance. It is necessary to note that  $f_{nadir}$  represents the frequency value measured when the maximum dynamic deviation of system frequency is achieved. Furthermore,  $f_{nadir}$  is the peak value of frequency on detecting an over-frequency event. If frequency falls, the lowest value of system frequency should be treated as the  $f_{nadir}$ .

In addition, the case study under variable wind speed is carried out in Section 5.4.3. To describe the frequency performance, the mean value of  $|\Delta f|$ , which is acquired by averaging the absolute value of frequency deviation  $\Delta f$ , and  $f_{nadir}$  are adopted.

#### **5.4.1 System Frequency Decline under Constant Wind Speed**

**Case. A:** If the wind speed is 8m/s, an under-frequency event occurs at 40s because the load increases by (75+j7.5) MVA.

The simulation results of Case. A are presented in Figure 5.8-Figure 5.11. Table 5.1 and Table 5.2 provide the data acquired from the simulation. If Scheme B or Scheme C is applied, each wind turbine can realize de-loading operation. Consequently, under normal condition, the rotor speed of each wind turbine is 0.9473 p.u.. Such value is higher than the rotor speed determined by the optimal TSR, which is 0.8 p.u. in this research.

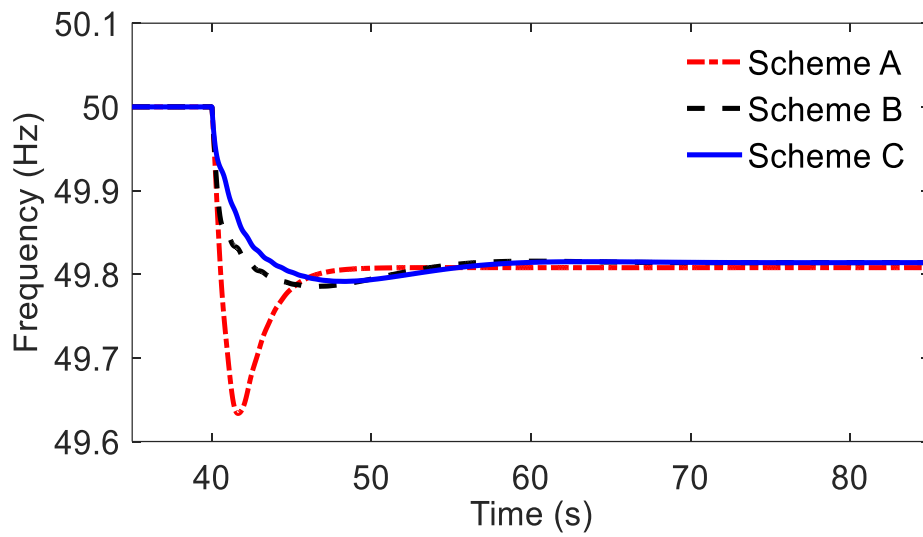


Figure 5.8 Performance of system frequency in Case. A

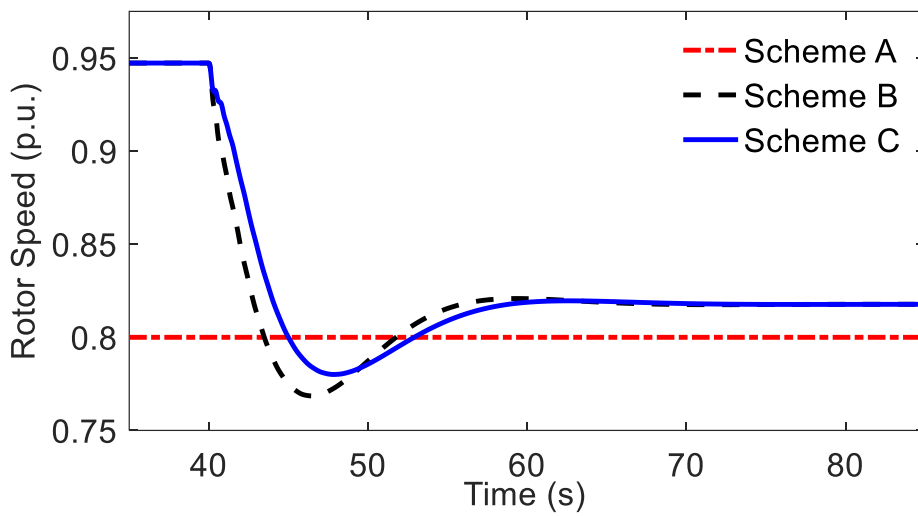


Figure 5.9 Performance of wind turbine rotor speed in Case. A

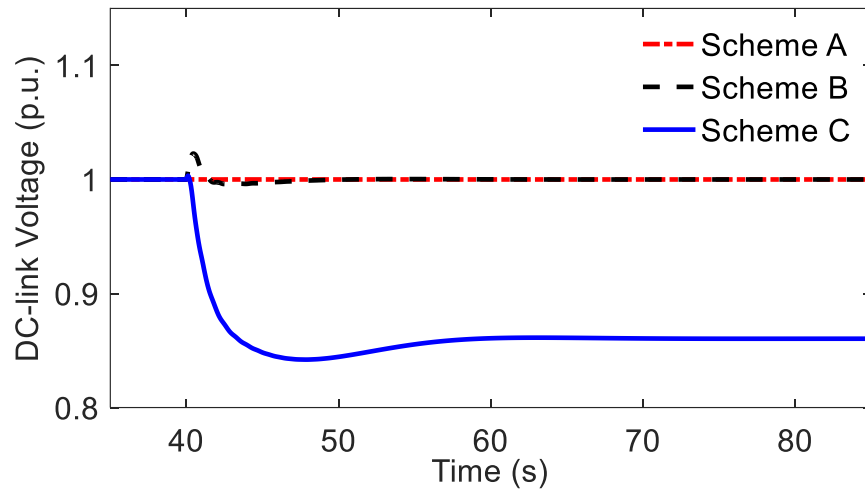


Figure 5.10 Performance of DC-link voltage of the VSC-HVDC system in Case. A

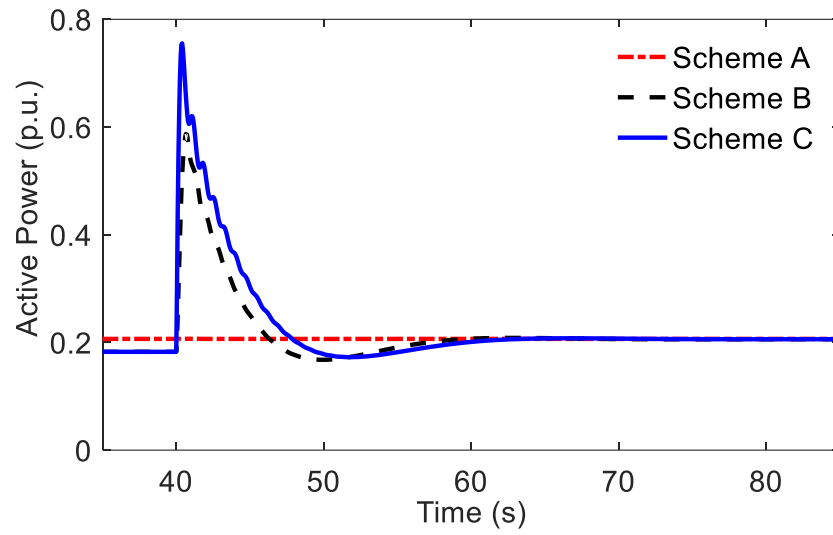


Figure 5.11 Performance of active power injected into the main grid in Case. A

Table 5.1 Frequency performance of Case. A

Schemes	Maximum  ROCOF (Hz/s)	$f_{nadir}$ (Hz)	$f_{final}$ (Hz)
Scheme A	0.3889	49.6336	49.8078
Scheme B	0.3340	49.7853	49.8139
Scheme C	0.3043	49.7914	49.8139

Table 5.2 Wind turbine performance of Case. A

Schemes	Initial Value of $\omega_r$ (p.u.)	Final Value of $\omega_r$ (p.u.)	Initial Value of $P_m$ (p.u.)	Final Value of $P_m$ (p.u.)
Scheme A	0.8	0.8	0.2163	0.2163
Scheme B	0.9473	0.8177	0.1947	0.2160
Scheme C	0.9473	0.8177	0.1947	0.2160

According to Table 5.1 and Table 5.2, the PMSG-WTs with Scheme A can keep the rotor speed constant so that the wind turbines cannot participate in frequency control. Nevertheless, due to the application of Scheme B or Scheme C, the rate of frequency change can be attenuated, and the frequency nadir can become higher. In addition, as the power reserve is released and more active power is generated, the rise in the final value of system frequency can be observed. It is noteworthy that the implementation of Scheme C can lead to the reduction of DC-link voltage. Consequently, the energy preserved in the DC capacitor can be delivered to the main grid, and therefore the transient behavior of onshore system frequency can be improved further.

#### 5.4.2 System Frequency Rise under Constant Wind Speed

**Case. B:** If the wind speed is 8m/s, an over-frequency event occurs at 40s because the load decreases by  $(75+j7.5)$  MVA.

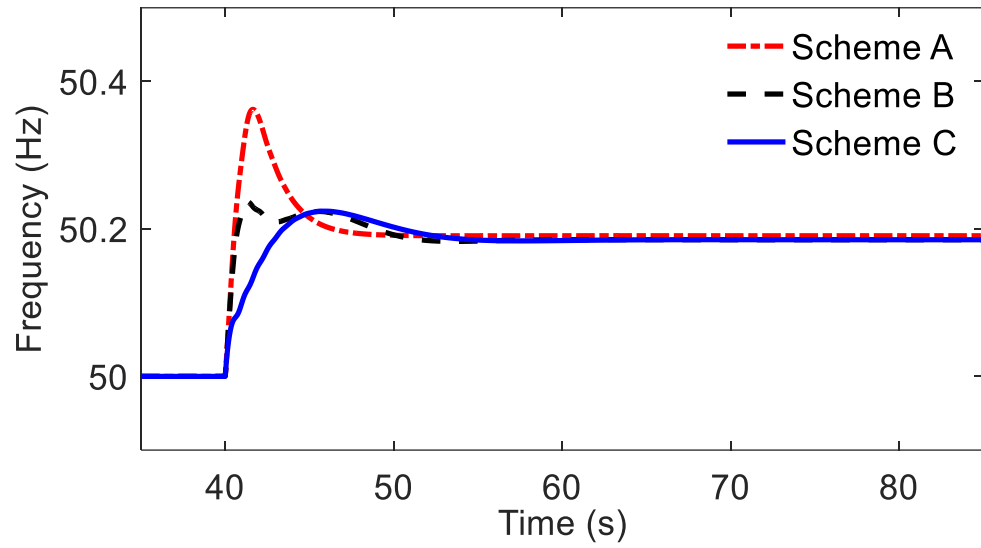


Figure 5.12 Performance of system frequency in Case. B

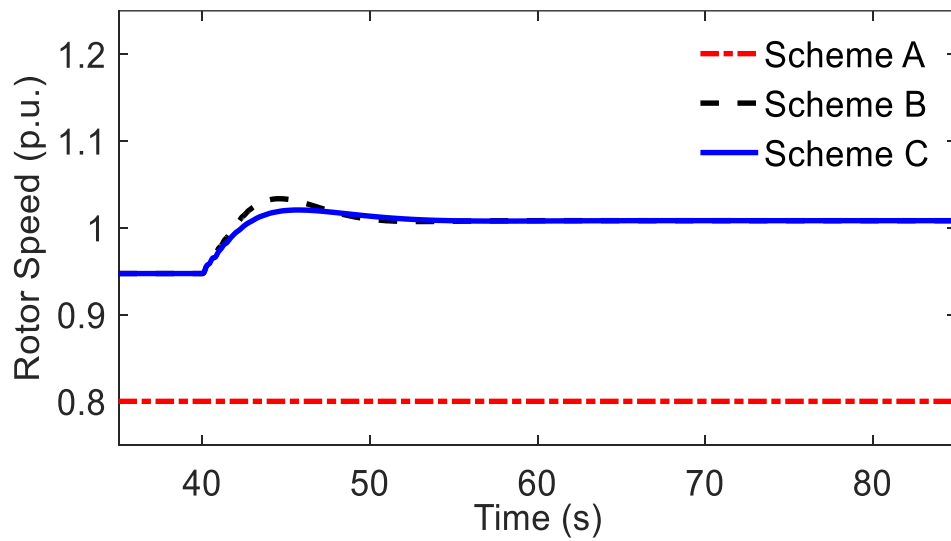


Figure 5.13 Performance of wind turbine rotor speed in Case. B

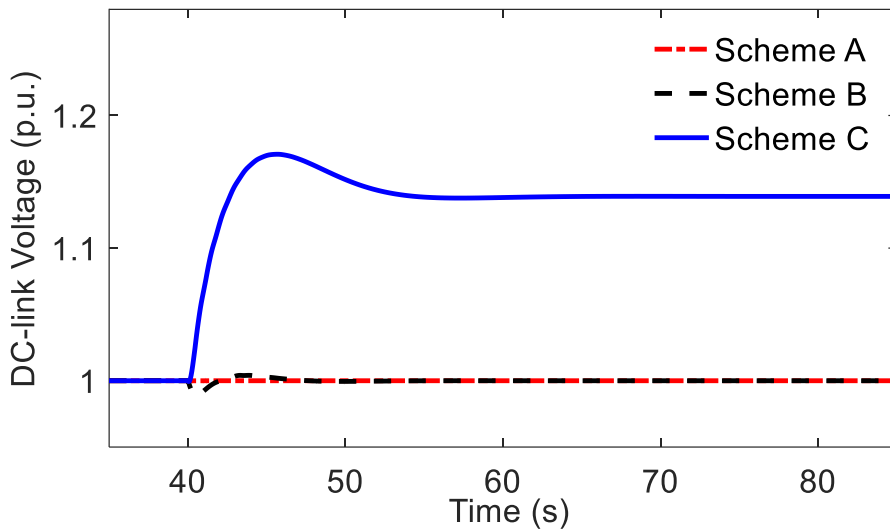


Figure 5.14 Performance of DC-link voltage of the VSC-HVDC system in Case. B

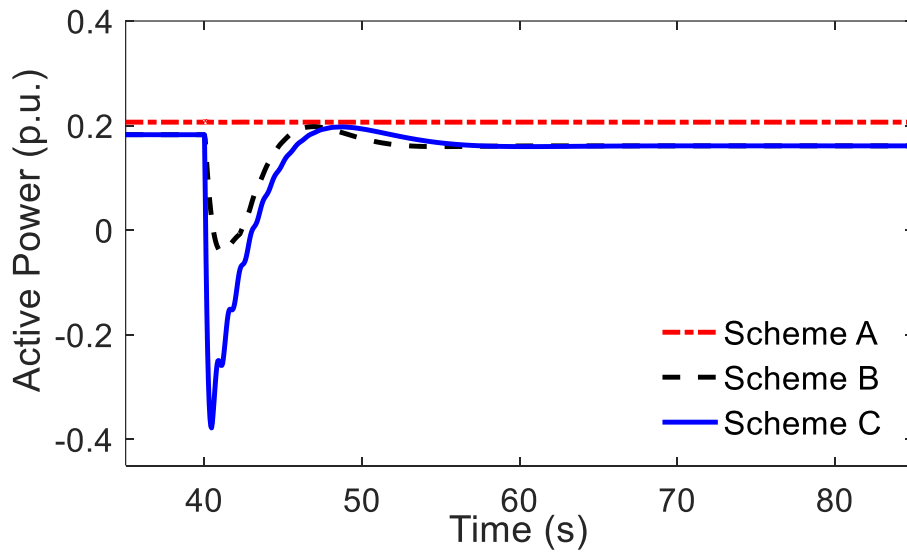


Figure 5.15 Performance of active power injected into the main grid in Case. B

Figure 5.12 and Table 5.3 describe the frequency performance of Case. B. According to the simulation results, if Scheme A is applied and no frequency control actions are performed, both the highest rate of frequency change and the greatest peak value of system

frequency can be acquired. On the contrary, by using Scheme B or Scheme C, such over-frequency event can make the wind turbine accelerate so that the power extracted from the wind can decrease and surplus active power can be absorbed by the rotor. As a result, the power imbalance can be mitigated effectively, and the performance of onshore system frequency can be improved significantly.

Compared to Scheme B, the utilization of the DC capacitor is involved into Scheme C. If frequency rises, the Scheme C will be activated, and thus the DC-link voltage will increase. Therefore, additional active power can be stored into the DC capacitor, and the extra improvement in the transient performance of system frequency can be attained.

Table 5.3 Frequency performance of Case. B

Schemes	Maximum  ROCOF (Hz/s)	$f_{nadir}$ (Hz)	$f_{final}$ (Hz)
Scheme A	0.3832	50.3622	50.1907
Scheme B	0.3412	50.2365	50.1853
Scheme C	0.3105	50.2241	50.1853

Table 5.4 Wind turbine performance of Case. B

Schemes	Initial Value of $\omega_r$ (p.u.)	Final Value of $\omega_r$ (p.u.)	Initial Value of $P_m$ (p.u.)	Final Value of $P_m$ (p.u.)
Scheme A	0.8	0.8	0.2163	0.2163
Scheme B	0.9473	1.0082	0.1947	0.1705
Scheme C	0.9473	1.0082	0.1947	0.1705

### 5.4.3 System Frequency Decline under Variable Wind Speed

*Case. C* If the wind speed is variable, an under-frequency event occurs at 180s because the load increases by (75+j7.5) MVA.

The simulation under variable wind speed is conducted in this section. Figure 5.16 depicts the wind speed profile used for this study. Relevant data can be acquired from [105]. It is noteworthy that the load remains constant from 100s~180s. At 180s, the load rises suddenly.

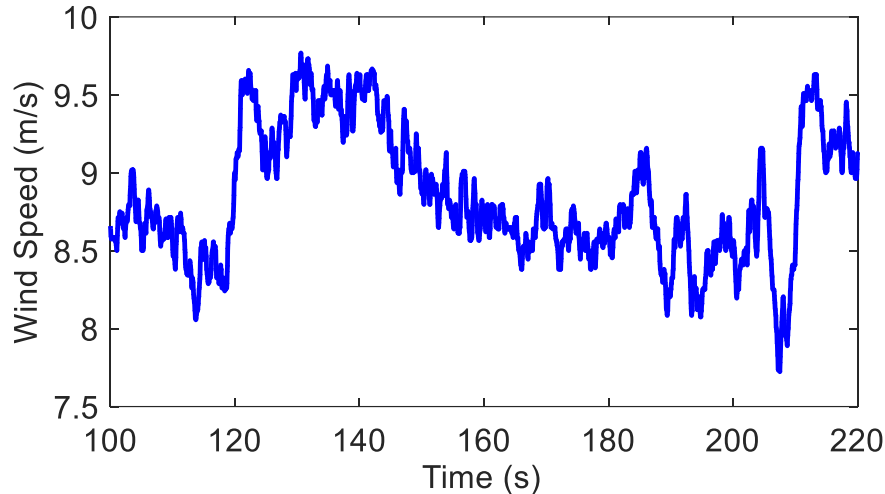


Figure 5.16 Variable wind speed profile used in Case. C

The simulation results during 100s~180s are presented in Figure 5.17-Figure 5.20. Table 5.5 provides the data for the assessment of system frequency. According to the figures, under variable wind speed, both the active power produced by the wind turbines and the frequency of main grid will fluctuate, especially if Scheme A is applied. By using Scheme B or Scheme C, the wind turbines can react to frequency deviation so that the frequency fluctuation can be mitigated. Moreover, the wind turbine with Scheme C can arrange the DC capacitor to participate in frequency regulation, and thus the system frequency can be smoothed further.

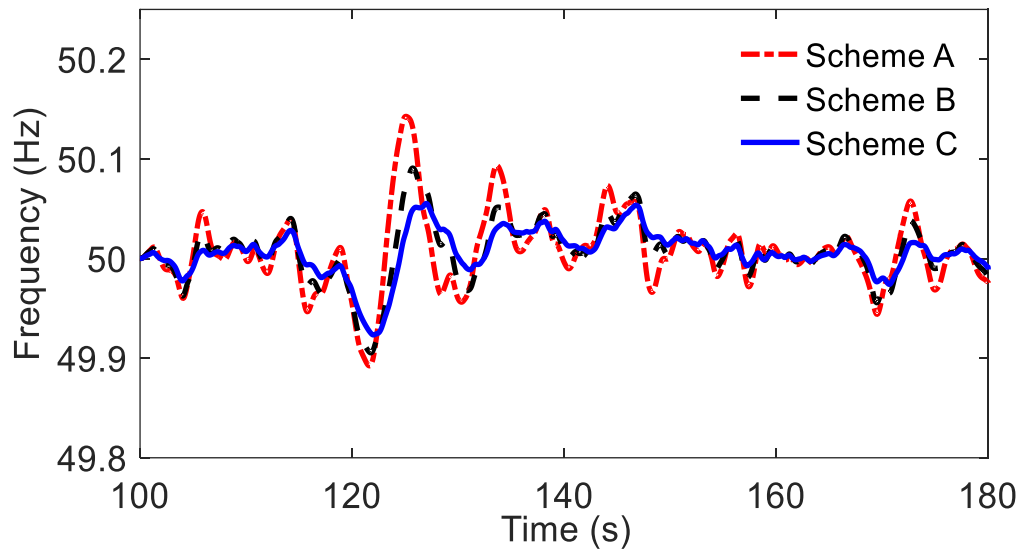


Figure 5.17 Performance of system frequency in Case. C (100~180s)

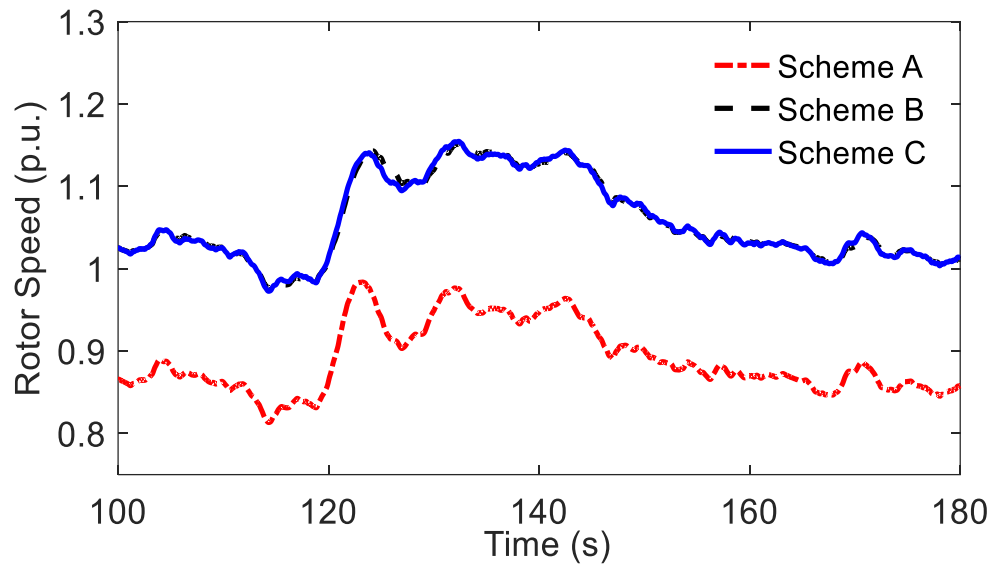


Figure 5.18 Performance of wind turbine rotor speed in Case. C (100~180s)

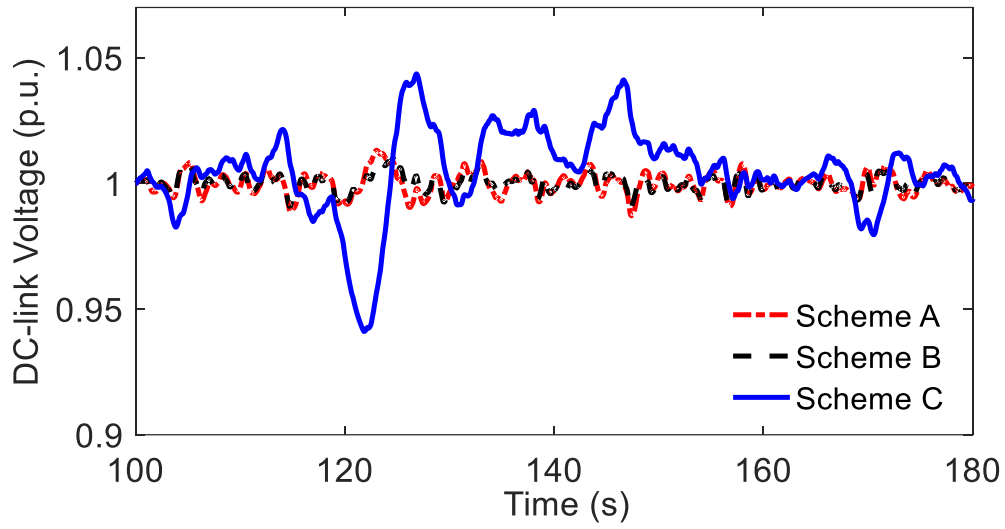


Figure 5.19 Performance of DC-link voltage of the VSC-HVDC system in Case. C (100~180s)

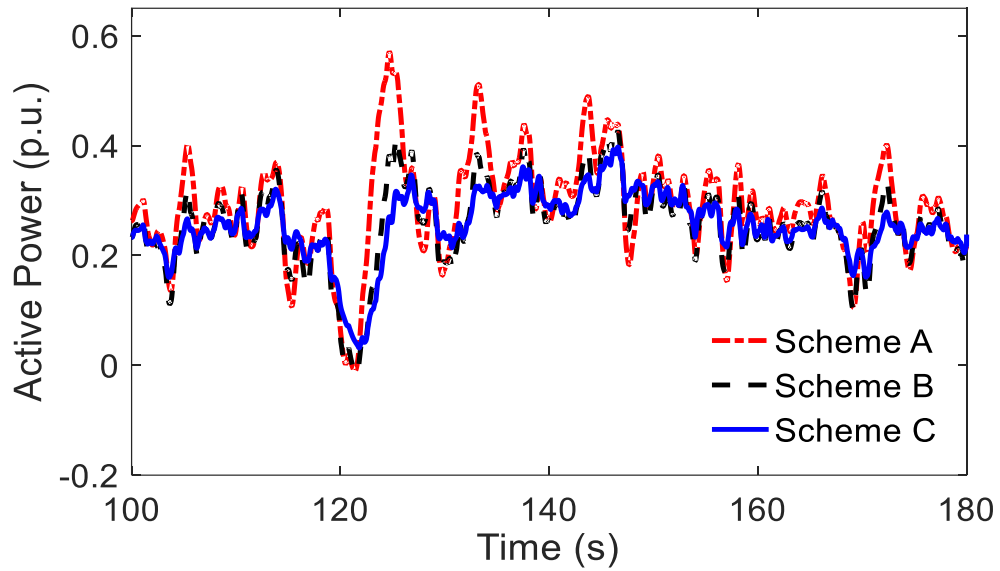


Figure 5.20 Performance of active power injected into the main grid in Case. C (100~180s)

Table 5.5 Frequency performance of Case. C

Schemes	mean value of $ \Delta f $ (Hz) during 100s~180s	$f_{nadir}$ (Hz) during 170s~220s
Scheme A	0.0269	49.6469
Scheme B	0.0217	49.7600
Scheme C	0.0169	49.7691

Figure 5.21 shows the fall of system frequency caused by the load increase. Table 5.5 provides relevant data. The table reveals that the lowest value of  $f_{nadir}$  can be acquired if neither the wind turbines nor the VSC-HVDC system performs frequency control. However, the application of Scheme B or Scheme C can result in the improvement in  $f_{nadir}$ . Moreover, the transient behavior of system frequency can be improved further by using the Scheme C. The reason is that the energy preserved in the DC capacitor can be exploited, and thus additional frequency support can be offered.

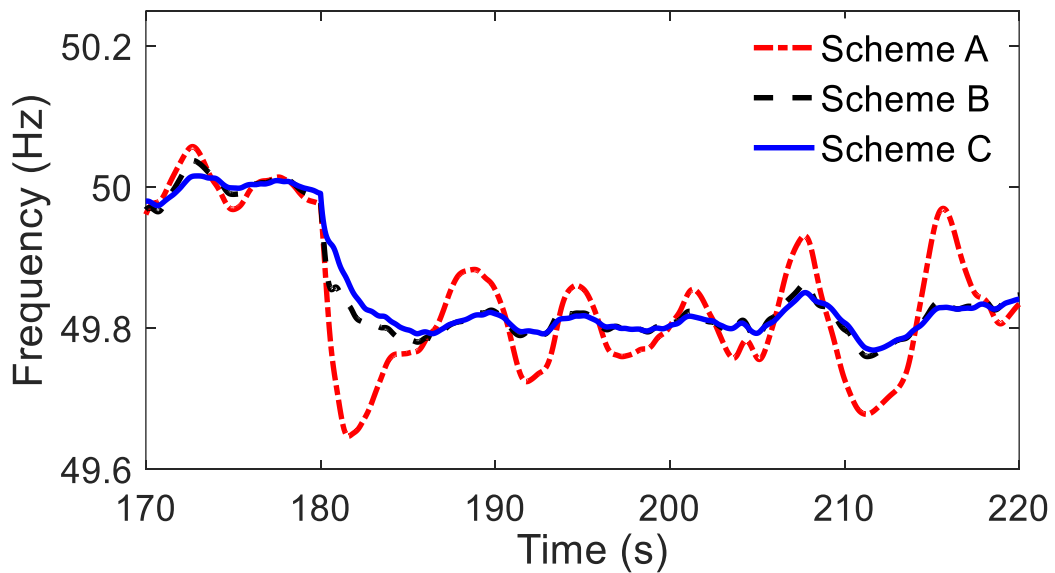


Figure 5.21 Performance of system frequency in Case. C (170~220s)

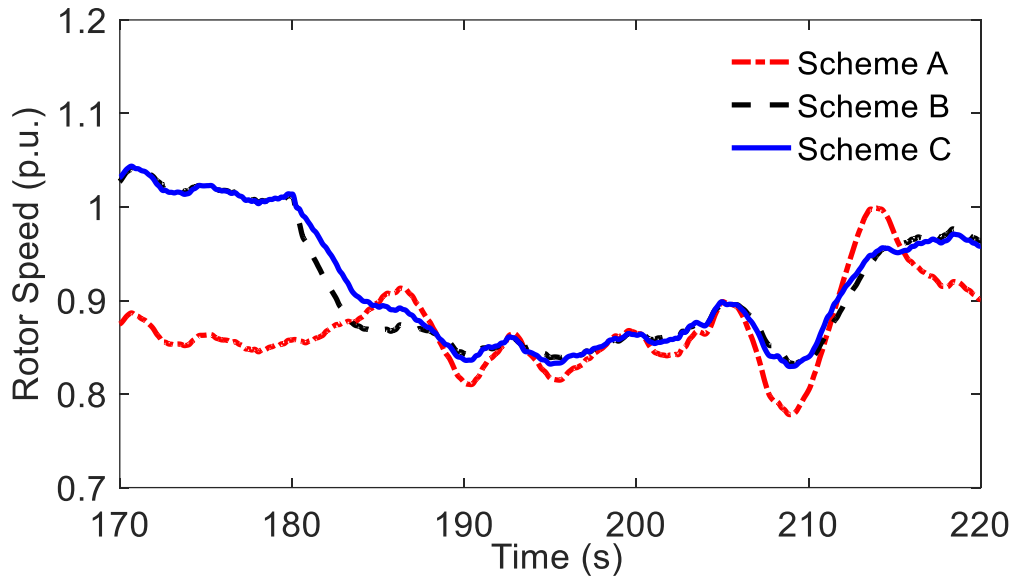


Figure 5.22 Performance of wind turbine rotor speed in Case. C (170~220s)

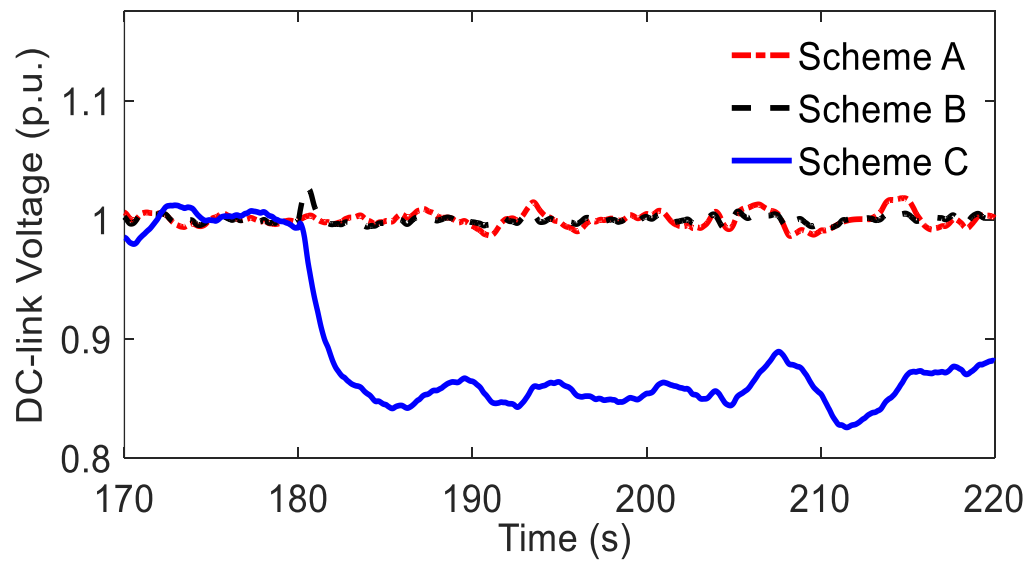


Figure 5.23 Performance of DC-link voltage of the VSC-HVDC system in Case. C (170~220s)

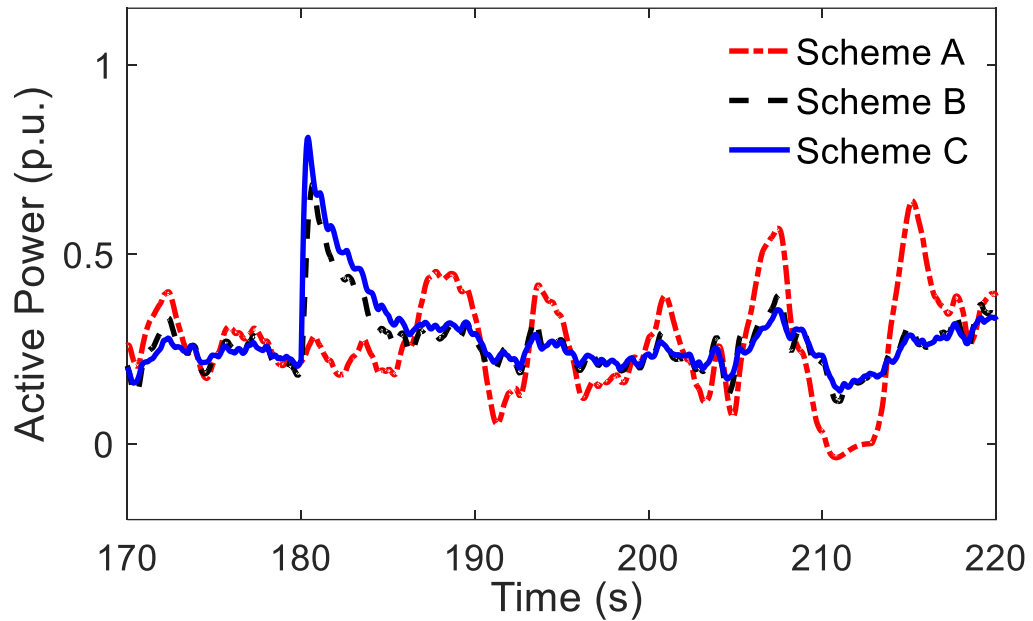


Figure 5.24 Performance of active power injected into the main grid in Case. C (170~220s)

## 5.5 Summary

In order to exploit the available resources provided by the VSC-HVDC system and offshore wind farm to provide frequency response, a coordinated frequency control scheme is presented in this chapter. As soon as frequency deviates, both the modified DC-link voltage control and the extended rotor speed control will be activated. Furthermore, the extended rotor speed control can utilize the kinetic energy preserved in rotor and the power reserve provided by individual wind turbine by adjusting the turbine speed. Besides, the modified DC-link voltage control manages to change the voltage of DC capacitors, and thus the energy stored in the capacitors can also be extracted to perform virtual inertia control. According to the simulation results, the proposed coordinated frequency control scheme can arrange the wind turbines and the VSC-HVDC system to participate in

frequency regulation together so that the performance of onshore system frequency can be improved significantly.

In the future, the amount of power reserve provided by each wind turbine can be investigated. It is noteworthy that the determination of the de-loading level may be associated with power system operation framework and electricity market mechanism. Besides, some dependable methods enabling the offshore wind power plants to acquire the frequency information of onshore power system can be developed. If the PMSG-WTs are erected in the offshore wind farm, the frequency control schemes considering the utilization of the DC capacitors installed in each wind turbine can be discussed further.

## **Chapter 6      Conclusions and Suggestions for Future**

### **Research**

#### **6.1 Conclusions**

The frequency control schemes applied in variable speed wind turbines are emphasized in this thesis. Traditionally, the wind turbines are arranged to maximize the power extracted from wind without providing necessary support to the power system. Since more and more wind turbines are integrated into transmission network, it is expected that they should play an important and active role in power system control and operation.

Considering that the increasing penetration of wind energy may impose challenges to system frequency control, some grid codes issued recently have required the WPPs to contribute to frequency regulation. To satisfy these technical requirements, various advanced control strategies enabling the wind turbines to provide frequency response are proposed in existing research literatures. As the power reserve kept by traditional resources may become exhausted if the integration level of wind energy is too high, some papers recommend that under normal condition, the wind turbines can operate in de-loading mode instead of MPPT mode to acquire power reserve so that the burden of power system can be released to some extent.

For individual PMSG-WT, the energy preserved in DC capacitor, the kinetic energy stored in rotor and the power reserve obtained from de-loading operation can be utilized for frequency regulation. However, from the literature review provided in this thesis, it can be learnt that limited research on exploiting all these resources to perform frequency control has been carried out.

To maximize the frequency support provided by the PMSG-WT as much as possible, a combined primary frequency control scheme is developed in this study. Such control scheme includes a modified DC-link voltage control and an extended rotor speed control. If the proposed control strategy is applied, both the kinetic energy stored in rotor and the power reserve acquired from de-loading operation can be employed to provide frequency response. Meanwhile, the deployment of DC capacitor for frequency control is also involved in the proposed control scheme to improve frequency performance further. The advantage of the proposed control scheme can be proved through simulation. It is noteworthy that the extended rotor speed control can also be implemented in each DFIG-WT so that the power reserve and kinetic energy offered by the DFIG-WT can be utilized together to enhance frequency support.

Based on the combined primary frequency control strategy described in Chapter 4, a coordinated frequency control scheme for the offshore wind power plant integrated via VSC-HVDC system is designed in Chapter 5. In this control method, the extended rotor speed control is implemented in each wind turbine so that the power reserve kept in advance and kinetic energy preserved in rotor can be deployed to provide frequency response. In addition, the modified DC-link voltage control is applied in the VSC-HVDC

system, and thus the DC capacitors can participate in frequency control at the same time. The simulation results prove that by using the proposed coordinated frequency control scheme, the frequency performance can be improved significantly.

## **6.2 Suggestions for Future Research**

In this thesis, the combined frequency control strategy is designed for individual PMSG-WT. Such frequency control methodology can also be applied in the offshore wind farm connected to VSC-HVDC transmission system. Based on this study, the following topics can be investigated in the future.

### **6.2.1 Improvement of Proposed Frequency Control Schemes**

The research in this thesis focuses on how to deploy the power reserve offered by each wind turbine to provide frequency response. For simplicity of the simulation test, the de-loading level of individual wind turbine is fixed. In the future, the amount of de-loading level can be discussed further. Besides, in order to implement the proposed control schemes, it is essential to investigate the setting of the control parameters by using some methods such as frequency domain response or root-locus analysis. Furthermore, to prove the advantage of these control schemes, a more complicated and realistic power system model should be set up for case study.

In addition, as the DC capacitors installed in each wind turbine or VSC-HVDC system are assigned to provide frequency support by adjusting the DC-link voltage, the methods to restore the DC-link voltage can be explored.

### **6.2.2 The Impacts of Proposed Frequency Control Schemes**

The impact of conventional frequency control methods used in wind turbines on power system performance is analyzed in [123]. If these frequency control schemes are replaced by the ones proposed in this thesis, the model of the whole system should be modified, and thus the effect on the power system should be studied again. Particularly, considering that no additional energy storage systems are involved in the proposed control schemes, the region of the frequency and voltage control should be investigated further.

Besides, the penetration level of wind energy can be limited, because the power fluctuation can lead to frequency deviation [124]. A method to estimate the penetration limit of wind power is provided in [124]. As some new frequency control approaches are discussed in this research, it would be interesting to examine that whether the penetration limit of wind energy will change if these control methods are applied in VSWTs.

### **6.2.3 Development of Multiple Wind Turbines Control Schemes**

This thesis emphasizes the design of frequency control schemes implemented in individual VSWT. Based on this research, the control framework of multiple wind turbines or a wind farm can be developed in the future. Recent studies on this topic have been provided in [125-127]. The control strategies proposed in [125] and [126] are based on the conventional frequency control schemes used in each wind turbine, while [127] aims to optimize the power extracted by the whole wind farm. In addition, some advanced multi-agents control theories such as distributed control methods and mean-field theory based control approach have been developed by the experts on mathematics and

cybernetics [128]. Based on these achievements and the research in this thesis, it would be interesting to explore novel control schemes for multiple wind turbines or a wind farm.



## Appendices

### A. Parameters Used in Chapter 3

Wind turbine: Rated wind speed is 12m/s; inertia constant of wind turbine is 3s; time constant of pitch servo is 0.25s; the damping coefficient of turbine is 0.01 p.u.; the damping coefficient of shaft is 0.01 p.u.; the stiffness of shaft is 0.5 p.u..

DFIG: Base power is 1.5MW, Base voltage is 575V; Base current is 1505A; the maximum power is 1.1 p.u.; the synchronous speed is 1 p.u.; the rated rotor speed is 1.1 p.u.; inertia constant of generator is 0.5s; stator leakage inductance is 0.171 p.u.; rotor leakage inductance is 0.156 p.u.; mutual inductance is 3.5 p.u.; the rated DC-link voltage is 1200V; the damping coefficient of rotor is 0.01 p.u..

### B. Parameters Used in Chapter 4

(1) Parameters of the wind turbine:

WT: Rated wind speed is 13.33m/s; inertia constant  $H_t = 2.5s$ ; damping coefficient  $D_{sh} = 1.11p.u.$ ; shaft stiffness coefficient  $K_{sh} = 1.5p.u.$ ; time constant of the pitch servo  $T_p = 0.25s$ ;  $\beta_{max} = 27deg$ .

PMSG: Rated power is 2MW; inertia constant  $H_g = 0.62s$ ; friction coefficient  $B = 0.01p.u.$ ; stator resistance  $R_s = 0.006p.u.$ , d-axis synchronous reactance (p.u.):  $x_d = 1.305$ ,  $x'_d = 0.296$ ,  $x''_d = 0.252$ ; q-axis synchronous reactance (p.u.):  $x_q = 0.474$ ,  $x'_q = 0.474$ ,  $x''_q = 0.243$ ,  $U_{dc.N} = 2000V$ ,  $C_{dc} = 1500000\mu f$ ,  $L_g = 0.15p.u.$ ,  $R_g = 0.003p.u.$

(2) Parameter of excitation system in thermal power plant 1&2:

Regulator gain  $K_{ES} = 300$ ; time constant  $T_{ES} = 0.01s$ .

(3) Parameter of governor in thermal power plant-1:

Servo-motor time constant  $T_{sm} = 0.025s$ , gate closing rate  $V_{G.MIN} = -0.1 p.u./s$ ; gate opening rate  $V_{G.MAX} = 0.1 p.u./s$ ; Governor time constants  $T_2 = 0s$ ,  $T_3 = 0.3s$ ,  $T_4 = 4s$ ,  $T_5 = 0.1s$ ; Turbine torque fractions  $F_2 = 0$ ,  $F_3 = 0.3$ ,  $F_4 = 0.4$ ,  $F_5 = 0.3$ ; droop value  $R_p = 4\%$ .

(4) Parameter of governor in thermal power plant-2:

Servo-motor time constant  $T_{sm} = 0.025s$ , gate closing rate  $V_{G.MIN} = -0.1 p.u./s$ ; gate opening rate  $V_{G.MAX} = 0.1 p.u./s$ ; Governor time constants  $T = 0.2s$ ; droop value  $R_p = 4\%$

(5) Parameter of synchronous generator in thermal power plant-1:

Nominal power 50 MVA; d-axis synchronous reactance:  $x_d = 2.54 p.u.$ ,  $x'_d = 0.237 p.u.$ ,  $x''_d = 0.183 p.u.$ ; q-axis synchronous reactance  $x_q = 2.31 p.u.$ ,  $x'_q = 0.392 p.u.$ ,  $x''_q = 0.191 p.u.$ ; inertial constant 5s; friction factor 0.01; stator resistance 0.0021 p.u.

(6) Parameter of synchronous generator in thermal power plant-2:  
 Nominal power:25 MVA; d-axis synchronous reactance:  $x_d=2.349$  p.u.,  $x'_d=0.219$  p.u.,  $x''_d=0.169$  p.u.; q-axis synchronous reactance  $x_q=2.136$  p.u.,  $x'_q=0.362$  p.u.,  $x''_q=0.177$  p.u.; inertial constant 5s; friction factor 0.01; stator resistance 0.002 p.u.

### C. Parameters Used in Chapter 5

(1) Parameters of the wind turbine:

WT: Rated wind speed is 13.33m/s; inertia constant  $H_t = 2.5$ s; damping coefficient  $D_{sh} = 1.11$ p. u.; shaft stiffness coefficient  $K_{sh} = 1.5$ p. u.; time constant of the pitch servo  $T_{servo} = 0.25$ s;  $\beta_{max} = 27deg$ .

PMSG: Rated power is 2MW; inertia constant  $H_g = 0.62$ s; friction coefficient  $B = 0.01$ p.u. ; stator resistance  $R_s = 0.006$ p.u , d-axis synchronous reactance (p.u.):  $x_d=1.305$ ,  $x'_d=0.296$ ,  $x''_d=0.252$ ; q-axis synchronous reactance (p.u.):  $x_q=0.474$ ,  $x'_q=0.474$ ,  $x''_q=0.243$ ,  $L_g = 0.15$ p.u.,  $R_g = 0.003$ p.u..

(2) Parameter of excitation system in thermal power plant 1&2:

Regulator gain  $K_{ES} = 300$ ; time constant  $T_{ES} = 0.01$ s.

(3) Parameter of governor in thermal power plant-1:

Servo-motor time constant  $T_{sm} = 0.025$ s, gate closing rate  $V_{G.MIN} -0.1$  p.u./s; gate opening rate  $V_{G.MAX} 0.1$  p.u./s; Governor time constants  $T_2=0$ s,  $T_3=0.3$ s,  $T_4=4$ s,  $T_5=0.1$ s; Turbine torque fractions  $F_2=0$ ,  $F_3=0.3$ ,  $F_4=0.4$ ,  $F_5=0.3$ ; droop value  $R_p=4\%$ .

(4) Parameter of governor in thermal power plant-2:

Servo-motor time constant  $T_{sm} = 0.025$ s, gate closing rate  $V_{G.MIN} -0.1$  p.u./s; gate opening rate  $V_{G.MAX} 0.1$  p.u./s; Governor time constants  $T=0.2$ s; droop value  $R_p=4\%$

(5) Parameter of synchronous generator in thermal power plant-1:

Nominal power 500 MVA; d-axis synchronous reactance:  $x_d=2.54$  p.u.,  $x'_d=0.237$  p.u.,  $x''_d=0.183$  p.u.; q-axis synchronous reactance  $x_q=2.31$  p.u.,  $x'_q=0.392$  p.u.,  $x''_q=0.191$  p.u.; inertial constant 5s; friction factor 0.01; stator resistance 0.0021 p.u.

(6) Parameter of synchronous generator in thermal power plant-2:

Nominal power:250 MVA; d-axis synchronous reactance:  $x_d=2.349$  p.u.,  $x'_d=0.219$  p.u.,  $x''_d=0.169$  p.u.; q-axis synchronous reactance  $x_q=2.136$  p.u.,  $x'_q=0.362$  p.u.,  $x''_q=0.177$  p.u.; inertial constant 5s; friction factor 0.01; stator resistance 0.002 p.u.

(7) Parameters of VSC-HVDC system:

Rated VSC AC rms voltage:110kV; nominal DC voltage: 200kV; DC capacitance: 10000uF; resistance of DC cable: 0.015ohm/km; inductance of DC cable: 0.792mH/km; capacitance of DC cable:  $14.4 \times 10^{-9}$ F/m.

## References

- [1] "GLOBAL WIND ENERGY OUTLOOK 2016," Global Wind Energy Council.
- [2] V. Akhmatov, *Induction generators for wind power*. Multi-Science Pub., 2005.
- [3] R. G. d. Almeida and J. A. P. Lopes, "Participation of Doubly Fed Induction Wind Generators in System Frequency Regulation," *IEEE Transactions on Power Systems*, vol. 22, no. 3, pp. 944-950, 2007.
- [4] D. Ochoa and S. Martinez, "Fast-Frequency Response Provided by DFIG-Wind Turbines and its Impact on the Grid," *IEEE Transactions on Power Systems*, vol. 32, no. 5, pp. 4002-4011, 2017.
- [5] S. Ghosh, S. Kamalasadán, N. Senroy, and J. Enslin, "Doubly Fed Induction Generator (DFIG)-Based Wind Farm Control Framework for Primary Frequency and Inertial Response Application," *IEEE Transactions on Power Systems*, vol. 31, no. 3, pp. 1861-1871, 2016.
- [6] D. Gautam, V. Vittal, and T. Harbour, "Impact of Increased Penetration of DFIG-Based Wind Turbine Generators on Transient and Small Signal Stability of Power Systems," *IEEE Transactions on Power Systems*, vol. 24, no. 3, pp. 1426-1434, 2009.
- [7] B. Singh and S. N. Singh, "Wind Power Interconnection into the Power System: A Review of Grid Code Requirements," *The Electricity Journal*, vol. 22, no. 5, pp. 54-63, 2009/06/01/ 2009.
- [8] M. Altin, G. Ö, R. Teodorescu, P. Rodriguez, B. B. Jensen, and L. Helle, "Overview of recent grid codes for wind power integration," in *2010 12th International Conference on Optimization of Electrical and Electronic Equipment*, 2010, pp. 1152-1160.
- [9] M. Tsili and S. Papathanassiou, "A review of grid code technical requirements for wind farms," *IET Renewable Power Generation*, vol. 3, no. 3, pp. 308-332, 2009.
- [10] G. C. Tarnowski, P. C. Kjar, P. E. Sorensen, and J. Ostergaard, "Variable speed wind turbines capability for temporary over-production," in *2009 IEEE Power & Energy Society General Meeting*, 2009, pp. 1-7.
- [11] L. R. Chang-Chien, W. T. Lin, and Y. C. Yin, "Enhancing Frequency Response Control by DFIGs in the High Wind Penetrated Power Systems," *IEEE Transactions on Power Systems*, vol. 26, no. 2, pp. 710-718, 2011.
- [12] N. R. Ullah, T. Thiringer, and D. Karlsson, "Voltage and Transient Stability Support by Wind Farms Complying With the E.ON Netz Grid Code," *IEEE Transactions on Power Systems*, vol. 22, no. 4, pp. 1647-1656, 2007.
- [13] L. Yang, Z. Xu, J. Ostergaard, Z. Y. Dong, and K. P. Wong, "Advanced Control Strategy of DFIG Wind Turbines for Power System Fault Ride Through," *IEEE Transactions on Power Systems*, vol. 27, no. 2, pp. 713-722, 2012.
- [14] D. Xie, Z. Xu, L. Yang, J. Østergaard, Y. Xue, and K. P. Wong, "A Comprehensive LVRT Control Strategy for DFIG Wind Turbines With Enhanced

- Reactive Power Support," *IEEE Transactions on Power Systems*, vol. 28, no. 3, pp. 3302-3310, 2013.
- [15] M. Mohseni and S. M. Islam, "Review of international grid codes for wind power integration: Diversity, technology and a case for global standard," *Renewable and Sustainable Energy Reviews*, vol. 16, no. 6, pp. 3876-3890, 2012/08/01/ 2012.
- [16] X. Liu, Z. Xu, and K. P. Wong, "Recent advancement on technical requirements for grid integration of wind power," *Journal of Modern Power Systems and Clean Energy*, vol. 1, no. 3, pp. 216-222, 2013.
- [17] *Technical regulation 3.2.5 for wind power plants with a power output greater than 11 kW.*, 2010.
- [18] *Requirements for Offshore Grid Connections in the Grid of TenneT TSO GmbH*, 2012.
- [19] *ISO Rules Part 502 Facilities Division 502 Technical Requirements Section 502.1 Wind Aggregated Generating Facilities Technical Requirements.*, 2013.
- [20] *EirGrid Grid Code Version 4.0*, 2012.
- [21] *Technical rule for connecting Wind Farm to power network.*, 2009.
- [22] A. D. Hansen, P. Sørensen, F. Iov, and F. Blaabjerg, "Centralised power control of wind farm with doubly fed induction generators," *Renewable Energy*, vol. 31, no. 7, pp. 935-951, 2006/06/01/ 2006.
- [23] S.-I. Moon, G.-C. Pyo, and J.-W. Park, "Study on development of Grid code and operation scheme of Jeju Island with high wind penetration," in *Proceedings of the 21st world energy congress, Montréal, Canada*, 2010, pp. 12-16.
- [24] A. M. Howlader, N. Urasaki, A. Yona, T. Senjyu, and A. Y. Saber, "A review of output power smoothing methods for wind energy conversion systems," *Renewable and Sustainable Energy Reviews*, vol. 26, pp. 135-146, 2013/10/01/ 2013.
- [25] A. Uehara *et al.*, "A coordinated control method to smooth wind power fluctuations of a PMSG-based WECS," *IEEE Transactions on energy conversion*, vol. 26, no. 2, pp. 550-558, 2011.
- [26] C. Jauch, *Stability and control of wind farms in power systems*. October, 2006.
- [27] T. Domínguez *et al.*, "Renewable energy supervision and real time production control in Spain," in *Int. Conf. on Renewable Energies and Power Quality, OCREPQ*, 2008, vol. 8, pp. 1-6.
- [28] A. D. Hansen and L. H. Hansen, "Market penetration of wind turbine concepts over the years," in *Proc. of EWEC*, 2007, vol. 2007.
- [29] *Specifications for Connecting Wind Farms to the Transmission Network – Second Edition*, 2000.
- [30] S. Musunuri and H. L. Ginn, "A fast maximum power extraction algorithm for wind energy systems," in *2011 IEEE Power and Energy Society General Meeting*, 2011, pp. 1-7.
- [31] W. Qiuwei, X. Zhao, and J. Østergaard, "Grid integration issues for large scale wind power plants (WPPs)," in *IEEE PES General Meeting*, 2010, pp. 1-6.

- [32] C. Abbey and G. Joos, "Effect of low voltage ride through (LVRT) characteristic on voltage stability," in *IEEE Power Engineering Society General Meeting, 2005*, 2005, pp. 1901-1907 Vol. 2.
- [33] A. Arulampalam, G. Ramtharan, N. Jenkins, V. K. Ramachandaramurthy, J. B. Ekanayake, and G. Strbac, "Trends in wind power technology and grid code requirements," in *2007 International Conference on Industrial and Information Systems*, 2007, pp. 129-134.
- [34] S. Heier, "Grid integration of wind energy conversion systems," *ISBN 0*, vol. 471, p. 97143, 1998.
- [35] S. Mueen *et al.*, "Comparative study on transient stability analysis of wind turbine generator system using different drive train models," *IET Renewable Power Generation*, vol. 1, no. 2, pp. 131-141, 2007.
- [36] N. A. Orlando, M. Liserre, R. A. Mastromauro, and A. Dell'Aquila, "A survey of control issues in PMSG-based small wind-turbine systems," *IEEE transactions on Industrial Informatics*, vol. 9, no. 3, pp. 1211-1221, 2013.
- [37] R. Pena, J. Clare, and G. Asher, "Doubly fed induction generator using back-to-back PWM converters and its application to variable-speed wind-energy generation," *IEE Proceedings-Electric Power Applications*, vol. 143, no. 3, pp. 231-241, 1996.
- [38] A. Koerber and R. King, "Combined Feedback-Feedforward Control of Wind Turbines Using State-Constrained Model Predictive Control," *IEEE Transactions on Control Systems Technology*, vol. 21, no. 4, pp. 1117-1128, 2013.
- [39] S. Musunuri and H. L. Ginn, "Comprehensive review of wind energy maximum power extraction algorithms," in *2011 IEEE Power and Energy Society General Meeting*, 2011, pp. 1-8.
- [40] M. Cirrincione, M. Pucci, and G. Vitale, "Growing neural gas (GNG)-based maximum power point tracking for high-performance wind generator with an induction machine," *IEEE Transactions on Industry Applications*, vol. 47, no. 2, pp. 861-872, 2011.
- [41] S. M. R. Kazmi, H. Goto, H.-J. Guo, and O. Ichinokura, "A novel algorithm for fast and efficient speed-sensorless maximum power point tracking in wind energy conversion systems," *IEEE Transactions on Industrial Electronics*, vol. 58, no. 1, pp. 29-36, 2011.
- [42] J. Chen, J. Chen, and C. Gong, "Constant-bandwidth maximum power point tracking strategy for variable-speed wind turbines and its design details," *IEEE Transactions on Industrial Electronics*, vol. 60, no. 11, pp. 5050-5058, 2013.
- [43] B. Ni and C. Sourkounis, "Energy yield and power fluctuation of different control methods for wind energy converters," in *Industry Applications Society Annual Meeting (IAS), 2010 IEEE*, 2010, pp. 1-7: IEEE.
- [44] R. Cardenas, R. Peña, S. Alepuz, and G. Asher, "Overview of control systems for the operation of DFIGs in wind energy applications," *IEEE Transactions on Industrial Electronics*, vol. 60, no. 7, pp. 2776-2798, 2013.

- [45] N. Freire, J. Estima, and A. Cardoso, "A comparative analysis of PMSG drives based on vector control and direct control techniques for wind turbine applications," *Przeegląd Elektrotechniczny*, vol. 88, no. 1, pp. 184-187, 2012.
- [46] J. Mohammadi, S. Vaez-Zadeh, S. Afsharnia, and E. Daryabeigi, "A combined vector and direct power control for DFIG-based wind turbines," *IEEE Transactions on Sustainable Energy*, vol. 5, no. 3, pp. 767-775, 2014.
- [47] X. Wang, X. Ruan, S. Liu, and K. T. Chi, "Full feedforward of grid voltage for grid-connected inverter with LCL filter to suppress current distortion due to grid voltage harmonics," *IEEE Transactions on Power Electronics*, vol. 25, no. 12, pp. 3119-3127, 2010.
- [48] D. Chen, J. Zhang, and Z. Qian, "An improved repetitive control scheme for grid-connected inverter with frequency-adaptive capability," *IEEE Transactions on Industrial Electronics*, vol. 60, no. 2, pp. 814-823, 2013.
- [49] S. A. Amamra, K. Meghriche, A. Cherifi, and B. Francois, "Multilevel Inverter Topology for Renewable Energy Grid Integration," *IEEE Transactions on Industrial Electronics*, vol. 64, no. 11, pp. 8855-8866, 2017.
- [50] J. Morren and S. W. De Haan, "Ridethrough of wind turbines with doubly-fed induction generator during a voltage dip," *IEEE Transactions on energy conversion*, vol. 20, no. 2, pp. 435-441, 2005.
- [51] J. López, E. Gubía, E. Olea, J. Ruiz, and L. Marroyo, "Ride through of wind turbines with doubly fed induction generator under symmetrical voltage dips," *IEEE Transactions on Industrial Electronics*, vol. 56, no. 10, pp. 4246-4254, 2009.
- [52] M. Mohseni, S. M. Islam, and M. A. S. Masoum, "Impacts of Symmetrical and Asymmetrical Voltage Sags on DFIG-Based Wind Turbines Considering Phase-Angle Jump, Voltage Recovery, and Sag Parameters," *IEEE Transactions on Power Electronics*, vol. 26, no. 5, pp. 1587-1598, 2011.
- [53] S. Xiao, G. Yang, H. Zhou, and H. Geng, "An LVRT Control Strategy Based on Flux Linkage Tracking for DFIG-Based WECS," *IEEE Transactions on Industrial Electronics*, vol. 60, no. 7, pp. 2820-2832, 2013.
- [54] X. Dawei, R. Li, P. J. Tavner, and S. Yang, "Control of a doubly fed induction generator in a wind turbine during grid fault ride-through," *IEEE Transactions on Energy Conversion*, vol. 21, no. 3, pp. 652-662, 2006.
- [55] R. Zhu, Z. Chen, X. Wu, and F. Deng, "Virtual Damping Flux-Based LVRT Control for DFIG-Based Wind Turbine," *IEEE Transactions on Energy Conversion*, vol. 30, no. 2, pp. 714-725, 2015.
- [56] J. Yao, H. Li, Y. Liao, and Z. Chen, "An Improved Control Strategy of Limiting the DC-Link Voltage Fluctuation for a Doubly Fed Induction Wind Generator," *IEEE Transactions on Power Electronics*, vol. 23, no. 3, pp. 1205-1213, 2008.
- [57] S. Muyeen, R. Takahashi, T. Murata, and J. Tamura, "A variable speed wind turbine control strategy to meet wind farm grid code requirements," *IEEE Transactions on power systems*, vol. 25, no. 1, pp. 331-340, 2010.
- [58] S. Alepuz, A. Calle, S. Busquets-Monge, S. Kouro, and B. Wu, "Use of stored energy in PMSG rotor inertia for low-voltage ride-through in back-to-back NPC

- converter-based wind power systems," *IEEE Transactions on Industrial Electronics*, vol. 60, no. 5, pp. 1787-1796, 2013.
- [59] G. Mandic, A. Nasiri, E. Muljadi, and F. Oyague, "Active torque control for gearbox load reduction in a variable-speed wind turbine," *IEEE Transactions on Industry Applications*, vol. 48, no. 6, pp. 2424-2432, 2012.
- [60] J. Licari, C. E. Ugalde-Loo, J. B. Ekanayake, and N. Jenkins, "Damping of torsional vibrations in a variable-speed wind turbine," *IEEE transactions on energy conversion*, vol. 28, no. 1, pp. 172-180, 2013.
- [61] M. Molinas, J. A. Suul, and T. Undeland, "Torque transient alleviation in fixed speed wind generators by indirect torque control with STATCOM," in *Power Electronics and Motion Control Conference, 2008. EPE-PEMC 2008. 13th*, 2008, pp. 2318-2324: IEEE.
- [62] H. Geng, D. Xu, B. Wu, and G. Yang, "Active damping for PMSG-based WECS with DC-link current estimation," *IEEE Transactions on Industrial Electronics*, vol. 58, no. 4, pp. 1110-1119, 2011.
- [63] A. Dixit and S. Suryanarayanan, "Towards pitch-scheduled drive train damping in variable-speed, horizontal-axis large wind turbines," in *Decision and Control, 2005 and 2005 European Control Conference. CDC-ECC'05. 44th IEEE Conference on*, 2005, pp. 1295-1300: IEEE.
- [64] *International Standard IEC 61400-1 Third Edition: Wind Turbines-Part 1 Design Requirements*.
- [65] J. M. Mauricio, A. E. León, A. Gómez-Expósito, and J. A. Solsona, "An electrical approach to mechanical effort reduction in wind energy conversion systems," *IEEE Transactions on Energy Conversion*, vol. 23, no. 4, pp. 1108-1110, 2008.
- [66] L. C. Henriksen, M. H. Hansen, and N. K. Poulsen, "Wind turbine control with constraint handling: a model predictive control approach," *IET control theory & applications*, vol. 6, no. 11, pp. 1722-1734, 2012.
- [67] J. Lin, Y. Sun, Y. Song, W. Gao, and P. Sorensen, "Wind power fluctuation smoothing controller based on risk assessment of grid frequency deviation in an isolated system," *IEEE Transactions on Sustainable Energy*, vol. 4, no. 2, pp. 379-392, 2013.
- [68] R. Cardenas, R. Pena, G. Asher, and J. Clare, "Control strategies for enhanced power smoothing in wind energy systems using a flywheel driven by a vector-controlled induction machine," *IEEE Transactions on industrial electronics*, vol. 48, no. 3, pp. 625-635, 2001.
- [69] C. Abbey and G. Joos, "Supercapacitor energy storage for wind energy applications," *IEEE Transactions on Industry Applications*, vol. 43, no. 3, pp. 769-776, 2007.
- [70] Q. Li, S. S. Choi, Y. Yuan, and D. Yao, "On the determination of battery energy storage capacity and short-term power dispatch of a wind farm," *IEEE Transactions on Sustainable Energy*, vol. 2, no. 2, pp. 148-158, 2011.
- [71] A. M. Howlader, N. Urasaki, S. Chakraborty, A. Yona, T. Senjyu, and A. Y. Saber, "Fuzzy controller based output power leveling enhancement for a permanent

- magnet synchronous generator," in *Fuzzy Systems (FUZZ), 2011 IEEE International Conference on*, 2011, pp. 656-661: IEEE.
- [72] T. Senjyu, R. Sakamoto, N. Urasaki, T. Funabashi, H. Fujita, and H. Sekine, "Output power leveling of wind turbine generator for all operating regions by pitch angle control," *IEEE Transactions on Energy conversion*, vol. 21, no. 2, pp. 467-475, 2006.
- [73] M. Molinas, J. A. Suul, and T. Undeland, "Extending the life of gear box in wind generators by smoothing transient torque with STATCOM," *IEEE Transactions on Industrial Electronics*, vol. 57, no. 2, pp. 476-484, 2010.
- [74] Y. Liao, K. Zhuang, J. Yao, H. Li, and J.-b. He, "Dual-mode power control strategy simulation study of direct-driven permanent magnet synchronous generator for wind turbine," *Proc. CSEE*, vol. 29, no. 33, pp. 76-82, 2009.
- [75] F. Wilches-Bernal, J. H. Chow, and J. J. Sanchez-Gasca, "A Fundamental Study of Applying Wind Turbines for Power System Frequency Control," *IEEE Transactions on Power Systems*, vol. 31, no. 2, pp. 1496-1505, 2016.
- [76] K. V. Vidyanandan and N. Senroy, "Primary frequency regulation by deloaded wind turbines using variable droop," *IEEE Transactions on Power Systems*, vol. 28, no. 2, pp. 837-846, 2013.
- [77] M. F. M. Arani and E. F. El-Saadany, "Implementing Virtual Inertia in DFIG-Based Wind Power Generation," *IEEE Transactions on Power Systems*, vol. 28, no. 2, pp. 1373-1384, 2013.
- [78] R. Chen, W. Wu, H. Sun, Y. Hu, and B. Zhang, "Supplemental control for enhancing primary frequency response of DFIG-based wind farm considering security of wind turbines," in *2014 IEEE PES General Meeting | Conference & Exposition*, 2014, pp. 1-5.
- [79] J. M. Mauricio, A. Marano, A. Gomez-Exposito, and J. L. M. Ramos, "Frequency Regulation Contribution Through Variable-Speed Wind Energy Conversion Systems," *IEEE Transactions on Power Systems*, vol. 24, no. 1, pp. 173-180, 2009.
- [80] F. Díaz-González, M. Hau, A. Sumper, and O. Gomis-Bellmunt, "Participation of wind power plants in system frequency control: Review of grid code requirements and control methods," *Renewable and Sustainable Energy Reviews*, vol. 34, pp. 551-564, 2014/06/01/ 2014.
- [81] L. Holdsworth, J. B. Ekanayake, and N. Jenkins, "Power system frequency response from fixed speed and doubly fed induction generator-based wind turbines," *Wind Energy*, vol. 7, no. 1, pp. 21-35, 2004.
- [82] Y. Fu, Y. Wang, and X. Zhang, "Integrated wind turbine controller with virtual inertia and primary frequency responses for grid dynamic frequency support," *IET Renewable Power Generation*, vol. 11, no. 8, pp. 1129-1137 Available: <http://digital-library.theiet.org/content/journals/10.1049/iet-rpg.2016.0465>
- [83] M. F. M. Arani and Y. A. R. I. Mohamed, "Dynamic Droop Control for Wind Turbines Participating in Primary Frequency Regulation in Microgrids," *IEEE Transactions on Smart Grid*, vol. PP, no. 99, pp. 1-1, 2017.

- [84] M. F. M. Arani and Y. A. R. I. Mohamed, "Analysis and Impacts of Implementing Droop Control in DFIG-Based Wind Turbines on Microgrid/Weak-Grid Stability," *IEEE Transactions on Power Systems*, vol. 30, no. 1, pp. 385-396, 2015.
- [85] O. Anaya-Lara, F. Hughes, N. Jenkins, and G. Strbac, "Contribution of DFIG-based wind farms to power system short-term frequency regulation," *IEE Proceedings-Generation, Transmission and Distribution*, vol. 153, no. 2, pp. 164-170, 2006.
- [86] Y. Wang, J. Meng, X. Zhang, and L. Xu, "Control of PMSG-Based Wind Turbines for System Inertial Response and Power Oscillation Damping," *IEEE Transactions on Sustainable Energy*, vol. 6, no. 2, pp. 565-574, 2015.
- [87] R. Melício, V. M. F. Mendes, and J. P. d. S. Catalão, "A pitch control malfunction analysis for wind turbines with permanent magnet synchronous generator and full-power converters: proportional integral versus fractional-order controllers," *Electric Power Components and Systems*, vol. 38, no. 4, pp. 387-406, 2010.
- [88] M. Seixas, R. Melício, and V. Mendes, "Offshore wind energy system with DC transmission discrete mass: modeling and simulation," *Electric Power Components and Systems*, vol. 44, no. 20, pp. 2271-2284, 2016.
- [89] Z. Wu, W. Gao, J. Wang, and S. Gu, "A coordinated primary frequency regulation from Permanent Magnet Synchronous Wind Turbine Generation," in *2012 IEEE Power Electronics and Machines in Wind Applications*, 2012, pp. 1-6.
- [90] Z. S. Zhang, Y. Z. Sun, J. Lin, and G. J. Li, "Coordinated frequency regulation by doubly fed induction generator-based wind power plants," *IET Renewable Power Generation*, vol. 6, no. 1, pp. 38-47, 2012.
- [91] Y. Li, Z. Xu, and K. P. Wong, "Advanced Control Strategies of PMSG-Based Wind Turbines for System Inertia Support," *IEEE Transactions on Power Systems*, vol. 32, no. 4, pp. 3027-3037, 2017.
- [92] J. Licari, J. Ekanayake, and I. Moore, "Inertia response from full-power converter-based permanent magnet wind generators," *Journal of Modern Power Systems and Clean Energy*, journal article vol. 1, no. 1, pp. 26-33, June 01 2013.
- [93] H. Xin, Y. Liu, Z. Wang, D. Gan, and T. Yang, "A New Frequency Regulation Strategy for Photovoltaic Systems Without Energy Storage," *IEEE Transactions on Sustainable Energy*, vol. 4, no. 4, pp. 985-993, 2013.
- [94] P. Zarina, S. Mishra, and P. Sekhar, "Exploring frequency control capability of a PV system in a hybrid PV-rotating machine-without storage system," *International Journal of Electrical Power & Energy Systems*, vol. 60, pp. 258-267, 2014.
- [95] P. Moutis, A. Vassilakis, A. Sampani, and N. Hatziaargyriou, "DC switch driven active power output control of photovoltaic inverters for the provision of frequency regulation," *IEEE Transactions on Sustainable Energy*, vol. 6, no. 4, pp. 1485-1493, 2015.
- [96] C. Rahmann, V. Vittal, J. Ascui, and J. Haas, "Mitigation control against partial shading effects in large-scale PV power plants," *IEEE Transactions on Sustainable Energy*, vol. 7, no. 1, pp. 173-180, 2016.

- [97] E. I. Batzelis, G. E. Kampitsis, and S. A. Papathanassiou, "Power reserves control for PV systems with real-time MPP estimation via curve fitting," *IEEE Transactions on Sustainable Energy*, vol. 8, no. 3, pp. 1269-1280, 2017.
- [98] X. Lyu, Z. Xu, J. Zhao, and K. P. Wong, "Advanced frequency support strategy of photovoltaic system considering changing working conditions," *IET Generation, Transmission & Distribution*, vol. 12, no. 2, pp. 363-370, 2017.
- [99] R. K. Varma and M. A. Kelishadi, "Simultaneous Fast Frequency Control and Power Oscillation Damping by Utilizing PV Solar System as PV-STATCOM," *IEEE Transactions on Sustainable Energy*, 2019.
- [100] Y. Wang, H. Bayem, M. Giralt-Devant, V. Silva, X. Guillaud, and B. Francois, "Methods for Assessing Available Wind Primary Power Reserve," *IEEE Transactions on Sustainable Energy*, vol. 6, no. 1, pp. 272-280, 2015.
- [101] A. Buckspan, L. Pao, J. Aho, and P. Fleming, "Stability analysis of a wind turbine active power control system," in *American Control Conference (ACC), 2013*, 2013, pp. 1418-1423: IEEE.
- [102] J. Zhu, C. D. Booth, G. P. Adam, A. J. Roscoe, and C. G. Bright, "Inertia Emulation Control Strategy for VSC-HVDC Transmission Systems," *IEEE Transactions on Power Systems*, vol. 28, no. 2, pp. 1277-1287, 2013.
- [103] "Dynamic Models for Steam and Hydro Turbines in Power System Studies," IEEE Committee Report, *IEEE Transactions on Power Apparatus and Systems*, vol. PAS-92, 1973.
- [104] P. Kundur, N. J. Balu, and M. G. Lauby, *Power system stability and control*. McGraw-hill New York, 1994.
- [105] "DTU Database on Wind Characteristics," <http://www.winddata.com/>, accessed on 10 May 2014.
- [106] X. Liu and A. Lindemann, "Control of VSC-HVDC Connected Offshore Windfarms for Providing Synthetic Inertia," *IEEE Journal of Emerging and Selected Topics in Power Electronics*, vol. PP, no. 99, pp. 1-1, 2017.
- [107] T. Ackermann, *Wind power in power systems*. John Wiley & Sons, 2005.
- [108] J. N. Sakamuri, M. Altin, A. D. Hansen, and N. A. Cutululis, "Coordinated frequency control from offshore wind power plants connected to multi terminal DC system considering wind speed variation," *IET Renewable Power Generation*, vol. 11, no. 8, pp. 1226-1236, 2017.
- [109] C. Feltes, H. Wrede, F. W. Koch, and I. Erlich, "Enhanced Fault Ride-Through Method for Wind Farms Connected to the Grid Through VSC-Based HVDC Transmission," *IEEE Transactions on Power Systems*, vol. 24, no. 3, pp. 1537-1546, 2009.
- [110] P. Kou, D. Liang, Z. Wu, Q. Ze, and L. Gao, "Frequency Support From a DC-Grid Offshore Wind Farm Connected Through HVDC Link: A Communication Free Approach," *IEEE Transactions on Energy Conversion*, 2018.
- [111] Y. Phulpin, "Communication-Free Inertia and Frequency Control for Wind Generators Connected by an HVDC-Link," *IEEE Transactions on Power Systems*, vol. 27, no. 2, pp. 1136-1137, 2012.

- [112] B. Silva, C. Moreira, L. Seca, Y. Phulpin, and J. P. Lopes, "Provision of inertial and primary frequency control services using offshore multiterminal HVDC networks," *IEEE Transactions on Sustainable Energy*, vol. 3, no. 4, pp. 800-808, 2012.
- [113] C. Li, P. Zhan, J. Wen, M. Yao, N. Li, and W. J. Lee, "Offshore Wind Farm Integration and Frequency Support Control Utilizing Hybrid Multiterminal HVDC Transmission," *IEEE Transactions on Industry Applications*, vol. 50, no. 4, pp. 2788-2797, 2014.
- [114] A. Junyent-Ferr, Y. Pipelzadeh, and T. C. Green, "Blending HVDC-link energy storage and offshore wind turbine inertia for fast frequency response," *IEEE Transactions on sustainable energy*, vol. 6, no. 3, pp. 1059-1066, 2015.
- [115] H. Liu and Z. Chen, "Contribution of VSC-HVDC to Frequency Regulation of Power Systems With Offshore Wind Generation," *IEEE Transactions on Energy Conversion*, vol. 30, no. 3, pp. 918-926, 2015.
- [116] I. M. Sanz, B. Chaudhuri, and G. Strbac, "Inertial response from offshore wind farms connected through DC grids," *IEEE Trans. Power Syst*, vol. 30, no. 3, pp. 1518-1527, 2015.
- [117] Y. Li, Z. Xu, J. Østergaard, and D. J. Hill, "Coordinated Control Strategies for Offshore Wind Farm Integration via VSC-HVDC for System Frequency Support," *IEEE Transactions on Energy Conversion*, vol. 32, no. 3, pp. 843-856, 2017.
- [118] Y. Li and Z. Xu, "Coordinated Control of Wind Farms and MTDC Grids for System Frequency Support," *Electric Power Components and Systems*, vol. 45, no. 4, pp. 451-464, 2017/02/25 2017.
- [119] A. B. T. Attya and J. L. Dominguez-García, "Insights on the provision of frequency support by wind power and the impact on energy systems," *IEEE Transactions on Sustainable Energy*, vol. 9, no. 2, pp. 719-728, 2018.
- [120] S. G. Vennelaganti and N. R. Chaudhuri, "Ratio-based Selective Inertial and Primary Frequency Support through MTDC Grids with Offshore Wind Farms," *IEEE Transactions on Power Systems*, 2018.
- [121] A. E. Leon, "Short-term frequency regulation and inertia emulation using an MMC-based MTDC system," *IEEE Transactions on Power Systems*, vol. 33, no. 3, pp. 2854-2863, 2018.
- [122] F. D. Bianchi and J. L. Domnguez-Garca, "Coordinated Frequency Control Using MT-HVDC Grids With Wind Power Plants," *IEEE Transactions on Sustainable Energy*, vol. 7, no. 1, pp. 213-220, 2016.
- [123] H. Ye, W. Pei, and Z. Qi, "Analytical modeling of inertial and droop responses from a wind farm for short-term frequency regulation in power systems," *IEEE Transactions on Power Systems*, vol. 31, no. 5, pp. 3414-3423, 2016.
- [124] C. Luo, H. G. Far, H. Banakar, P.-K. Keung, and B.-T. Ooi, "Estimation of wind penetration as limited by frequency deviation," *IEEE Transactions on Energy Conversion*, vol. 22, no. 3, pp. 783-791, 2007.
- [125] X. Gao, K. Meng, Z. Y. Dong, D. Wang, M. S. El Moursi, and K. P. Wong, "Cooperation-Driven Distributed Control Scheme for Large-Scale Wind Farm

- Active Power Regulation," *IEEE Transactions on Energy Conversion*, vol. 32, no. 3, pp. 1240-1250, 2017.
- [126] Z. Wang and W. Wu, "Coordinated Control Method for DFIG-Based Wind Farm to Provide Primary Frequency Regulation Service," *IEEE Transactions on Power Systems*, vol. 33, no. 3, pp. 2644-2659, 2018.
- [127] S. Zhong and X. Wang, "Decentralized Model-Free Wind Farm Control Via Discrete Adaptive Filtering Methods," *IEEE Transactions on Smart Grid*, 2016.
- [128] A. De Paola, D. Angeli, and G. Strbac, "Distributed control of micro-storage devices with mean field games," *IEEE Transactions on Smart Grid*, vol. 7, no. 2, pp. 1119-1127, 2016.